THESIS
3
2000

LIBRARY
Michigan State
University

This is to certify that the

dissertation entitled

EXPERIMENTAL INVESTIGATION OF THE BEHAVIOR OF RC
DECK SLAB WITH ADDED LATERAL RESTRAINT

presented by

Made Sukrawa

has been accepted towards fulfillment
of the requirements for

Ph.D. degree in Civil Engineering

William E. Saul
Major professor

Date 7/24/00

MSU is an Affirmative Action/Equal Opportunity Institution

PLACE IN RETURN BOX to remove this checkout from your record.
TO AVOID FINES return on or before date due.
MAY BE RECALLED with earlier due date if requested.

DATE DUE	DATE DUE	DATE DUE
JUN 2 1 2002		

6/01 c:/CIRC/DateDue.p65-p.15

EXPERIMENTAL INVESTIGATION OF THE BEHAVIOR OF RC DECK SLAB WITH ADDED LATERAL RESTRAINT

By

Made Sukrawa

A DISSERTATION

Submitted to
Michigan State University
in partial fulfillment of the requirements for
the degree of

DOCTOR OF PHILOSOPHY

In Civil Engineering

Department of Civil and Environmental Engineering
College of Engineering

2000

ABSTRACT

EXPERIMENTAL INVESTIGATION OF THE BEHAVIOR OF RC DECK SLAB WITH ADDED LATERAL RESTRAINT

By: Made Sukrawa

The present study proposes a new method of retrofitting an existing composite reinforced concrete bridge deck slab by increasing its lateral restraint, by connecting the top flanges of steel girders with tie rods. To verify the method, experimental and analytical investigations were conducted. Experimental investigation was conducted by testing a 1/5 scale composite steel I-beam bridge. Two different deck panels were incorporated into the construction of a three-girder simply supported bridge. One panel was retrofitted with tie rods, and the other panel was used as a control panel. With a span to thickness ratio of 12.5, the model deck slab was reinforced with 0.2% isotropic welded wire mesh. Each slab panel was consecutively tested at four different load points with a statically applied concentrated load. The behavior of the slab panels was measured with dial and strain gages to determine the stiffness and strength of the panels. The load response history of the slab, the center beam, and the tie rods was observed at load increments of 2,224 N (500 lbs) until the slab failed.

The slab panel with tie rods was significantly stronger and stiffer than the control slab panel. At lower load levels, the net deflection of the slab with tie rods reduced by a factor of 34%, and at higher load levels, the reduction was up to 50%. The cracked and failure loads of the slabs with tie rods increased by factors of 30% and 13.7%, respectively. Compared to a half axle load of 72.5 kN (16.3 kip) with an impact factor of

1.3, safety factors of 15.9 and 13.9 were obtained for the slab with and without tie rods, respectively. Thus, with added lateral restraint the safety factor of the slab increased by a factor of 14.4%.

Prediction of the load response history of the bridge was conducted by developing 3-D nonlinear finite element (FE) models using a commercial finite element software ABAQUS. The models incorporated each component of the bridge including the tie rods. The deck slab was modeled using 3-D solid elements with steel reinforcement embedded in the concrete elements. Several models were developed for studying the sensitivity of the models to various modeling parameters. The response of each model was compared to the observed response. In addition to the FE analysis, strength analyses using punching shear theory of restrained slabs and the ACI Code provisions on punching shear strength of concrete slabs were also utilized for comparison.

The arching action in the deck slab was well predicted by 3-D solid elements, through the development of strains in the tie rods in the vicinity of the load. The observed load response history of the bridge was also accurately simulated in the FE models up to a load level about 60% of the failure load. At higher load levels however, the FE models showed stiffer response than the observed one. The responses of the FE models were strongly dependent on the material model for the concrete.

Strength analysis using the punching shear model of restrained slabs predicted the punching strength of the slabs with corresponding restraint factor values of 0.663 and 0.786 for the slab panel without and with tie rods, respectively. The addition of tie rods increased the lateral restraint of the slab by a factor of 18.6%. The ACI Code provisions gave nominal shear strengths significantly lower than the observed values.

To:

The People of Bontihing - Bali

ACKNOWLEDGEMENTS

The author wishes to express sincere gratitude to Dr. William E. Saul for his professional encouragement, guidance, and especially his personal friendship throughout this endeavor. The author also wishes to thank the committee members: Dr. Ronald S. Harichandran, Dr. Frank J. Hatfield, and Dr. Charles R. McCluer for their valued technical input and suggestions throughout the course of this research.

The research was partly funded by Civil and Environmental Engineering Department - Michigan State University, and The Great Lakes Fabricator & Erectors Association of Michigan. The author also gratefully acknowledges the Structural Lab of Michigan DOT for their help and the use of their lab.

Most importantly, the work would not have been possible without the financial support from the Engineering Education Development Project of the Department of Education and Culture of Indonesia. The author also appreciates the financial supports through fellowships from the College of Engineering, Office for International Students and Scholars, and the Graduate School of Michigan State University. Finally, invaluable support and understanding of the author's wife, Putu Sumiarthi, are most appreciated.

TABLE OF CONTENTS

LIST OF TABLES ix

LIST OF FIGURES x

CHAPTER 1

INTRODUCTION 1

1.1 Enhancing Arching Action in RC Deck Slabs 1

1.2 Hypothesis 3

1.3 Purpose and Scope of Research 5

CHAPTER 2

LITERATURE REVIEW 8

2.1 Introduction 8

2.2 Experimental Investigations of RC Deck Slabs for Bridges 9

2.2.1 Tests by Batchelor et al 9

2.2.2 Test by Dorton et al., and Csagoly et al. 11

2.2.3 Test by Beal 12

2.2.4 Test by Fang et al. 13

2.2.5 Test by Puckette et al. 14

2.2.6 Test by Perdikaris 15

2.3 External Reinforcement in Deck Slab and Steel Beam 16

2.4 Empirical Design Method of RC Deck Slabs for Bridges 18

2.5 Shear Strength of Reinforced Concrete Slabs 22

2.5.1 Empirical Methods 22

2.5.2 Rational Model of Punching Shear 25

2.6 Finite Element Analysis of Reinforced Concrete Slab 28

CHAPTER 3

THEORY AND ANALYSIS 36

3.1 Introduction 36

3.2 Rational Model of Punching Shear Strength of Restrained Slabs 38

3.2.1 Mechanical Model for Simply Supported Slabs 42
3.2.2 Mechanical Model of Restrained Slabs 45
3.3 Analyses of Punching Strength of RC Slabs with Additional Lateral restraint 48
3.4 ACI Provision on Punching Shear Strength of Concrete Slab 53
3.5 Finite Element Analysis 55
3.5.1 Geometric Model 56
3.5.2 Material Models 60
3.5.2.1 Concrete Model 61
3.5.2.2 Steel Model 64
3.5.3 Input Files 64
3.5.4 Finite Element Analyses Results 68

CHAPTER 4

DESIGN AND CONSTRUCTION OF MODEL BRIDGE 76
4.1 Introduction 76
4.2 Design of Prototype Bridge 77
4.2.1 Reinforced Concrete Deck Slab 78
4.2.2 Design of Tie Rods 80
4.2.3 Design of Steel Girders 81
4.2.4 Design of Edge Beams 81
4.2.5 Design of Shear Connectors 83
4.3 Design of Scaled Model Bridge 83
4.4 Properties of Material for Model Bridge 88
4.4.1 Micro Concrete 90
4.4.2 Steel Reinforcement 92
4.4.3 Structural Steel 93
4.5 Construction of Model Bridge 93
4.5.1 Concrete Cylinders 94
4.5.2 Curing 95

CHAPTER 5

EXPERIMENTAL PROGRAM 97

5.1 Introduction 97
5.2 Instrumentation 98
5.3 Load Testing of Model Bridge 99
5.4 Recorded Data 102
    5.4.1 Cylinder Test 102
    5.4.2 Loading Test 105

CHAPTER 6

PRESENTATION AND DISCUSSION OF RESULTS 113
6.1 Introduction 113
6.2 Punching Strength of Slabs (Analyses and Test Results) 114
6.3 Load Deflection Diagram of Slabs (FEM and Test Results) 119
6.4 Deflection of Center Beam (FEA and Test Results) 127
6.5 Strain in Tie Rods (FEA and Test Results) 131
6.6 Summary of Results 134

CHAPTER 7

CONCLUSION AND RECOMMENDATION 137
7.1 Summary and Conclusion 137
7.2 Recommendation 141
REFERENCES 143

APPENDICES

APPENDIX A: PUNCHING SHEAR MODEL OF RESTRAINED SLAB, DERIVATION OF EQUATIONS 149
APPENDIX B: FLOW DIAGRAM AND CODE LISTING TO CALCULATE PUNCHING SHEAR STRENGTH OF RESTRAINED SLAB.. 163
APPENDIX C: EXAMPLE OF FINITE ELEMENT INPUT AND OUTPUT FILES 169

LIST OF TABLES

Table 3.1 Punching Load of Slab (Restrained Slab Theory) 52
Table 3.2 Shear Strength of Model Slab (ACI Formulae) 55
Table 3.3 Description of FE Models 68
Table 3.4 Summary of FEA Results 69
Table 4.1 Properties of Prototype Bridge 84
Table 4.2. Scale Factor 85
Table 4.3 Properties of Prototype and 1/5 Scale Model Bridges 89
Table 5.1 Results of Cylinder Tests 103
Table 5.2 Crack Load, Failure Load, and Maximum Deflections of Test Slab 107
Table 6.1 Ratios of FEA and Test Results 117

LIST OF FIGURES

Figure 1.1 Compressive Membrane Forces in a Cracked Slab 4
Figure 1.2 Effect of Adding Tie Rod 4
Figure 2.1 K and N Model of Punching Shear 27
Figure 2.1 Tension Stiffening Model of RC 31
Figure 3.1. Crack Pattern of Restrained Deck Slab (Plan View) 40
Figure 3.2. Mechanical Punching Model of Restrained Slab 41
Figure 3.3 Sector Element (Wedge) Showing Forces and Notations 41
Figure 3.4 Geometry of Equivalent Circular Slab 51
Figure 3.5.a Plan View of FE model Showing Mesh of the Deck 59
Figure 3.5.b Cross Section of FE model Showing Element Connectivity 59
Figure 3.5.c Isometric View of FE model without the Deck Elements 60
Figure 3.6 Predicted Load Deflection Diagram of Slab with Tie Rods 70
Figure 3.7 Load Deflection Diagram of Slab Using Different Elements 71
Figure 3.8 Predicted Load Deflection Diagram of Slab without Tie Rods 72
Figure 3.9 Predicted Load Deflection Diagram of Center Beam 73
Figure 3.10 Predicted Load Strain Diagram of Tie Rods 75
Figure 4.1 Plan View of Prototype Bridge 79
Figure 4.2 Longitudinal Section Showing Edge Beam and Diaphragm 82
Figure 4.3 Cross Section of Model Bridge 87
Figure 4.4 Detail of Tie Rod 88
Figure 5.1 Experimental Set-Up on Loading Frame 99
Figure 5.2 Arrangement of Dial Gages and Strain Gage Position 100
Figure 5.3 Loading, Tie Rods, and Strain Gage Positions 101
Figure 5.4 Typical Crack Pattern 106
Figure 5.5 Top View of Punching Failure at LP3 108
Figure 5.6 Bottom View of Punching Failure at LP2 108

Figure 5.7 Load Deflection Diagram of Slab 109
Figure 5.8 Load Deflection Diagram of Center Beam 110
Figure 5.9 Load Strain Diagram of Tie Rods 111
Figure 6.1 Analysis Results: Punching Strength of Slab 115
Figure 6.2 Observed Load Deflection Diagram of Slab Loaded near Mid-span 121
Figure 6.3 Observed Load Deflection Diagram of Slab Loaded near the Edges 122
Figure 6.4 Measured and Predicted Load Deflection Diagram of Slab Loaded at LP3 124
Figure 6.5 Measured and Predicted Load Deflection Diagram of Slab Loaded at LP7 125
Figure 6.6 Measured and Predicted Load Deflection Diagram of Center Beam Loaded At LP3 (Slab with Tie Rods) 128
Figure 6.7 Measured and Predicted Load Deflection Diagram of Center Beam Loaded at LP7 (Slab without Tie Rods) 129
Figure 6.8 Measured and Predicted Load Strain Diagram of Tie Rods Directly Underneath the Applied Load 132
Figure 6.9 Measured and Predicted Load Strain Diagram of Tie Rods Adjacent to the Applied Load 133
Figure A.1 Isometric View of Conical Shell Element for Simply Supported Slab 150
Figure A.2 Cross Section of Mechanical Model Showing Notations 150
Figure A.3 Mechanical Model of Simply Supported Slab 156
Figure A.4 Mechanical Model of Restrained Slab 157
Figure A.5 Boundary Forces 160
Figure C.1 Magnified Displaced Shape of FE Model of the Bridge............................. 183
Figure C.2 Contour of E33, Strain in 3-Direction 184
Figure C.3 Contour of S33, Stress in 3-Direction 185

CHAPTER 1

INTRODUCTION

1.1 Enhancing Arching Action in RC Deck Slabs

Although common practice is to assume flexure for the design of a reinforced concrete (RC) deck slab, it has been repeatedly shown that, when subjected to a concentrated wheel load, the slab fails in punching shear (AASHTO 1994). By definition, punching shear failure is denoted by a local failure, when a plug of concrete is punched out of the slab immediately underneath the load.

A laterally restrained deck slab exhibits internal arching action that strengthens the slab through the confinement provided by a complex three-dimensional membrane stress around the loaded area. The lateral restraint is provided by the supporting components, surrounding slab, and rigid appurtenances acting compositely with the slab. As a result, the slab fails in shear, rather than in flexure, with a load capacity much higher than required to sustain a truck wheel load.

Despite the extra strength, in a composite RC slab and steel girder system, the girders always last longer than the slab because the slab is directly impacted by traffic, de-icing chemicals, climate, and other aggressive environmental effects. Such exposure causes the slab to readily deteriorate. Consequently, it requires replacement during the service life of the bridge. Strengthening an existing deck slab is one way to extend its service life. In addition to restoring its function, retrofitting a bridge deck is also intended to upgrade the bridge's status to a higher performance level, or to meet additional capacity requirements (Xanthakos 1996). In this case, retrofitting is aimed at increasing the durability of the slab.

There are a number of ways to strengthen existing RC deck slab structures. One way is to use the concrete-thickness increasing method, where the slab is retrofitted by adding another layer of concrete with reinforcement. This method is not very popular because it adds dead load stress on the supporting girders, which may not have been considered in the design. It also requires adjustment of the vertical alignment of the pavement adjoining the bridge. Bonding between the old and the new concrete is another problem that arises in this method.

The carbon-fiber-sheet gluing method is the most recent process employed to strengthen concrete structures. In this method carbon fiber sheets are glued to the concrete under surface by means of an epoxy resin (Masajiro et al, 1994). This method is suitable to increase the flexural strength of the slab.

In this study, an alternate method called the lateral-restraint increasing method is proposed. The method proposed herein is based on the addition of tension members (tie rods) to connect the top flanges of the supporting steel girders beneath the slab. The additional lateral restraint is expected to minimize the lateral movement of the girders, thus enhancing arching action in the slab, and therefore, increasing the strength and stiffness of the slab. The advantage of this method, relative to the others, is its ease of application that neither entails traffic interruption nor requires special materials or tools.

Extensive research on the load capacity of RC deck slabs was reported by a number of workers, where load tests on small and full scale deck slabs were conducted (Bachelor et al. 1978, Csagoly et al 1978, Beal 1982, Fang et al. 1986, Puckette et al.

1989, Agarwal 1990). RC slabs with various steel reinforcement ratios and arrangements, were built and tested up to failure. Orthotropic and isotropic steel arrangements were used; the first represents the conventional practice, where the steel ratio in the transverse direction of the bridge is higher than that in the longitudinal direction; the later represents the same steel ratios in both directions of the bridge. The results of these experiments showed that the arching action enhanced the shear strength of the slab.

Taking advantage of arching action, extensive tests on steel-free fiber-reinforced concrete (SFFRC) deck slabs were reported (Mufti et al. 1993, Bakht and Mufti 1996). Instead of conventional reinforcement, steel straps were used as external reinforcement, where the straps were attached to the top flanges of the steel girders to increase the lateral restraint of the slab. The experiments showed that the addition of steel straps resulted in a punching failure load twice as high as the failure load of a slab without restraining straps.

1.2 Hypothesis

From the aforementioned research, it can be concluded that the behavior of RC deck slabs on steel beams can be improved by increasing their lateral restraint. The lateral restraint in RC deck slabs is provided by the shear connectors, internal steel reinforcement, and the supporting components of the deck. Adding shear connectors or internal steel reinforcement to an existing deck slab is not practical. It is possible, however, to increase the lateral restraint of the slab by using external reinforcement, similar to that used for the SFFRC deck slabs. By adding tension members to connect the underside of the top flanges of the steel beams, it is hypothesized to increase the lateral restraint of the slab, and therefore, improve the strength and stiffness of the deck slab.

The enhancement of lateral restraint through the addition of a tie rod is illustrated in Figures 1.1 and 1.2. Figure 1.1 shows the formation of flexural cracks and in-plane forces corresponding to the stress distribution in a restrained slab. The compressive membrane action produces net in-plane forces at the slab boundaries that cause the supporting girders to move both vertically and laterally. Figure 1.2 shows the diagram of the compressive arch tied by steel reinforcement and a tie rod.

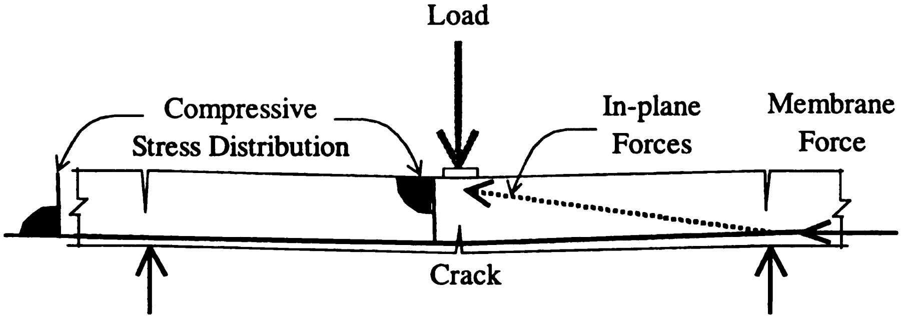
Load
Compressive
Stress Distribution
In-plane
Forces
Membrane
Force
Crack

Figure 1.1 Compressive Membrane Forces in a Cracked Slab

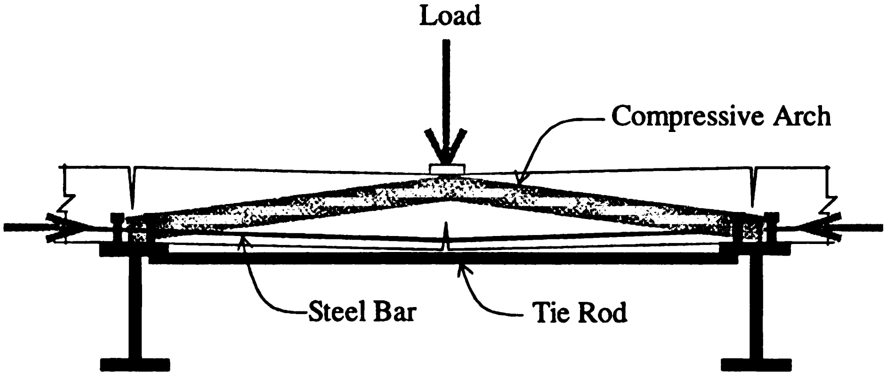
Load
Compressive Arch
Steel Bar
Tie Rod

Figure 1.2 Effect of Adding Tie Rod

Adding a tie rod to the arch horizontally (connecting top flanges of the girders) will reduce the lateral movement of the arch, and hence, enhance the arching action in the slab. The compressive membrane forces together with the external load develop three-dimensional compression in the slab, which considerably increases the strength and stiffness of the concrete around the loaded area.

To test the validity of this hypothesis, an experimental study was conducted. Analytical studies based on a rational model of punching shear and finite element analyses (FEA) were conducted to verify the experimental results. The application of the concept of adding tie rods for retrofitting an existing or a newly constructed RC deck slab is the original contribution of this research.

1.3 Purpose and Scope of Research

The main objective of this research is to study the effect of adding lateral restraint (tie rods) to an existing composite RC deck slab and steel girder system on the behavior of the slab subjected to a static concentrated load. For this purpose, experimental testing and theoretical analyses were conducted. The load response history of the slab, the steel beam, and the tie rods is used to measure the effect of adding tie rods. In addition to the main objective, there are a number of other purposes of this research. They are:

- To verify the adequacy of the strength and stiffness of RC deck slabs with minimum steel reinforcement under service load and overload conditions.
- To develop three-dimensional, nonlinear finite element (FE) models of the bridge to predict the load response history of the slabs with and without additional tie rods.

- To verify the application of the rational and empirical approaches, to predict the punching shear strength of a restrained RC deck slab with and without additional lateral restraint.

As a preliminary study, to prevent bias observation due to uncontrolled conditions of the deck slabs, only a newly constructed slab (without deterioration) is considered. The deck slab is assumed to be deficient because there is a need to increase the performance and durability of the deck. Having stated the purposes and scope (limitation), the steps of this research are listed in the following order:

- Literature Review: reviews the experimental work related to the arching action in the deck slab for bridges, and the theoretical and numerical analyses of RC deck slabs.
- Theory and Analyses: include derivation of the equations to calculate the punching shear strength of an RC slab, and development of finite element models using finite element (FE) software ABAQUS.
- Design and Construction of Model Bridge: design the prototype and small-scale bridge, prior to building the model bridge.
- Experimental Program: includes instrumentation, and load testing of the model bridge.
- Presentation and Discussion of Results: evaluate the results from the analyses and lab experiment, and verify the validity of the analyses methods based on the test results.
- Conclusion and Recommendation: draw conclusions from the test and analyses results, and provide recommendations related to application of the concept of adding lateral restraint to an existing or a newly constructed deck slab.

The results of these experimental and analytical studies will be applicable to retrofit RC deck slabs on steel girders for bridges, and it can be extended to other slab structures subjected to concentrated loads. Therefore, through this research, a new method of retrofitting an existing RC deck slab is to be verified.

CHAPTER 2

LITERATURE REVIEW

2.1 Introduction

Experiments on punching shear failure of reinforced concrete slabs discovered that the presence of in-plane compression due to restraint in the slab boundaries substantially increased the shear strength of the slab. These findings have influenced bridge researchers to review and investigate the shear strength of RC deck slabs for bridges. For the past three decades, after the composite I-beam bridge became popular in North America, extensive research into the behavior of RC deck slabs for bridges has been conducted.

Research on the shearing strength of composite bridge deck slabs was initiated at the University of Illinois in 1946. Since then, more extensive tests were conducted to specifically investigate the behavior of deck slabs under concentrated loads. Tests at Queen's University were among the pioneer studies in this area (Hewitt 1972; Hewitt and Batchelor 1975; Batchelor et al. 1978). More detail on this experimental program is discussed in the following sections, together with a number of other related experimental work.

Taking advantage of arching action in the slab, external reinforcement has been used to provide additional lateral restraint. Experimental work initiated at the Technical University of Nova Scotia, TUNS, was part of an effort to eliminate internal reinforcement in deck slabs (Mufti et. al. 1993; Bakht and Mufti 1996; Newhook 1997). This particular work is also reviewed in detail.

The application of these findings for bridge deck design was marked by the inclusion of the empirical design method, for the first time, in both the Ontario Highway Bridge Design Code, OHBDC 1983 and the American Association of State Highway and Transportation Official (AASHTO 1994) design specifications for bridges. These design methods were reviewed in detail in consideration of the benefits gained utilizing arching action in the design as compared to the conventional method. Finally, reviews on theories on the punching shear strength of reinforced concrete slabs and finite element analyses of RC slabs are presented in the last parts of this chapter.

2.2 Experimental Investigations of RC Deck Slabs for Bridges

A number of experimental projects have been reported investigating the behavior of small model and full scale RC deck slabs for bridges subjected to concentrated loads. Among the published work are those conducted by: Batchelor et al., Dorton et al. and Csagoly et al., Agarwal, Beal, Fang et al., Puckette et al., and Perdikaris et al. In general, the natures of the investigations are similar, however, the focus of each differs somewhat. Therefore, it is necessary to discuss some of them emphasizing their focus.

2.2.1 Tests by Batchelor et al.

Experimental investigations of the ultimate strength of deck slabs of composite steel concrete bridges were conducted by testing one-eight scale models of 24.4 m (80 ft.) span prototype bridges. Three-girder and four-girder model bridges were designed with beam spacing of 0.45 and 0.30 m (18 and 12 in.), respectively. The model bridges were tested to failure with static concentrated loads at Queen's University in conjunction with the Ontario Ministry of Transportation and Communications (Hewitt 1972; Hewitt and Batchelor 1975; Batchelor et al. 1978). The 22 mm (0.9 in.) thick model slabs were divided into strips where each strip was reinforced with various steel ratios ranging from 0 to 0.6 %. Orthotropic and isotropic steel arrangements were used to represent both the conventional practice and the proposed application, respectively.

The results from a total of 68 failure tests showed that nearly all of the slabs failed in punching shear. Only one panel of reinforced slab and some panels of unreinforced slabs failed in flexure. The average ultimate strength of the four-beam model slabs ranged from 16.5 kN (3,710 lbs) for the plain concrete slab to 23.66 kN (5,319 lbs) for the slab with 0.6% isotropic reinforcement. The slab with orthotropic reinforcement failed at about 24 kN (5,400 lbs).

It was reported that at a load of between 25 and 50 percent of the ultimate load visible cracking in the form of longitudinal and diagonal cracks were observed on the underside of the slab. Subsequently, transverse cracks appeared on the upper-side of the slab, on either side of the loaded area in the vicinity of the beams. The cracking pattern followed that the higher the percentage of reinforcement, the more symmetrical and closely spaced the cracking was. The deflection behavior of the slab followed that the slab with lower steel ratio failed after relatively larger deflection. The net deflection of the slab with 0.2% steel ratio, at failure load of about 18 kN (4,047 lbs), was about 7.5 mm (0.3 in.).

The conclusion of the experiment suggested that the strength of the deck was not significantly affected by the position of the load on the deck, previous failures of the slab in adjacent panels, dead load stress and deflection, or the strength of the concrete. It also recommended the use of 0.2 % isotropic steel reinforcement to account for the temperature and shrinkage requirements, which amounts to a reduction of 66 % of the conventional steel requirement. With the recommended minimum steel, the slab can still be expected to have a safety factor against punching failure of about 9. In addition to the experimental work, a theory to calculate the punching shear strength of a restrained slab was proposed based on the theory initiated by Kinnunen and Nylander for simply supported slabs. More detail on this theory is discussed later in this chapter and in Chapter 3.

2.2.2 Tests by Dorton et al., and Csagoly et al.

Field testing of existing, and newly designed and built bridges was conducted by the Ontario Ministry of Transportation and Communication, using a simulated wheel load of 445 kN (100,000 lbs), about four to five times the actual AASHTO truck wheel load (Dorton et al. 1976; Csagoly et al. 1978). A total of 40 bridges were tested with a wide range of spans, slab thickness, age, bridge types, and degrees of deterioration. The deck slabs of the existing bridges were designed according to the 1973 AASHTO specifications, where four different bridge types were selected: Non-composite steel beam and concrete slab; Composite steel beam and concrete slab; Monolithic concrete beam and concrete slab; Composite AASHTO girders and concrete slab. For the composite steel girder bridges, the slab thickness varied from 180 to 215 mm (7 to 9 in.) with beam spacing from 1.84 to 3.51 m (8 to 12 ft.).

From 32 bridges examined, neither serious cracking was noticed in any of the deck slabs, nor visible cracking observed on the top surface of the slabs in the transverse negative moment regions. Directly under the load on the bottom surface of the slab, hairline cracking was observed during the test. However, the cracks disappeared upon removal of the load. For the composite steel beam bridges, the deflection of the slab under the simulated load varied from 0.7 to 3.05 mm (0.02 to 0.12 in.) depending on the beam spacing. It was concluded that even under a load 4 to 5 times larger than the maximum half-axle weight combined with the deterioration of some decks, no failure of restrained slabs were ever observed. Consequently, the deck slabs that were designed according to the 1973 AASHTO Specification were considered overly designed.

For the newly designed and built bridge, a three-span-continuous steel girder bridge was load tested. The deck slab was designed based on the new findings from lab tests conducted at Queen's University, in which steel reinforcement ratio as low as 0.2% was used. The deflection of the deck, subjected to the same load as that used to test the existing bridges, was reported to vary from 1 to 3.1 mm (0.04 to 0.122 in.) for the interior panels and 1.1 to 2.8 mm (0.044 to 0.111 in.) for the exterior panels. It was concluded that the deck slabs could be safely designed allowing for internal arching action, making possible a large reduction in the steel reinforcement. Agarwal (1990) reported load tests similar to those mentioned above with comparable results.

2.2.3 Tests by Beal

Lab testing of two bridge models with a scale factor of 1 to 5.9 was conducted at the New York State DOT (Beal 1981; Beal 1982). The prototype bridge was comprised of five steel girders spaced at 2.75 m (9 ft.) center to center with 22 m (72 ft.) of span length. In the first model the 216 mm thick slab was heavily reinforced to represent the standard bridge deck design according to the 1977 AASHTO Specification. For the second model, a 200 mm thick slab was reinforced with minimum isotropic steel representing the new practice of design in Ontario. The strain in the steel reinforcement was measured and used to estimate the bending moment on both uncracked and cracked conditions of the slab. For the uncracked test, field tests were also conducted for comparison.

The conclusion of the tests was that, the service load stress, predicted by the existing design procedure and method, did not develop in the slab. Under a service load of 92.6 kN (20.8 kips), the maximum induced stress in a conventionally reinforced slab was 57.2 MPa (8.3 ksi). A value of 80.6 MPa (11.7 ksi) was observed for the slab with lighter steel reinforcement. The maximum ratio of the measured and theoretical induced moment were 0.65 and 0.62 for the conventional and lightly reinforced slab, respectively. A 100 % increase of wheel load would not overstress the steel reinforcement and, accordingly, it was concluded that no methodology is needed to predict induced stresses resulting from the passage of occasional overload permit vehicles. Tests to failure resulted in punching shear capacities always larger than six times the design wheel load, regardless of the reinforcement pattern. Thus, a 59% reduction in total steel reinforcement did not reduce the strength of the slab below a safe level.

2.2.4 Tests by Fang et al.

Lab testing of a full-scale model bridge was conducted at the University of Texas at Austin (Fang et al. 1986, Fang et al. 1990). The 190 mm (7.5 in.) slab was supported on three steel girders spaced at 2.13 m (7 ft.). The span length of the model bridge was 14.94 m (49 ft.). Isotropic steel reinforcement amounted to 60% of the existing AASHTO specified requirement was used. The level of stress in the deck due to design and fatigue loading was recorded.

The research concluded that at the design load level, the overall behavior of the deck slab, including the local stiffness of the deck at the loaded point, was satisfactory. Under overload condition, about three times the design load, the behavior of the slab was essentially linear. Fatigue loading did not significantly change the behavior of the deck due to the design load, even under the overload cited above. Another important assessment from their conclusions was that the compressive membrane forces did not significantly affect the performance of the bridge at loads below cracking.

2.2.5 Tests by Puckette et al.

The University of Wyoming in conjunction with the Wyoming Highway Department and the Federal Highway Administration (Puckette et al. 1989) conducted tests on two noncomposite steel girder bridges. One deck slab was reinforced according to conventional practice, and the other used minimum isotropic reinforcement. The stresses in the longitudinal and transverse steel were measured at 133.44 kN (30,000 lbs) applied load. The AASHTO design load was 92.52 kN (20.8 kips) which corresponds to a 71.168 kN (16 kips) prototype wheel loads with a 1.3 impact factor.

The maximum observed stress in the bottom transverse steel under the 133.44 kN (30,000 lbs) load was 45.5 MPa (6.6 ksi) and 54.5 (7.9 ksi) for the conventional and isotropic slabs, respectively. The stresses in the other steel reinforcement of the slab were even lower. It was concluded that a slab with isotropic steel arrangement performed satisfactorily under the AASHTO design load.

2.2.6 Tests by Perdikaris et al.

Perdikaris did a number of tests related to the behavior of RC deck slabs under static and moving loads for slabs with various degrees of edge restraint. Among the test specimens was a 1 to 6.6 scale model bridge tested at Case Western Reserve University, in conjunction with the Ohio DOT and the Federal Highway Administration (Perdikaris and Beim 1988; Petrou and Perdikaris 1990; Petrou 1991). The 15.24 m (50 ft.) prototype bridge was supported by four non composite steel girders spaced at 2.13 m (7 ft.). The 216 mm (8.5 in.) slab with orthotropic and isotropic reinforcement was loaded with pulsating and moving loads in addition to static loads. The pulsating load was applied sinusoidally at a fixed point at frequencies between 1 and 8 Hz. The maximum load was about 60% of the static ultimate strength of the slab and the minimum load was 1.779 kN (400 lbs). The constant magnitude of moving load was applied at a maximum speed of 460 mm/s (1.5 ft./sec).

The results of the tests showed that the orthotropically reinforced slab was stronger and stiffer than the slab with isotropic reinforcement. However, the later slab still had a safety factor of 14 in terms of the static failure load. In term of cracking load the safety factor was about four. At the design load of 92.6 kN (20,800 lbs), the expected stress in the steel reinforcement was about 20.7 MPa (3 ksi), which is a negligible amount compared to the yield stress of the steel. Under the pulsating load, the slab with isotropic reinforcement showed lower fatigue strength than the one with orthotropic reinforcement. Under moving load, however, the fatigue life (number of load passages) of the isotropically reinforced slab was about 20 times the fatigue life of the slab with orthotropic reinforcement. With a reduction of 43% in steel content, the slab with isotropic reinforcement failed at a 37% lower load, but its ductility increased by about 270%, as compared to the orthotropic reinforcement.

Still other tests related to the application of the new design approach have been done. The common conclusion of the tests was that a deck slab reinforced with as low as 0.2% isotropic reinforcement is adequate to sustain the current AASHTO design load, including the provision for fatigue strength. The minimum specified reinforcement of 0.2% was intended to account for temperature and shrinkage induced stresses. It was also implied that the conventional design method of slab reinforcement was unnecessarily excessive.

2.3 External Reinforcement in Deck Slab and Steel Beam

Experiments on steel-free fiber reinforced concrete (SFFRC) deck slabs were conducted at TUNS (Mufti et. al. 1993; Bakht and Mufti 1996; Newhook 1997). These experiments avoided using steel reinforcement and took advantage of the internal arching system, which develops in laterally restrained slabs. Fibers were used to control the cracking due to the effects of shrinkage and temperature in the concrete. Instead of internal steel reinforcement, external steel straps were used to provide lateral restraint of the slabs.

As reported by the investigators, the initial experiment was guided by trial and error where each experiment was conceived after studying the results of the preceding ones. In the first experiment, a half-scale model of a two-girder bridge was constructed. A 100 mm (4 in.) thick steel-free fiber reinforced concrete slab was supported by two W460x82 steel girders, spaced at 1,067 mm (42 in.) center to center, with a longitudinal span of 3,500 mm (137.8 in.). Three C200x17 diaphragms were placed at the inner portion of the girders, but none at the ends. Therefore, the free edges of the slabs were not restrained. Pairs of 75-mm (3 in.) long shear studs, spaced at 305-mm (12 in.) center to center, were used to connect the slabs with the girders. The deck slab contained 38-mm (1.5 in.) long polypropylene fibers with 0.88% of volume fraction (0.34% by weight). The deck slab was tested under a central rectangular patch load measuring 257 by 127 mm^2 (10 by 5 in.). The slab failed in flexure at a load of 173 kN (38.9 kip).

In the second model, end diaphragms were added to the steel framework, with the other dimensions the same as in the first experiment. Interestingly enough, the slabs failed at a load of 222 kN (49.9 kip), but not in punching shear. The first two models led to a third model where 64 x 10 mm (2.5 x 0.4 in.) steel straps spaced at 457 mm (18 in.) centers were welded to the top flanges of the steel girders. This model resulted in a punching shear failure at a load of 418 kN (93.9 kip). Taking advantage of the localized failure, the slab was tested at two other locations at distances of 0.86S and 0.43S from the closer transverse free edge, where S is the spacing of the girders. The failure loads for the two locations were 316 and 209 kN (71 and 47 kips), respectively, with a hybrid between punching shear and flexure failure modes. The decrease in load capacities near the transverse edges was believed to be due to the lack of longitudinal restraint. In the fourth model, three girders were used to study the behavior of the slab under pairs of loads, one on either side of an internal girder. Testing at mid span of this model resulted in simultaneous punching shear failures at a load of 418 kN (94 kip) for each loading pad.

In comparison, the AASHTO Specification requires that interstate highway bridges be designed for a maximum load of 145 kN (32 kip), which is a maximum HL-93 truck load (AASHTO 1994). In a full scale, the third and fourth models mentioned above would fail at a load of 1,672 kN (376 kip), which have more than enough factor of safety to sustain the maximum HL-93 truckload.

This experiment suggested that the transverse free edges of the slab need to be stiffened by edge beams with their major flexural rigidities in the horizontal plane and include shear connectors to ensure an effective transfer of in-plane forces from the slabs to the steel girders. Extensive work has been done as an extension of this experiment, including the dynamic performance of SFFRC deck slabs (Bakht and Mufti 1996; Mufti and Bakht 1996; Newhook 1997). These research findings have been extended to field verification by the construction of a full-scale highway bridge. These results have also been adopted by the Canadian Highway Bridge Design Code (CHBDC) into the design provisions for steel-free deck slabs on beams.

2.4 Empirical Design Method of RC Deck Slabs for Bridges

In addition to the conventional method of design, where the deck slab design is based on flexure, an empirical method has been adopted for the first time in the Ontario Bridge Design Code (OHBDC 1983). This method is based mainly on the presumption of significant compressive membrane action in the deck slab. Among the prerequisites for this method are as follows:

- The girder spacing shall not exceed 3.7 m (12.1 feet).
- The cantilever portion of the slab shall extend at least 1 m (3.3 feet) beyond the centerline of the exterior girders. The curb integral with the slab may be used instead of the 1 m overhang, provided that the combined cross-sectional area of the curb, plus the slab beyond the centerline of the exterior girder, is not less than the cross-sectional area of a 1 m length of the deck slab.
- The span length to thickness ratio of the slab shall not exceed 15. In skew slabs, the skew span shall be used in calculating this ratio.
- The slab thickness is not less than 225 mm (9 in.) and four layers of isotropic reinforcement bars ($\rho = 0.3\%$ for each layer) shall be used with spacing not to exceed 300 mm (12 in.).
- Diaphragms shall extend throughout the transverse cross section of the bridge between external girders, and the maximum spacing of such diaphragms shall be 8 m (26 feet) for steel I-beams and box girders.

Deck slabs that meet the above requirements need not be analyzed, and are presumed to have met crack control requirements and adequate shear strength. If the empirical method is not applicable, yield line methods rather than elastic analyses shall be used to determine the ultimate resistance. The serviceability limit state of cracking should also be checked.

The AASHTO LRFD Bridge Design Specifications 1994 (AASHTO 1994) permits for the first time an empirical design method for deck slabs. Excluded in the specification is the cantilevered overhang of the slab. Section 9.7.2 of AASHTO 1994 specifies the method with a long commentary. In order to use the empirical method certain conditions have to be satisfied. These conditions and the logical explanation behind them are discussed in the following:

- *The supporting components are made of steel and /or concrete.* Slabs supported by timber beams are not allowed to be designed with this method because there is not enough evidence to show adequate lateral shear transfer between the slab and the relatively soft timber beams.
- *The deck is fully cast-in-place and water cured.* Precast slabs are not allowed to be designed with this method because it does not provide a good lateral shear transfer between the deck and the beam. The development of bond strength between concrete and steel is enhanced in water cured concrete.
- *The deck is of uniform depth, except for haunches at girder flanges and other local thickening.* In the case of non-uniform thickness of the deck slab, the minimum thickness should be used as the slab thickness in the design.
- *The ratio of effective length to design depth does not exceed 18 and is not less than 6.*
- *Core depth of the slab is not less than 100 mm.* Core depth is the depth without concrete covers.

- *The effective length of slab shall be taken as the face-to-face distance (for slabs monolithic with beams), or the distance between flange tips plus the flange overhang (for slabs supported on steel or concrete girders), and does not exceed 4,100 mm.*
- *The minimum depth of the slabs is not less than 175 mm, excluding a sacrificial wearing surface where applicable.*
- *There is an overhang beyond the centerline of the outside girder of at least 5 times the depth of the slab. This condition is satisfied if the overhang is at least 3 times the depth of the slab, and a structurally continuous concrete barrier is made composite with the overhang.*
- *The specified 28-day strength of the concrete is not less than 28 MPa.*
- *The deck is made composite with the supporting structural components.* To satisfy this requirement, a minimum of two shear connectors at 600 mm centers shall be provided in the negative moment region of the continuous steel superstructures. For concrete girders, the use of stirrups extending into the deck is sufficient to satisfy the requirement.

Having satisfied all of the above conditions, the slab designed using the empirical method shall be provided with four layers of isotropic reinforcement. The minimum amount of reinforcement shall be 0.570 mm^2/mm for each bottom layer and 0.380 mm^2/mm for each top layer. The reinforcing steel shall be Grade 400 or better with spacing not to exceed 450 mm. It is also specified to use straight bars with lap splices.

Tests indicated that 0.2% reinforcement (based on effective depth) satisfies the strength requirement. The specified steel area for the bottom layers corresponds to 0.3% of the gross area for a 190 mm thick slab. The intent of the extra reinforcement is to

provide better crack control in the positive moment region. For the negative moment region, field measurements showed very low stress in the steel, consequently, 0.2% reinforcement was specified. The lower steel percentage is also intended to prevent spalling of the deck due to corrosion of the steel.

2.5 Shear Strength of Reinforced Concrete Slabs

There are a number of analysis methods available to calculate the shear strength of a concrete slab. However, most of the methods are empirical based on test results of slab structures supported on columns. Accordingly, direct application of the empirical methods to calculate the shear strength of a deck slab supported on beams is not appropriate. In the following discussions, two methods of analysis are reviewed, one being the empirical method used in the ACI Code, and the other is a rational model for calculating the punching shear capacity of a restrained concrete slab.

2.5.1 Empirical Methods

As reported by Joint ASCE-ACI Task Committee 426 (Joint ASCE-ACI 1974), the expression for ultimate shear strength of a slab can be divided into two categories. The first were the expressions dependent primarily on concrete strength, and the other were expressions dependent primarily on flexural effects such as bending moment and steel ratio. Among the expressions, none of them included the condition of the slab at the boundary. Nonetheless, it is interesting to note the conclusion of the committee regarding the factors that primarily affect the shear strength of a concrete slab. Among the factors was the restraint (provided by the external frames) where the in-plane compression due to the presence of restraint considerably enhances the capacity of the slab. However, it was stated that the degree of strength enhancement is difficult to calculate.

Another significant finding from the committee of prime interest to designers is that the shear strength of a slab can be increased substantially by nonyielding portions of a structure surrounding the loaded area. Therefore, it is necessary to consider the stiffness of the slab and the rigidity against lateral movements of its supports to determine strength changes caused by the surrounding elements of the structure.

Comparing test results and calculated values (using various empirical formulae), the committee found that the shear capacity equation from the ACI 318-71 gives a lower bound value of the shear strength, which is preferable for the purpose of design. The complete form of the expression (in U.S. common units) is given by:

$$\frac{Vu}{4(c+d)} = \phi 4\sqrt{fc'}$$

where Vu is the ultimate shear strength of the slab with effective depth to centroid of reinforcement, d, and column (load) side length of c. The term on the right hand side is the limited shear stress of the slab subjected to bending in two directions, in which fc' has unit of pound per square inch (psi). For the purpose of comparing the calculated value to the experimental test result, the strength reduction factor, ϕ is taken equal to one.

The shear strength of nonprestressed slabs and footings according to the ACI 318-95 (ACI 1995) is given in three different expressions depending on the size and the

position of column, load, or reaction area. For slabs loaded (supported) at the center, its shear capacity is limited to the following two expressions:

ACI Equation 11-36: $Vc = (2 + \frac{4}{\beta_c})\sqrt{fc'}b_0 d$ and

ACI Equation 11-37: $Vc = 4\sqrt{fc'}b_0 d$

where Vc is the shear capacity of the slab without shear reinforcement, β_c is the ratio of long side to short side of concentrated load or loaded area, and b_0 is the perimeter of the critical section. The critical section can be calculated at a distance $d/2$ from the edges of the load or reaction area. For a value of β_c less than or equal to 2.0 equation 11-37 governs.

For two-way prestressed slabs and footing, the ACI Code formula for shear strength is:

ACI Equation 11-38: $Vc = (\beta_p \sqrt{fc'} + 0.3 f_{pc}) b_0 d + V_p$

The constant β_p has a limiting value of 3.5, and the compressive stress (at the centroid of the cross section), f_{pc} is limited to a value between 125 psi and 500 psi. V_p is the vertical component of effective prestress force at the section.

It is obvious that the ACI Code formulae will not be appropriate for slabs with varying boundary conditions and steel reinforcement. However, for comparison purpose, these equations can be used to obtain an estimate of the shear capacity of restrained slabs. The compressive stress, f_{pc} in ACI equation 11-38 can be viewed as being due to the compressive membrane forces resulting from arching action in the slab.

Other groups of researchers proposed different empirical formulae to estimate the shear strength of a deck slab. Among the groups are: Jiang and Shen, and Azad et al.

Jiang and Shen (1986) proposed a plasticity-based failure model in the form of a simple formula to calculate the punching shear strength of a concrete slab as given by:

$$Vjs = 0.074 fc' \pi (d_o + h) h$$

In this formula, d_o is the diameter of the loaded area and h is the thickness of the slab. Azad et al. (1994) proposed a modification to the ACI 318-89 formula to calculate the shear strength of a concrete slab, in which the critical section was to be determined using the shear plane angle equal to 30 degree instead of 45 degree. For a rectangular load area of size a and b, the resulting equation for the perimeter of critical section is given by:

$$b_o = 2(a+b) + 6.93d$$

Azad et al. also compared the theoretical shear strength values given by the Jiang and Shen model and Azad' formulae to a limited number of test results. It was shown that using a shear plane angle of 30 degrees to determine the perimeter of critical section in the ACI formula yielded a shear strength value closer to the test results, on the safe side. The Jiang and Shen formula was reported to hold true for deck slabs with lower concrete strength.

2.5.2 Rational Model of Punching Shear

The empirical approaches have been of value in the studies of punching shear capacity of reinforced concrete slabs. The application of each approach is limited to the conditions upon which the approach was made. For a slab in general, a rational mechanical model that accounts for arching action, boundary conditions, and steel reinforcement is necessary.

The first rational model to calculate the punching shear capacity of a reinforced concrete slab was proposed by Kinnunen and Nylander (1960). The K and N model was developed based on extensive tests of circular slabs supported on a central column. The load was applied along the perimeter of the slab, which therefore represents a simply supported circular slab with a concentrated load at the column. To apply this model for the analysis of bridge deck slabs, it is necessary to introduce boundary forces along the perimeter of the slab. For that purpose, Hewitt and Batchelor (1972) modified the K and N model. The punching model of a restrained slab proposed by Hewitt and Batchelor became the model, specifically developed for RC deck slabs. However, both models are not as popular as the empirical approaches because they involve a great deal of analysis and entail somewhat vague assumptions. Petrou and Perdikaris (1996) proposed an approach, where the slab was modeled as a truss with springs along the slab boundaries. This model involved so many constants and assumptions that it proved difficult to follow. For that reason, the model is not included in this study. In the following section, the basic principles of the K and N, and Hewitt and Batchelor models are discussed, while a more detail discussion is presented in Chapter 3.

The theory proposed by Kinnunen and Nylander was based on extensive experiments conducted in the late 1950's in Stockholm, Sweden (Kinnunen and Nylander 1960, Kinnunen 1963). Referring to Figure 2.1, Kinnunen and Nylander argued that the outer portion of the slab, which is bounded by the shear crack and by radial cracks, is loaded through a compressed conical shell that develops from the column (load) to the end of the shear crack. The conical shell is assumed to have a shape and varying thickness in such a manner that the compressive stress at the intersection with the column and the root of the shear crack are approximately equal.

The criterion of failure, as argued by Kinnunen and Nylander is as follows: *The strength and effective modulus of elasticity of the slab increase due to the presence of a three-dimensional state of compressive stress in the conical shell. The tangential strain at the top surface of the slab at a distance (B/2 + y) from the center of the column was taken as a measure of the supporting strength of the conical shell. Failure takes place when the strain reaches such a high value that the strength of the conical shell is impaired. Thus, failure is described as the failure of the conical shell in compression, which takes place when the tangential strain reaches a characteristic value.*

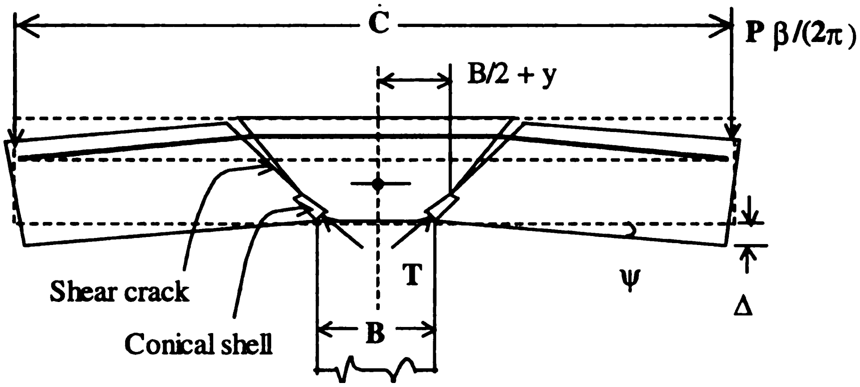

Figure 2.1 K and N Model of Punching Shear

The punching load was calculated by assuming a dimension of the conical shell and then following a convergent iterative procedure. They found that their theory gave values for the punching load which were in satisfactory agreement with results of their own tests as well as those of others. For the case of a two-way reinforced slab the calculated values were lower than the test results. Kinnunen, in his later paper, argued that the higher test values were attributed to the dowel and membrane effects, and consequently, the calculated value should be corrected by increasing the value by 20 percent.

Modification of the K and N model was proposed by Hewitt and Batchelor (Hewitt 1972, Hewitt and Batchelor 1975, Batchelor et al. 1978). The proposed model incorporated boundary restraining forces and moments (fixed boundary actions) into an idealized model developed for simply supported slabs by Kinnunen and Nylander.

The compressive membrane and fixed boundary action forces depend greatly on the slab deflection and the degree of edge restraint. When a slab fails in punching, the ultimate resisting moment of the slab does not necessarily develop. Although the boundary forces could theoretically be calculated using the stress-strain relationship for reinforcement and the concrete, the stress distribution and the resultant in-plane forces at the instant of failure by punching is extremely difficult to calculate or verify. Consequently, an empirical factor called the "restraint factor", Fr, was introduced to account for the fraction of boundary forces at the instance of punching failure. The factor, Fr, has a value between zero and one, depending on the slab's condition at the boundary. A value between 0.52 and 0.74 was appropriate for the deck slabs tested by Hewitt and Batchelor.

As reported by Petrou (Petrou 1991), Bousias modified the Hewitt and Batchelor model, by including the effect of compressive reinforcement. A rectangular compressive block was used instead of a parabolic stress distribution to calculate the boundary forces at failure. Such modifications resulted in a punching load about 17 to 20% higher than that of the Hewitt and Batchelor model. In view of this difference, it was concluded that the value of the restraint factor used by Hewitt and Batchelor has to be reduced, thus this modification resulted in a different value for the restraint factor. To limit the discussion this model will not be included in the analysis.

2.6 Finite Element Analysis of Reinforced Concrete Slab

Application of finite element analyses, FEA, for reinforced concrete structures has increased steadily because of the development of relatively powerful finite element procedures over the last four decades. However, the analysis results obtained from the FEA still vary considerably as compared to experimental results, particularly those involving ultimate capacity of the structure. One possible cause of the problem is that the reinforced concrete materials exhibit a complex structural response with various nonlinearities. Interaction between concrete and the steel reinforcement embedded in the concrete complicate the behavior of the composite concrete material. In addition, the presence of cracks in concrete affects the overall behavior of the structure that requires the model to include the post-cracking behavior of concrete. However, modeling the post-elastic behavior of concrete remains a poorly understood area.

Ngo and Scordelis (1967) published the first paper on finite element analysis of reinforced concrete beams in 1967. This first model included cracking and bond simulation capability that enabled the computation of stress in the vicinity of the crack. This led to the development of a discrete crack model. The second model tried to locate the zones of cracking and how its development affected the overall behavior of the structure. This second approach led to the development of a smeared crack model

(Schnobrich 1985). Subsequent studies have been undertaken to study the overall behavior of special types of structures, such as RC plates and shells. Emphasis was placed on the development of a smeared crack model within a layered plate and shell element. Among those who worked on this approach are Hand et al. (1973), and Lin and Scordelis (1975).

Finite element analysis of RC plate and shell structures gained its popularity because their geometry is usually complex. The rapid development of shell elements in the aerospace industry is another factor that improves the FEA of RC plate and shell structures. Many investigators used a corner supported two-way RC slab for a numerical example. This frequently referenced slab was tested by McNeice at the University of London, England in 1967 (Jofriet and McNeice 1971). Using an effective section approach to account for the crack development in the flexural response, Jofriet and McNeice reported two FE models of the McNeice slab that yielded load deflection diagrams very similar to the test results.

Using nonlinear layered analysis, Hand et al. (1973) reported the FE model of McNeice slab. Lin and Scordelis (1975) also analyzed the same slab, in which tension stiffening was included in the material model for reinforced concrete. Improved results were reported with the inclusion of tension stiffening. Another researchers (Gilbert and Warner 1978) reported the analysis of McNeice slab utilizing different methods of incorporating tension stiffening. In addition to modifying the stress strain relation for concrete, Gilbert and Warner used modified steel properties (increased E values) to assign the tension stiffening. They claimed that the second approach was as satisfactory as the first one, but it required less computer time.

The importance of including a realistic tension stiffening model was emphasized when analyzing lightly reinforced sections or structures that are endangered by stability failures (Schnobrich 1985). As a global property of reinforced concrete, the tension stiffening is a consequence of the presence of steel within the concrete. Accordingly, different models of tension stiffening have been used in the literature. One of the models most commonly used is as shown in Figure 2.2. This model is similar to the post-cracking response of concrete in tension when gradually unloaded. The factor β characterizes the length of the descending branch of the concrete stress-strain curve.

Based on limited experimental results, Vecchio and Collins reported reasonably high tension stiffening effects of up to one hundred times greater than the cracking strain. Admittedly, Collins' graph of measured tension stiffening, as reproduced by Schnobrich (1985), was obtained from a heavily reinforced section with a reinforcement percentage of 1.875% in at least one direction. The value of $\beta = 20$ is sufficiently conservative and was used by many investigators. Schnobrich suggested that the upper bound value of $\beta\varepsilon_t$ should be equal to the yield strain of the steel reinforcement.

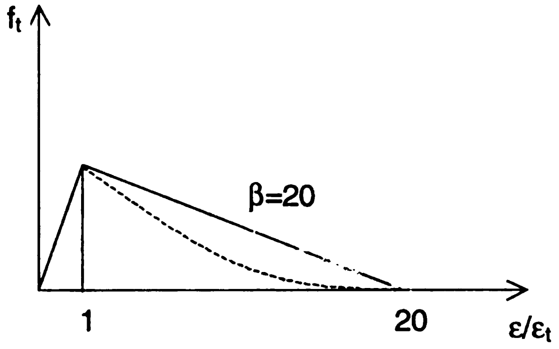

Figure 2.2 Tension Stiffening Model for Reinforced Concrete

Hsu and Zhang (1996) proposed a different approach to account for tension stiffening for an RC membrane element, in which they considered two effects simultaneously. First, the tensile stress strain in concrete; second, the stress strain curve in steel embedded in concrete. They argued that after the cracking of concrete, higher steel strains are located at the cracks, while between the cracks the strains are smaller. Therefore, the steel stress strain curve should be modified accordingly. They demonstrated the effects of using simplified, modified, and accurate constitutive laws for concrete and steel in tension, on the response of six full scale RC panels tested at the University of Houston. It was shown that using the accurate constitutive laws into the softened truss model produced an accurate prediction of load-deformation response throughout the loading history.

The importance of incorporating tension stiffening in the concrete model was also shown in the example manual of a commercially available FE program, ABAQUS (H, K & S, Inc. 1996; H, K & S, Inc. c 1999). They also used McNeice slab as an example of non-linear analysis of RC structures. Three different values of tension stiffening: 0.0005, 0.001, and 0.002 were used to obtain three different load deflection diagrams. The model with a tension stiffening value of 0.001 yielded a load deflection diagram that best matched the test result. It was also shown that with a tension stiffening value of 0.0005, the responses of the slab model became brittle and failed at a lower load level. Using a value of 0.002 very ductile response was obtained, in which the analysis continued until a much larger deflection than the maximum test value was reached.

To date shell elements are widely used for the analysis of RC slab structures. Even to model punching shear, Polak proposed the use of layered plate and shell element

(Polak 1998). Huria et al. (1993) reported a nonlinear FEA of an RC slab bridge using an isoparametric shell element. Abbasi et al. (1992) and Azad et al. (1994) also reported a finite element analysis of a reinforced concrete deck slab using plate and shell elements. Unfortunately, they only reported the ultimate load values instead of the load deflection relationships. The later is more meaningful in studying the behavior of deck slabs under lower load levels. Gonzales-Vidosa et al. (1988) used axisymmetric solid elements to model symmetrical punching of RC slabs. They claimed that the FE package they were using could be used in studying the punching problem in RC slabs with confidence. Admittedly, their package was limited for the analysis of RC elements subjected to plane-stress and axisymmetrical loading conditions.

The analysis of a complex 1:6 scale model of a reactor vessel has served as a yardstick for the FEA of general concrete structures. This structure was built and experimentally tested in 1987 at Sandia National Laboratories (Noguchi and Schnobrich 1991; Bathe et al. 1989; H, K & S, Inc. 1996). Pretest predictions of the structure (using axisymmetric solids) were provided by 10 organizations using six different FE programs including ABAQUS, ADINA, and NFAP. There was significant variation in the reported predictions. However, the experimental results also showed considerable variation. Therefore, the differences in the analytical predictions did not seem severe, especially for the prediction of the global response of the structure. The broader band of analysis values lied on the values of tension stiffening. As reported by Schnobrich, the consensus of the investigators was that a no tension concrete model gave the best correlation with the observation of the test. The explanation for this is that the cracking state has been developed prior to the full pressure test. The actual failure of this containment structure

occurred at locations not predicted by the FEA. For this reason, post-test analyses were undertaken using three-dimensional models to verify their ability to reproduce the local failure behavior. Bathe et al. (1989) claimed to have a high degree of confidence in the ADINA system and the concrete model mentioned above. However, they admitted that concrete still remains a very complex material to model numerically. They suggested improvement of the material model through the open exchange of ideas and mutual respect between software developers and structural analysts.

Different from the aforementioned researchers, Wegner and Mufti used three-dimensional solid elements (instead of shell elements) to model a fiber reinforced concrete deck slab for the bridge mentioned earlier in this chapter (Wegner and Mufti 1994). They used a commercial program, ADINA to model every component in their bridge to obtain as realistic a model as possible. The deck slab was modeled using 20-node, three-dimensional isoparametric elements, while two-node beam elements were used for the steel girders. Vertically oriented rigid links (made of beam elements with high section properties) were used to connect the beam elements to the deck elements. The links were capable of transmitting both vertical forces and shear forces between the steel girders and the concrete deck, where full composite action was assumed. Channel section diaphragms were also modeled using beam elements, and steel straps were modeled using truss elements capable of transmitting axial forces only. A total of eleven different models were developed and their respective results of nonlinear analysis were reported in the form of load-deflection curves.

The failure loads resulting from each model were reported as being widely scattered, which shows that the models were very sensitive to a number of modeling parameters, and therefore required some experimentation to tune the numerical procedures to a particular application. Among the models that gave results closest to the load tests was the one incorporating the entire system (without taking advantage of conditions of symmetry). The load was applied over a realistic area (rather than at a single node), and the girder top flanges were also modeled to represent the effect of a shortened span for the slab. A model with a reduced value of concrete modulus of elasticity was also developed. Interestingly enough, this model gave analysis results closest to the experimental result. They concluded that the three-dimensional isoparametric element used to model the deck slab produced overly stiff responses, and suggested the need for improvement of numerical techniques to be more reliable.

There are a number of works related to the FEA of RC structures reported in the literature including those published in foreign languages (Aoyama and Noguchi 1985; Noguchi and Schnobrich 1991). Despite the overwhelming number of papers on the FEA of concrete structures, very view studies have addressed a true three-dimensional problem. Currently however, several commercial general-purpose FE programs have incorporated three-dimensional model for concrete into their element library. Among the programs are: ABAQUS, ADINA, and DIANA. For the present study, ABAQUS was used to analyze the model bridge in Chapter 3.

CHAPTER 3

THEORY AND ANALYSIS

3.1 Introduction

Extensive research into the behavior of RC deck slabs discovered that the primary action by which these slabs resist a concentrated wheel load is not flexure, as was traditionally believed, but a complex three dimensional membrane stress state referred to as internal arching action. Cracking of the deck in the positive moment region and the resulting upward shift of the neutral axis in that portion of the slab make the action possible. The arching action is sustained by in-plane membrane forces which develop as a result of lateral confinement provided by the surrounding concrete slab, rigid appurtenances and supporting components acting compositely with the slab.

By now, the arching action phenomenon has been widely accepted among bridge engineers, though some state DOT are still reluctant to use the empirical design method of deck slab design that takes advantage of the arching action. Despite the overwhelming data available through extensive experimental work, there is not yet a theoretically sound analytical work available. The complexity of the problem has contributed to the slow development of the analytical method. In addition, the nonlinear behavior of concrete subjected to a complex stress state is still insufficiently known. Accordingly, the available analysis methods rely on empirical coefficients that are not necessarily suitable for general application. Punching theory of a restrained slab proposed by Hewitt and

Batchelor is one of the rational approaches that incorporates empirical factors and coefficients. Moreover, this theory was a direct modification of the K and N theory for simply supported slabs for which design parameters were developed. Nevertheless, the theory could only predict the strength and deflection of the deck at failure. However, being a method developed specifically for deck slabs, the theory is helpful for understanding the phenomenon of arching action. For this reason the theory is analytically re-derived in this chapter. The theory is also utilized to calculate the deck strength under different lateral restraint conditions.

Petrou and Perdikaris (1990) reported predictions of deck strengths using yield line theory and the ACI Code formulae. The yield line theory was reported to under estimate the punching strength of the deck slab. Kuang and Morley (1992), in their experiment on punching shear behavior of restrained reinforced concrete, also concluded that Johansen's yield line theory is not suitable for predicting the punching load capacity of a restrained slab. In this study, however, the theory is not considered in the analysis. The ACI formulae, on the other hand, were reported to give strength values closer to the experimental results than those from the yield line theory.

Kuang and Morley compared the values of slab punching strength given by the British Standard, BS 8110 and the ACI 318-89. It was reported that for a slab with lower steel ratio the ACI formula gave punching strength values closer to the test results than the British Standard did. Nevertheless, the ACI formulae were developed for design purposes, which accordingly, are on the conservative side. Moreover, the formulae do not consider the effect of restraint provided by the slab boundaries, which admittedly under estimate the strength of a restrained slab. However, the formulae are simple and useful to rapidly estimate the shear strength of the deck. For these reasons, the formulae are included for comparison.

In this study, the behavior of a deck slab under lower load magnitudes is more important than its load capacity because in practical cases, the deck is subjected to a wheel load that is much lower (about 10%) than its ultimate capacity. An analytical method capable of predicting the response of the deck under any magnitude of applied loads would be more useful for understanding the deck behavior. More importantly, the method should also be able to explicitly incorporate the tie rods into the analysis in order to study their effect on the deck behavior.

Considering the successful application of numerical analyses for RC plate and shell structures, finite element analysis (FEA) is utilized in this study to analyze the deck slab as an integral part of a model bridge. Even though there are not many reports on the successful applications of FEA on three-dimensional RC deck slabs, it is widely used and readily available. The theory itself will not be discussed here because it has been widely accepted as a standard method for stress analysis. However, the material modeling for reinforced concrete is briefly summarized since the development of the constitutive model of the material is not yet as advanced as that of other structural materials.

3.2 Rational Model of Punching Shear Strength of Restrained Slabs

Theory of punching shear failure for simply supported RC slabs was proposed by Kinnunen and Nylander based on extensive experimental work conducted in the late 1950's in Stockholm, Sweden (Kinnunen and Nylander 1960, Kinnunen 1963). The theory was based on the observed behavior and failure mechanism of a circular slab supported by a central column. For a composite RC slab and steel girder system, the conditions at the boundaries of the slab are partially restrained. In order to use the model proposed by Kinnunen and Nylander (K and N model), some modifications of the model were required. For this purpose, Hewitt and Batchelor proposed a punching shear model for restrained slabs, where the boundary restraining force, F_b and the boundary restraining moment, M_b are incorporated into the K and N model (Hewitt and Batchelor, 1975, Batchelor et al 1978). M_b and F_b are forces per unit length of slab, acting in the plane of slab along its boundary.

Similar to the Hewitt and Batchelor reports, Mufti and Newhook (1998) showed that under a concentrated load, the failure mechanism of a deck slab supported on steel girders is as shown in Figure 3.1. Under an initiating load level, radial cracks formed on the bottom surface of the concrete slab, originating below the load. As the load increases, the radial cracks gradually propagated to the top surface of the slab to become full depth cracks. Circular cracks formed on the top surface of the slab at a diameter approximately equal to the girder spacing (this circular crack pattern is the basis of the assumed equivalent circular slab). At a load somewhat less than the failure load, an inclined shear crack developed, originating on the bottom surface of the slab at some distance away from the load, in a circular manner. At punching failure, the shear crack formed the upper surface of the punch cone. This failure mechanism was similar to that of the circular slabs tested by Kinnunen and Nylander. Accordingly, the deck slab could be analyzed as an equivalent circular slab.

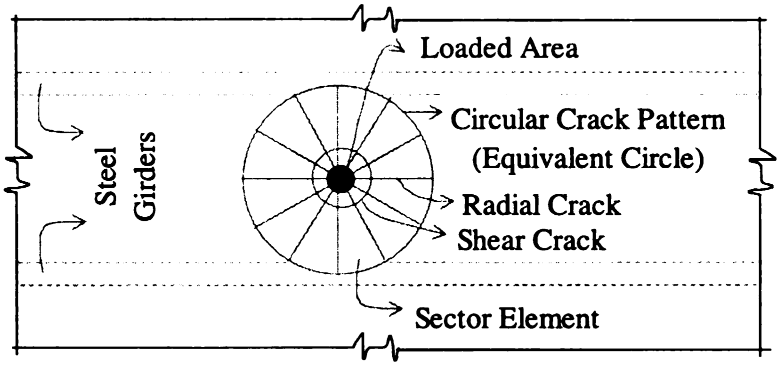

Figure 3.1. Crack Pattern of Restrained Deck Slab (Plan View)

Kinnunen and Nylander argued that the portion of the slab, which is bounded by the shear crack and radial cracks, is loaded through a compressed conical shell that develops from the circular column (concentrated load) to the end of the shear cracks. The imaginary conical shell is assumed to have the shape as shown in Figure 3.2, and its thickness varies in such a manner that the compressive stresses at the intersection with the column and the root of the shear crack are approximately equal. At the tip of the conical shell, at the top surface of the slab, the concrete is in a state of three-dimensional compressive stress where confinement provided by these stresses significantly increases the strength of the concrete in that area.

The section of the slab outside the shear cracks can be divided into wedges or sector elements of angle β bounded by shear cracks, radial cracks, and the outside edges of an equivalent circular slab as shown in Figures 3.1, 3.2, and 3.3. These sector elements are assumed to act as rigid bodies, and under failure loading, they rotate about a center of rotation, CR, with angle ψ. Figure 3.3 also shows forces in a sector element used as the basis for the derivation of equations to determine the punching strength of a restrained slab (Kinnunen and Nylander 1960, Kinnunen 1963, Hewitt and Batchelor 1975). The details of the derivation are given in Appendix A. In the following sections, the punching shear model of a circular slab is summarized.

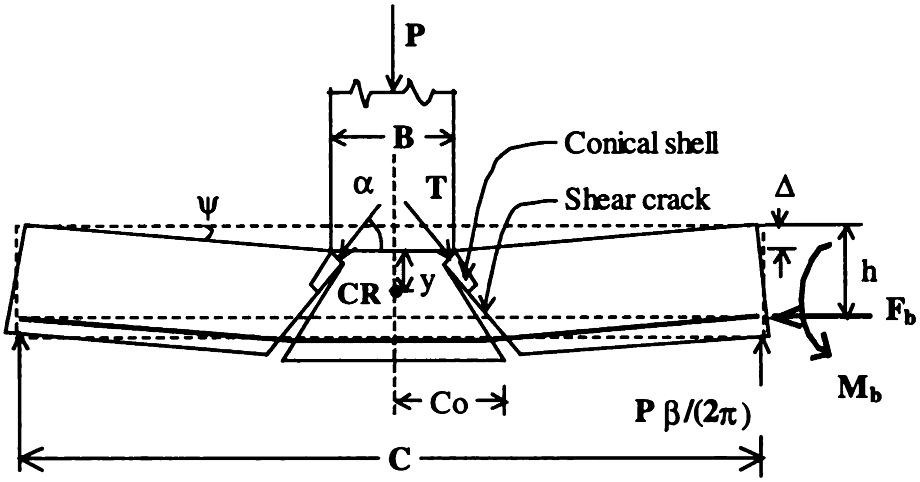
P
B
α
T
ψ
Conical shell
Shear crack
Δ
h
CR
y
F_b
M_b
Co
P β/(2π)
C

Figure 3.2. Mechanical Punching Model of Restrained Slab

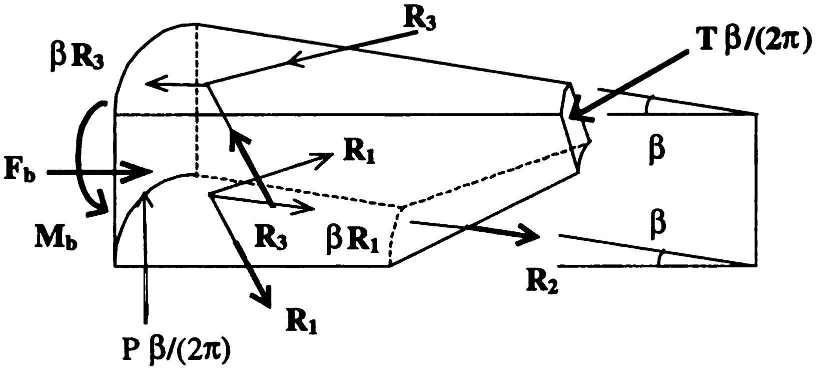
R_3
βR_3
T β/(2π)
F_b
R_1
β
M_b
R_3
βR_1
β
R_2
R_1
P β/(2π)

Figure 3.3 Sector Element (Wedge) Showing Forces and Notations

3.2.1 Mechanical Model for Simply Supported Slabs

Referring to Figure 3.2 and Figure A.2 in Appendix A, the load P, which is transmitted through the conical shell is given by the following expressions:

$$f_{(\alpha)} = \sin\alpha\cos\alpha(1-\tan\alpha) = \frac{\tan\alpha(1-\tan\alpha)}{1+\tan^2\alpha} \qquad \text{Equation (1)}$$

$$P = \pi\frac{B}{h}\frac{y}{h}\frac{(B+2y)}{(B+y)}f_t f_{(\alpha)}h^2 \qquad \text{Equation (2)}$$

The complete list of notation is given in Appendix A. The above equations are valid for both simply supported and restrained slabs.

If ψ is the angle of the rotation around the C.R., then using the expression for strain ε_s of reinforcing steel at a distance, $r = r_s$ (the boundary between the yield and elastic stress.ranges) from the center of the slab, the following expression is obtained:

$$\frac{r_s}{h} = \frac{\psi}{\varepsilon_s}(1-\frac{y}{h}) = \frac{E_s}{f_s}\psi(1-\frac{y}{h}) \qquad \text{Equation (3)}$$

Referring to Fig. A.3 in Appendix A, the resultant force in the ring reinforcement, R_1 is calculated using $dA_s = \rho\, h\, dr$ as follows:

For $r_s \geq C_0$: $R_1 = \rho f_{sy}h^2\left[(\frac{r_s}{h}-\frac{C_0}{h})+\frac{r_s}{h}\ln\frac{C/2}{r_s}\right]$ Equation (4.a)

For $r_s < C_0$: $R_1 = \rho f_{sy}h^2\left[\frac{r_s}{h}\ln\frac{C/2}{r_s}\right]$ Equation (4.b)

At failure, the steel reinforcement inside the shear crack yields, therefore the steel stress is equal to f_{sy}. Accordingly, the resultant force of the radial steel reinforcement, R_2 can be expressed as:

For $r_s \geq C_0$: $R_2 = \varepsilon_s E_s \rho h \beta C_0 = f_{sy} h \rho C_0 \beta = \rho f_{sy} h^2 \frac{C_0}{h} \beta$ Equation (5.a)

For $r_s < C_0$: $R_2 = \rho f_{sy} h^2 \frac{r_s}{h} \beta$ Equation (5.b)

The compressive strain in concrete has the relation: $\varepsilon_{ct} = \psi \frac{y}{r}$, and the corresponding resultant compressive force in concrete, R_3 can be written as:

$R_3 = \frac{h^2}{2} (\frac{y}{h})^2 f_{ct} (\frac{B}{2y} + 1) \ln \frac{C/2}{B/2 + y}$ with a radial component of $R_3\beta$.

Failure occurs when ε_{ct} at the top of the slab (under the load) reaches a limiting value. Based on measurement during their experiment, Kinnunen and Nylander proposed the following expressions for the Young's modulus and failure ratio of concrete:

$E_c = 10^5 (0.35 + 0.3 \frac{f_{cube}}{150})$ Equation (6)

$\frac{f_t}{f_{ct_{r=(B/2+y)}}} = 2.35$ Equation (7)

The term f_{cube} denotes the compressive strength of a 150-mm concrete cube in kilogram force per square centimeters. The failure ratio is expressed in terms of the ratio of the stress of concrete in the imaginary conical shell and the tangential concrete stress at radius r = (B/2 + y) from the center of the circular slab.

Hewitt and Batchelor converted the compressive strength of 6 by 12 in. cylinder (f_{cyl}) in psi units into f_{cube} using the following relation:

$$f_{cube} = \frac{f_{cyl}}{0.75 + 0.000025 f_{cyl}} \qquad \text{Equation (8)}$$

For slabs with two-way reinforcement, Kinnunen (1963) proposed the following equations:

$$\text{For } \frac{B}{h} \leq 2; \psi = 0.0035(1 - 0.22\frac{B}{h})(1 + \frac{B}{2y}) \qquad \text{Equation (9.a)}$$

$$\text{For } \frac{B}{h} > 2; \psi = 0.00195(1 + \frac{B}{2y}) \qquad \text{Equation (9.b)}$$

$$\text{and } \frac{C_o}{h} = \frac{B}{2h} + 1.8 \qquad \text{Equation (10)}$$

The expression for the stress in the conical shell, f_t becomes as follows:

$$\text{For } 0 < \frac{B}{h} \leq 2: \ f_t = 825(0.35 + 0.3\frac{f_{cube}}{150})(1 - 0.22\frac{B}{h}) \qquad \text{Equation (11.a)}$$

$$\text{For } \frac{B}{h} > 2: \ f_t = 0.00195 E_c = 460(0.35 + 0.3\frac{f_{cube}}{150}) \qquad \text{Equation (11.b)}$$

Referring to Fig. A.3 in Appendix A, the equilibrium condition is satisfied by taking moments with respect to the point of intersection of R_1 and $P\beta/(2\pi)$. It yields:

$$(K_y \tan\alpha - 1)(\frac{1 - \tan\alpha}{1 + \tan^2\alpha}) = \frac{1}{4.7}(1 + \frac{y}{B})\ln\left[\frac{C/2}{B/2 + y}\right]$$

$$\text{where } K_y = \frac{C/2 - B/2}{(h - y/3)}$$

Rearrangement of terms results in the second equation for punching load of a simply supported slab:

$$P = \frac{2\pi}{K_y}(R_1 + \frac{R_2}{\beta}) \qquad \text{Equation (12)}$$

Using equation (1) through (12) the punching load of a simply supported slab can be determined by solving the punching load P in equations (2) and (15) through an iterative procedure. For the case of a restrained slab, the equations for a simply supported slab are coupled with additional equations as a result of the additional boundary forces as given in the following section.

3.2.2 Mechanical Model of Restrained Slabs

The model for a restrained slab proposed by Hewitt and Batchelor is basically the one proposed by Kinnunen and Nylander, with moment and force at the level of the compression reinforcement at the boundary included. Referring to Figure A.4, taking moments with respect to the point of intersection of the resultant of the forces R_1 and $P\beta/(2\pi)$ gives:

$$\frac{2\pi R_3}{P} = K_y - \cot\alpha - \frac{M_b}{P}\frac{\pi C}{(h - y/3)},$$

where the notations are given in Appendix A.

Assuming a circular fan failure mode, the resisting moments M_b, is given by $4\pi M_b$. Therefore, replacing M_b/P with $X/(4\pi)$, in which X is a factor of the order unity, yields:

$$X = 4\pi\frac{M_b}{P} \qquad \text{Equation (13)}$$

Using $f_t/f_{ct} = 2.35$ and substituting the expressions for P and R_3 for simply supported slabs the following equations are obtained:

$$K_z = K_y - \frac{XC}{4(h - y/3)} \qquad \text{Equation (14)}$$

$$\frac{(1 + y/B)}{4.7}\ln\left[\frac{C/2}{B/2 + y}\right] = (K_z \tan\alpha - 1)\frac{(1 - \tan\alpha)}{(1 + \tan^2\alpha)} \qquad \text{Equation (15)}$$

Verification of these equations is obvious: if $M_b = 0$, then $X = 0$, and therefore, $K_z = K_y$ which is identical to that of simply supported slabs.

Referring to Fig. A.5 in Appendix A, the equilibrium equation is obtained by taking moments about the point of intersection of $T\beta/(2\pi)$ in the conical shell and the resultant of the forces, R_3. Then the second expression for punching load of a restrained slab is given by the following relation:

$$P = \frac{2\pi}{K_z}(R_1 + \frac{R_2}{\beta} + F_b\frac{C}{2}) \qquad \text{Equation (16)}$$

Again, if F_b and $M_b = 0$, then $X = 0$ and therefore, $K_z = K_y$. In that case Equation (16) is identical to Equation (12) for a simply supported slab. This means that the expressions for punching load of a restrained slab are those for a simply supported slab, provided that the boundary forces are zero.

In order to solve for the punching strength of a restrained slab, it is necessary to develop an expression for the boundary forces using static equilibrium at the slab boundary. Shown in Figure A.5 are resultant maximum boundary stresses and forces in

the slab. The maximum tensile force, F_t, per unit length of the boundary, at the level of tensile reinforcement, is given by:

$$F_t = h\rho f_{sy} \qquad \text{Equation (17)}$$

Likewise, the maximum compressive force per unit length of the slab boundary is given by:

$$F_c = kf_{\max}(\frac{t}{2} - \frac{\Delta}{4}) \qquad \text{Equation (18)}$$

At failure, the stresses in concrete and steel reinforcement at the slab boundary, do not necessarily reach maximum values. Accordingly, a restraint factor, F_r was introduced to account for the lower stresses in the slab boundary. The factor F_r is purely empirical, to make up the difference between the calculated and measured punching load. However, it is reasonable that the actual boundary restraints at failure are less than the maximum possible values. Accordingly, the following expressions are adopted:

$$M_b = F_r M_{b(\max)} = F_r \left[F_t(2h - t) - F_c(h - \frac{13}{16}t - \frac{3}{32}\Delta) \right] \qquad \text{Equation (19)}$$

$$F_b = F_r F_{b(\max)} = F_r \left[F_c - F_t \right] \qquad \text{Equation (20)}$$

Finally, assuming a small angle of rotation, ψ, the slab deflection at failure, Δ can be approximately expressed as:

$$\Delta = \psi \frac{(C - B)}{2} \qquad \text{Equation (21)}$$

This concludes the development of the equations necessary to solve for the punching load, P, of a circular restrained slab with a circular concentrated load through an iterative procedure. For the case of a non-circular slab with a non-circular loaded area, it is necessary to assume equivalent circles for the slab and load by equating their perimeters (Kinnunen and Nylander 1960).

Nylander reported that, the punching load calculated using the above mentioned theory for simply supported slabs is about 20% less than the observed values (Nylander 1963). The reason for this difference is that the formulae were derived based on the conditions at shear crack formation stage. The ultimate loads are substantially higher than the loads at the first crack stage, because when a shear crack crosses the steel reinforcement, the crack propagation is arrested due to the bond between the steel and the concrete. This phenomenon is known as dowel action. In addition to the dowel action, the compressive membrane forces developed under the applied load also cause the crack to stop. Both phenomena are logically sound and experimentally provable. However, it is not easy to establish analytical expressions that explain the phenomena because the dowel and membrane forces developed at failure are difficult to measure or calculate. An empirical factor of 1.2 was reported to give a corrected punching load very close to the measured value. The factor was adopted for restrained slabs by Batchelor and Hewitt. Accordingly, the corrected theoretical punching load, V is given by: $V = 1.2P$.

3.3 Analyses of Punching Strength of RC Slabs with Additional Lateral Restraint

Analyses of RC deck slabs with additional lateral restraint were conducted utilizing an empirical approach based on the punching shear model of a restrained slab developed by Kinnunen and Nylander, and Hewitt and Batchelor. For practical cases of deck slabs, the value of the restraint factor, F_r reported by Hewitt and Batchelor, ranges from 0.52 to 0.74 (Hewitt and Batchelor 1975). In this study, the lateral restraint for a slab with additional tie rods should be higher than that without tie rods. Consequently, the restraint factor, F_r for a slab with tie rods should be larger than that without tie rods, which also results in a higher punching load for slab with tie rods. Unfortunately, the exact values of these factors could not be determined until test results are obtained. Accordingly, the punching loads are determined using restraint factors between 0.5 and 0.9, where the slab in this study is expected to have a restraint factor value within this range.

For this analysis, a 1/5 scale model bridge is assumed, and the properties of the slab and its supporting structures are as designed in Chapter 4, and used in the experimental work in Chapter 5. The model bridge consists of three steel girders and a concrete deck of 40.6 mm (1.6 in.) thick, with girder spacing of 508 mm (20 in.). The load was applied through a 102 mm by 51 mm (4 in. by 2 in.) pad, which corresponds to a perimeter of 305 mm (12 in.). The geometry and dimensions of the equivalent circular slab used for the analysis are shown in Figure 3.4.

The steps required to determine the punching load capacity of a restrained slab with known value of the restraint factor are listed as follows:

1. Increment a value for deflection, Δ;
2. Calculate F_t and F_c from Equations (17) and (18), respectively;
3. Calculate M_b and F_b from Equations (19) and (20), respectively;
4. Increment a value for X;

5. Increment a value for y/h;
6. Calculate f_t from Equation (11.a) or (11.b), and tan α for $f\alpha$ from Equation (15) and (1);
7. Calculate P from Equation (2);
8. Calculate ψ , r_s and Co from Equations (9.a) or (9.b), (3) and (10);
9. Calculate R_1 from Equations (4.a) or (4.b), and R_2/β from Equation (5.a) or (5.b);
10. Calculate Δ and P from Equations (21) and (16);
11. Compare the values of P obtained from step 7 and step 10. If the difference is significant go to step 5;
12. Calculate X from Equation (13);
13. Compare the value of X in step 4 with that calculated in step 12. If the difference is significant go to step 4;
14. Calculate F_c from Equation (18) using the new value of Δ;
15. Compare the values of F_c calculated in step 2 and 14. If the difference is significant go to step 1;
16. Determine the corrected punching load, V = 1.2 P.

A computer program that implements the above steps was developed. The flowchart and the complete listing of the code are given in Appendix B, Flow Diagram and Code Listing to Calculate Punching Shear Strength of Restrained Slabs. Upon completion of the experimental tests, the restraint factors for the model slabs could be determined by equating the calculated and the experimentally observed values.

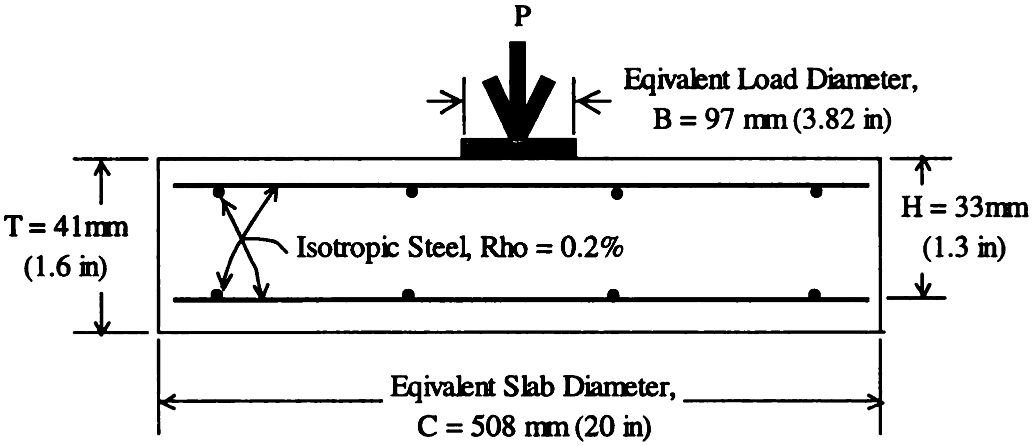
P
Eqivalent Load Diameter,
B = 97 mm (3.82 in)
T = 41mm
(1.6 in)
Isotropic Steel, Rho = 0.2%
H = 33mm
(1.3 in)
Eqivalent Slab Diameter,
C = 508 mm (20 in)

Figure 3.4 Geometry of Equivalent Circular Slab

The complete dimensions and properties of the slab, used as the input of the program, are as follows (notations are adopted from the code listing):

- Slab thickness, T = 40.6 mm (1.6 in.), slab effective depth, H = 33 mm (1.3 in.).
- Concrete compressive strength, FCCYL = 27.58 MPa (4.0 ksi).
- Steel reinforcement ratio, RHO = 0.2%.
- Restraint factor, FR is varied from 0.5 to 0.9.
- Equivalent diameter of slab (equal to beam spacing), C = 508 mm (20 in.).
- Equivalent diameter of load, B = 97 mm (3.82 in.).
- Yield stress of steel reinforcement, FSY = 500 MPa (72.5 ksi).
- Steel Young's modulus, ES = 200 GPa (29,000 ksi).

The program was run using the above input values and different values of the restraint factor. The punching load of the deck, for each value of the restraint factor is shown in Table 3.1. The net deflection of the slabs is also listed in the table along with the corrected punching load due to the dowel and compressive membrane forces effects.

Table 3.1 Punching Load of Slab (Restrained Slab Theory)

Restraint Factor, FR	Punching Load		Deflection (mm)	Corrected Punching Load	
	P (N)	P (lbs)		V (N)	V (lbs)
0.50	35,719	8,030	1.76	42,863	9,636
0.55	38,290	8,608	1.67	45,948	10,330
0.60	40,843	9,182	1.59	49,012	11,018
0.65	43,370	9,750	1.52	52,044	11;700
0.70	45,861	10,310	1.46	55,033	12,372
0.75	48,316	10,862	1.40	57,980	13,034
0.80	50,727	11,404	1.35	60,873	13,685
0.85	53,094	11,936	1.31	63,712	14,323
0.90	55,416	12,458	1.26	66,499	14,950

From the table, it is apparent that the punching strength of the model slab is directly proportional to the value of restraint factor, the higher the restraint factor the higher the punching load of the deck. The magnitude of the values, however, is not meaningful unless it is compared to a reference value such as wheel load used to design the bridge deck slab. In a full-scale bridge the load capacity of a 1/5-scale slab is 25 times the load capacity of the model slab. Accordingly, the theoretical load capacity of the prototype slab ranges from 1,071.57 to 1,662.52 kN (240.90 and 373.73 kip). Using an impact factor of 1.3 the concentrated load due to a truck load of 145 kN (32.597 kips) is 94.25 kN (21.188 kip). The corresponding factors of safety provided by these slabs range from 11.4 to 17.6. This is in good agreement with the values reported in the literature (Hewitt 1972, Beal 1982, Fang et al. 1986, Petrou and Perdikaris 1990). The numbers in Table 3.1 will be compared to the experimental test results to determine the actual value of restraint factors of the slabs with and without additional lateral restraint.

3.4 ACI Provision on Punching Shear Strength of Concrete Slab

The model deck slab previously analyzed using the restrained slab theory will now be analyzed using the ACI Code provision on punching shear strength of concrete slabs (Section 11.12.2 of the ACI 318-95 Code). Using a loaded area with ratio of long side to short side dimensions, β_c equal to 2, the expression for the nominal punching shear strength of a reinforced concrete slab without shear reinforcement is given in US customary units as:

$$V_c = 4\sqrt{f_c'}b_0 d \qquad \text{(ACI: 11-37)}$$

In SI units the above equation becomes (Hassoun, 1998):

$$V_c = \frac{1}{3}\sqrt{f_c'}b_0 d \qquad \text{(ACI-SI: 11-37)}$$

V_c is the nominal shear strength in pounds (lbs) and newton (N) for the U.S. customary and SI units, respectively. The concrete compressive strength, f_c', is 27.58 MPa (4,000 psi). The empirical nature of the formula requires that f_c' be provided in the units shown; the square root of f_c' has the same unit as f_c'. The perimeter of the critical section, b_0, is 437 mm (17.2 in), and the effective depth of the slab, d, is 33 mm (1.3 in).

Due to the arching action, the top portion of the slab around the loaded area is under compression, similar to that of a prestressed concrete slab. Consequently, the ACI formula for a prestressed concrete slab could be applied to restrained RC deck slabs. Since the magnitude of the stress is not known an assumed value can be used. For this purpose, the ACI Code formula for shear strength of a two-way prestressed concrete slab is also included in this analysis. Omitting the vertical component of effective prestress force, V_p, the expression of shear strength in U.S. customary units is given as:

$$Vc = (\beta_p \sqrt{fc'} + 0.3 f_{pc}) b_0 d \qquad \text{(ACI: 11-38)}$$

The Code limits the values of β_p and the compressive stress f_{pc} to 3.5 and 500 psi, respectively. In this case, a maximum value is assumed. Using these ACI formulae the ultimate shear strength of the model slab is calculated and the result is shown in Table 3.2.

It is apparent that the ACI Code formulae do not take into consideration the span length, the boundary conditions, or the flexural reinforcement of the slab. They also neglect the dowel action due to the presence of steel reinforcement. However, using the formula for a prestressed concrete slab (assuming the compressive membrane stress as the stress due to the prestressing), the shear strength of the slab increases considerably. In

the actual case, the magnitude of the membrane stress at failure could be higher than 500 psi, for which accordingly, the strength of the slab would be higher.

Table 3.2 Shear Strength of Model Slab (ACI Formulae)

ACI Formulae / Equations	Maximum Shear Strength	
	N	Lbs
ACI: 11-37	25,162	5,657
ACI: 11-38	36,936	8,304

3.5 Finite Element Analysis

The finite element modeling (FEM) of the model bridge was conducted to calculate the deck response under a full range of loads, from zero to failure load. Ideally, the FE model should also be able to verify the experimental test results. In this study, the FE model was designed to take into consideration the effect of each component in the bridge to mimic the load deflection curve observed during the experiment up to failure. For this purpose, it is necessary to model every component in the bridge, taking into consideration the non-linearity of the concrete material. In addition, previous test results showed that the deck slabs underwent large deformation. Therefore, geometric non-linearity should be included in the model.

ABAQUS was among the commercial finite element software available at the Division of Engineering and Computing Services (DECS) at MSU that has nonlinear capability. It also has a special feature to model the inelastic behavior of a concrete material. For this reason ABAQUS/Standard Version 5.8 was used in the present study.

To study the effect of adding tie rods, two distinct types of models were developed. One type for the slab panel with tie rods, and the other for the control slab panel without tie rods. For each type, several computer runs were necessary in order to study the sensitivity of the material model. From observations made during the experiment it was apparent that only the concrete slab underwent inelastic deformation, while the steel beams remained elastic up to the failure of the deck. Accordingly, special care was given in modeling the concrete material. Mesh sensitivity was beyond the scope of this study; however, three different element types and arrangements were incorporated in the FE models. Agreement between the FEA and the experimental test results was expected in this study.

3.5.1 Geometric Model

The unsymmetrical loading positions on the bridge required the FE model to incorporate the entire bridge. The model included the deck slab, steel girders, edge beams, diaphragms, and tie rods. The deck slab was modeled with a three-dimensional solid element, which in ABAQUS is referred to C3D type. The steel girders were divided into flanges and web, in which a 9-node shell element of type S9R5 was used for both the flanges and the web. The edge beams and the diaphragms were modeled using a beam element of type B31. Truss element of type T3D2 was used to model the tie rods.

During the development of the models, a shell element was used for the deck slab. However, the stress in the tie rods underneath the load was held to zero, because the shell element was meant to undergo flexure without in-plane displacement. Therefore, shell elements could not be utilized in this study because they could not model the arching action in the deck slab. Accordingly, a solid element was the only choice for the RC slab model.

There are a number of solid element types available in ABAQUS. Among the element types are: an 8-node linear, a 20-node quadratic, and a 27-node high order element. In this study, the 8-node element C3D8 was used as the reference element for the deck slab. Either one or two elements were used along the thickness of the slab. A model with four solid elements along the depth of the deck was also investigated. However, using four elements resulted in so large a model that it could not be solved within a reasonable period of time. For that reason, the model with four elements was not included in this study. For the purpose of comparison, a 27-node solid element with reduced integration (type C3D27R) was also used to model the RC slab. Some of its nodes were omitted to reduce the size of the model. The steel reinforcement was modeled as layers of rebar embedded in the concrete elements. The interactions between concrete and rebar, such as bond slip and dowel action, were approximately modeled in the material model for concrete.

The flanges and the webs of the steel beams were modeled using type S9R5 element, which is a 9-node shell element with reduced integration. This type of element was meant for a thin shell, which is appropriate to model the effect of bending of the top flanges on which the concrete slab was supported. The width of the flange and the depth of the web dictated the mesh sizes. A mesh of 50 x 100 mm. (2 x 4 in.) was used for the flanges and 100 x 150 mm. (4 x 6 in.) mesh were used for the web. The thickness of the flange and web elements was 4.34 mm and 2.90 mm, respectively. No evidence of bond failure between the flanges of the steel girders and the concrete was found during the demolition of the test specimen. Accordingly, no attempt was made to model slip between the top flanges of the steel beam and the concrete slab. In other words, a full composite action was assumed in the FE model.

The tie rods were modeled with type T3D2, a 2-node truss element. The cross sectional area of the rod was 161 mm^2 (0.25 in^2), which is the area of the square bar on which the strain gage was mounted. The truss element was chosen because the tie rod should only be subjected to axial tension due to the arching action in the slab. The diaphragms and the edge beams were modeled with a type B31 element, a linear three-dimensional beam element. The moment of inertia for the beam element were 395,420 mm^4 (0.95 in^4) with respect to the weak axis and 1,147,966 mm^4 (2.758 in^4) with respect to the strong axis. Based on these properties, the equivalent dimensions of the beam element could be determined. The composite action between the edge beams and the concrete slab was not included in the FE model since its effect is negligible if the load is applied at a distance away from the edge of the slab. The geometric model is shown in Figures 3.5.a, 3.5.b, and 3.5.c.

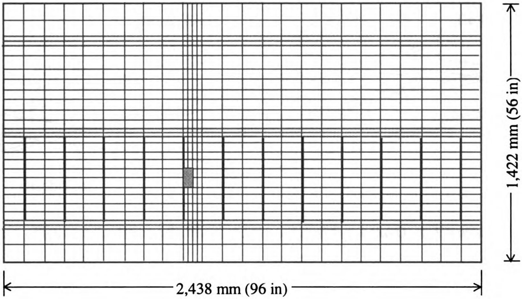
2,438 mm (96 in)
1,422 mm (56 in)

Figure 3.5.a Plan View of FE Model Showing Mesh of the Deck (Using 8-node Solid Elements), Tie Rods, and Loaded Area.

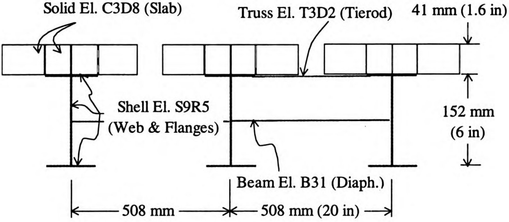
Solid El. C3D8 (Slab)
Truss El. T3D2 (Tierod)
41 mm (1.6 in)
Shell El. S9R5
(Web & Flanges)
152 mm
(6 in)
Beam El. B31 (Diaph.)
508 mm
508 mm (20 in)

Figure 3.5.b Cross Section of FE model Showing Elements Connectivity.

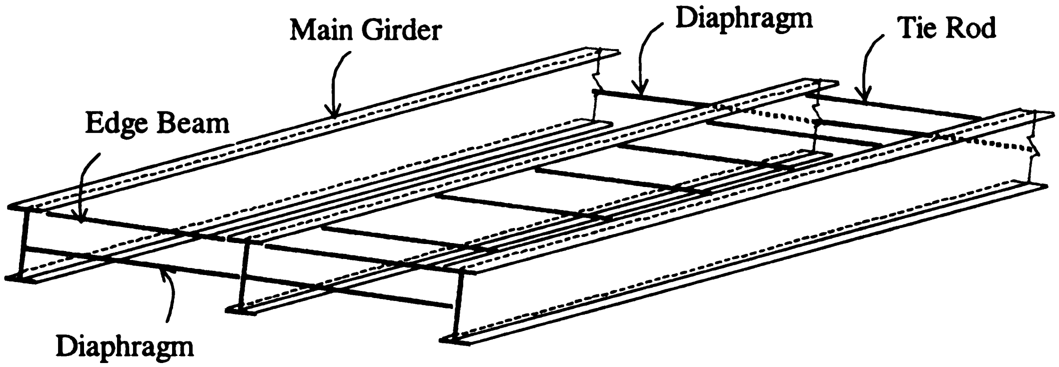

Figure 3.5.c Isometric View of FE model without the Deck Elements

3.5.2 Material Models

The reinforced concrete modeling in ABAQUS was accomplished by combining plain concrete elements and rebar elements. These elements were superimposed on the mesh of plain concrete elements, and were used with standard metal plasticity models that describe the behavior of the rebar material. A one-dimensional strain theory was used for the rebar element. With this modeling approach, the concrete behavior was considered independently of the rebar. The effect associated with the rebar/concrete interface, such as bond slip and dowel action, was modeled approximately by introducing tension stiffening into the concrete model. The purpose of the tension stiffening is to simulate the load transfer across cracks through the rebar. More detail on the reinforced concrete model is explained in the following sections.

3.5.2.1 Concrete Model

The concrete material was modeled by specifying its Young's modulus, Poisson's ratio, compressive behavior, tension behavior, uniaxial and multiaxial behavior, post-failure stress strain relation, and cracked shear retention. The Young's modulus of concrete was used for the elastic part of the stress strain relation, while the compressive behavior was necessary to model the non-linear behavior of the material. The uniaxial tension, uniaxial compression, and multiaxial compression behavior of the concrete were used to determine the failure ratios in tension and compression. The postfailure stress strain relation was required to introduce the tension stiffening behavior of the concrete element. Finally, cracked shear retention was used to model the diminishing shear stiffness of the cracked concrete.

In the present study, cylinder tests were conducted to obtain the compressive and tensile strength of the concrete. The detail of the tests is presented in Chapter 5. The remaining concrete parameters required to model the concrete material were determined utilizing well known relationships. The value of Poisson's ratio of concrete is between 0.15 and 0.2 with a higher value for lower strength concrete (Mehta and Monteiro 1996). In this study a value of 0.2 was used for all models. Different values of Poisson's ratio were tried in some models but there were no significant differences in the results. For the compressive stress strain relation, a hypothetical model was developed based on test data conducted by Kupfer and Gerstle (Kupfer et al 1973). The model is incorporated in the material model input for the concrete element.

For the basic FE model, the value of Young's modulus used was 25,000 MPa. (3,600 ksi), which is about one eight of the value for steel. Yielding of concrete was assumed to start at a stress of about 12.5% of its maximum stress, and the total strain corresponding to the maximum stress of 27.58 MPa (4,000 psi) is assumed to be about 0.003. For some models, the above values were arbitrarily assumed to study the sensitivity of the model with respect to each modeling parameter. A total strain of 0.005 was used for some models to include a hardening behavior. This behavior was made possible by the presence of compressive membrane action in the deck slab.

The tension behavior of the concrete material model included tension stiffening in order to model the strain softening behavior of the cracked concrete. The stress strain relation was assumed to be linear up to failure. After failure, the strain softening reduces the stress linearly to zero. The strain at which the stress is equal to zero for a heavily reinforced member was reported to be as high as one hundred times its failure strain (Schnobrich 1985). Assuming linear stress strain behavior under tension, the failure strain of the model concrete is about 0.0001. Accordingly, the maximum strain for the tension stiffening models could be as high as 0.01.

Knowing that the yield strain of a 500 MPa (72.5 ksi) steel is about 0.0025, then a reasonable value for the tension strain of concrete is equal to the yield strain of steel. At failure however, the steel strain could be much higher than 0.01. Accordingly, a tension stiffening value higher than 0.0025 is possible. Tension stiffening values between 0.0005 and 0.002 were used in ABAQUS for the analyses of a one way slab tested by Jain and Kennedy, and a two way slab tested by McNiece (H, K & S, Inc. c 1998; Jain and Kennedy 1974). The model using tension stiffening of 0.001 yields a load deflection curve that fits the experimental result best. Admittedly, this parameter should be calibrated to a particular case. It was also shown that, the higher the tension stiffening the more ductile the model. In this study, a value of 0.0025 was used as a standard value for tension stiffening. In some models, a tension stiffening value as high as 0.0075 was used to obtain longer solutions.

In addition to the above mentioned properties, ABAQUS requires additional input values to determine the failure surface of a concrete element which are termed failure ratios. The failure ratios include the ratio of the ultimate biaxial compressive stress to the ultimate uniaxial compressive stress, and the absolute value of the ratio of uniaxial tensile stress at failure to the ultimate uniaxial compressive stress. Kupfler et al. (1969) showed that the maximum biaxial strength is about 25% higher than the uniaxial compressive strength and occurs at $\sigma_1 = f_p$, where f_p is the prism compressive strength of concrete. Under $\sigma_1 = \sigma_2$, the biaxial compressive strength of concrete is about 16% greater than the uniaxial strength. The ratio of uniaxial tensile stress to uniaxial compressive stress was between 7% and 11% with higher values for lower strength concrete (Mehta and Monteiro, 1996). Based on the above data, values of 1.25 and 0.1 were used as reference values. In some models, values of 1.3 and 0.11 were used for the failure ratio in compression and tension, respectively.

The cracked shear retention feature in ABAQUS was meant to account for the reduction in shear modulus as the concrete cracks. The shear retention option assumes that the shear stiffness of open cracks reduces linearly to zero as the crack opening increases. If the option is omitted in the material data block, ABAQUS will assume full shear retention, where the shear response is not affected by the cracked element. In this study, the option was omitted, which means that there is no shear stiffness loss in the planes of crack, once they have formed. The reason for this assumption is due to the fact

that the deck slab undergoes a three-dimensional state of stress, in which the response is controlled by the material behavior normal to the crack planes, whereas the material behavior in the plane of the crack is not important. Accordingly, the choice of full shear retention not only has no influence in the results but also provides a more efficient numerical solution (H, K & S, Inc. b 1998).

3.5.2.2 Steel Model

The material model for steel was obtained by specifying its Young's modulus and Poisson's ratio for the elastic part, and the yield stress and plastic strain for the plastic portion. For the Young's modulus a value of 200,000 MPa (29,000 ksi) was used with a Poisson's ratio of 0.3. The yield stress for rebar was 500 MPa (72.5 ksi) and 250 MPa (36 ksi) for the structural steel. No plastic strain was included in the models since all of the structural steel is expected to be within its elastic stress range.

3.5.3 Input Files

ABAQUS/Standard version 5.8 runs as a batch application that requires an input file to be prepared prior to running the software. General pre-processor software such as Hypermesh can also be used to prepare the input file. However, for a three-dimensional model, such as the subject bridge model, it is easier to write the input file than to use a graphical pre-processor.

The input file contains model data and history data. Model data define the finite element model: the nodes, elements, element properties, material definitions, and any other data that specify the model itself. History data define what happens to the model, the sequence of events or loading for which the response of the model is sought. ABAQUS has some useful features for simplifying the writing of the input file. Among the features used in this model are node and element sets, node and element generations, and node copy. The complete features are described in the three volumes of ABAQUS/Standard User's Manual (H, K & S, Inc. b 1998).

For the purpose of modeling the bridge in this study, the input file was prepared in the following sequences. An example of input file is given in Appendix C.

1. Mesh Definition: includes definition of nodes and elements. Nodes are defined by number and coordinates, and elements are defined by number, type, and the node numbers that form the element.

2. Material Definition: specifies the name and the properties of the material. For an elastic material such as steel, only its Young's modulus is required. For elastic plastic materials such as concrete, the material definition is lengthy and complex, especially when properties beyond the elastic range are to be considered. Among the necessary data to define a concrete material are the compressive stress, Young's modulus, Poisson's ration, plastic strain, and failure ratios. The two-way reinforcement is modeled using the REBAR option where the area and the location of the steel reinforcement along the thickness of the element are specified.

3. Boundary Conditions: define the prescribed values of displacement at the boundaries. In this FE model, one end of the center beam is assumed to resist lateral, longitudinal,

and vertical displacements, while the other end is free to displace longitudinally. The other two beams are free to displace, except in the vertical direction.

4. Step Definition: specifies the history data such as the loading type and its magnitude, solution method, etc. For this model, a nonlinear static solution is expected, therefore, an incremented load is specified. Since considerable nonlinearity is expected in the response, including possible unstable regimes, the modified Riks method is used with automatic incrementation of the load. The option to specify this method in ABAQUS is STATIC, RIKS.
5. Output Requests: list all the output data to be created by ABAQUS. Unless specifically defined, by default ABAQUS will create a data file that lists the model definition and all of the output results that may cause memory problems. For problem of this type, a status file that contains information about the progress of the analysis is necessary. The status file is created using the MONITOR option, where the value of one degree of freedom of one node in the model is written (to the status file) at the end of each increment. Therefore, the status file can be examined as the analysis job is executing, which is very useful for large size problems with hours of running time. The other important output file is the restart file, which can be used for graphical post-processing using ABAQUS/Post. This file is created using the RESTART, WRITE options. With this restart file hard copies of the model can be created using ABAQUS/Plot.

During execution, ABAQUS, like other FE software, creates a number of sizable temporary scratch files. To manage these files, it is necessary to create an environment file that specifies how and where the scratch files should be written and saved.

Depending on the size of the problem, the size of scratch files could be more than a gigabyte, which accordingly, must be properly managed to avoid memory problem.

In the present study, a number of FE models were created to obtain a model that best mimics the experimental test results. The models were numbered and named, and the variables included in the models are summarized in Table 3.3. All of the models use one 8-node element along the depth of the deck, except for model m82 and m27. Model m82 uses two 8-node elements, and m27 represents a model with one 27-node element.

In addition to the input file, a sample status file is also given in Appendix C together with the output from ABAQUS/Plot as shown in Figures C1, C2, and C3. In Figure C1, a magnified deformed shape of the bridge model is shown. Figures C2 and C3 show the contour plot of strain and stress in 3-direction (vertical direction), respectively. The load response history of the bridge model is more important in studying the effect of adding tie rods to the deck slab. Accordingly, the FEA results were presented in the form of load deflection diagrams for the slab and the beam, and load strain diagram for the tie rods.

Each FE model shown in Table 3.3 uses a different model for the concrete material in order to study the effect of varying material properties on the response of the FE model. Model m6 uses a concrete model that represents the properties used for example problems in ABAQUS/Standard Example Manual (H, K & S, Inc. c 1998). However, these properties do not necessarily produce the best model for the subject case. The results of the FEA using varying concrete models are given in the following sections.

Table 3.3 Description of FE Models

FE Model		Concrete			Failure Ratio		Tension Stiff.
No	Name	Ec/Eco	f_{cy} / f_c	ε_{cy}	Comp.	Tension	
1	m1	100%	12.5%	0.0030	1.25	0.10	0.0025
2	m1a	100%	10.0%	0.0015	1.16	0.10	0.0020
3	m1b	100%	12.5%	0.0030	1.16	0.10	0.0040
4	m1c	100%	12.5%	0.0030	1.16	0.10	0.0060
5	m2	100%	12.5%	0.0050	1.30	0.11	0.0075
6	m3*	50%	12.5%	0.0050	1.30	0.11	0.0075
7	m4	100%	12.5%	0.0030	1.20	0.10	0.0100
8	m5	100%	50%	0.0030	1.20	0.10	0.0075
9	m6	100%	50%	0.0015	1.16	0.10	0.0020
10	m82	100%	12.5%	0.0050	1.30	0.11	0.0075
11	m27	100%	12.5%	0.0050	1.30	0.11	0.0075

Note: * Model m3 uses reduced Young's modulus. Eco = 24,822 MPa (3.6 E6 psi), and f_c = 27.58 MPa (4000 psi).

3.5.4 Finite Element Analysis Results

The results of the FEA are presented in tables and diagrams. Table 3.4 shows the summary of results of the analyses using various models. The complete description of each model is shown in Table 3.3. It is apparent from the table that the response of each model varies considerably. The models with tie rods fail at a higher load than those without tie rods. These results show that the addition of tie rods improve the strength of the slab. It also shows that the FEA can model the arching action in the slab. However,

the results are not meaningful unless they are compared to the test results. Therefore, further discussion on these results is given in Chapter 6 together with the results from the experimental program presented in Chapter 5.

Table 3.4 Summary of FEA Results

Model		Slab with Tie Rods				Slab without Tie Rods			
No	Name	P-max.		Δ-max.		P-max.		Δ-max.	
		N	lbs.	Mm	in.	N	lbs.	Mm	in.
1	M1	33,949	7,632	4.17	0.164	32,952	7,408	4.50	0.177
2	M1a	30,959	6,960	3.43	0.135				
3	M1b	38,504	8,656	4.80	0.189				
4	m1c	39,144	8,800	4.90	0.193				
5	m2	46,048	10,352	7.24	0.285	43,770	9,840	7.95	0.313
6	m3	60,851	13,680	11.91	0.469	42,418	9,536	8.59	0.338
7	m4	43,913	9,872	5.77	0.227	37,934	8,528	5.31	0.209
8	m5	56,368	12,672	5.89	0.232				
9	m6	30,817	6,928	3.02	0.119				
10	m82	15,088	3,392	1.45	0.057				
11	m27	15,871	3,568	1.61	0.063				

Figures 3.6, 3.7, and 3.8 show the load-deflection relationship of the deck slab with and without tie rods loaded near the mid-span of the bridge. Figure 3.7 shows the effect of using different element types and configurations, where three diagrams are

shown. In Figure 3.8, the load deflection diagram for the model without tie rods is shown, where the name with extension "nr" is associated with this model. In this case, the tie rods were removed from the model. It is apparent from the figures that the responses of the models vary according to the variables used to model the concrete material.

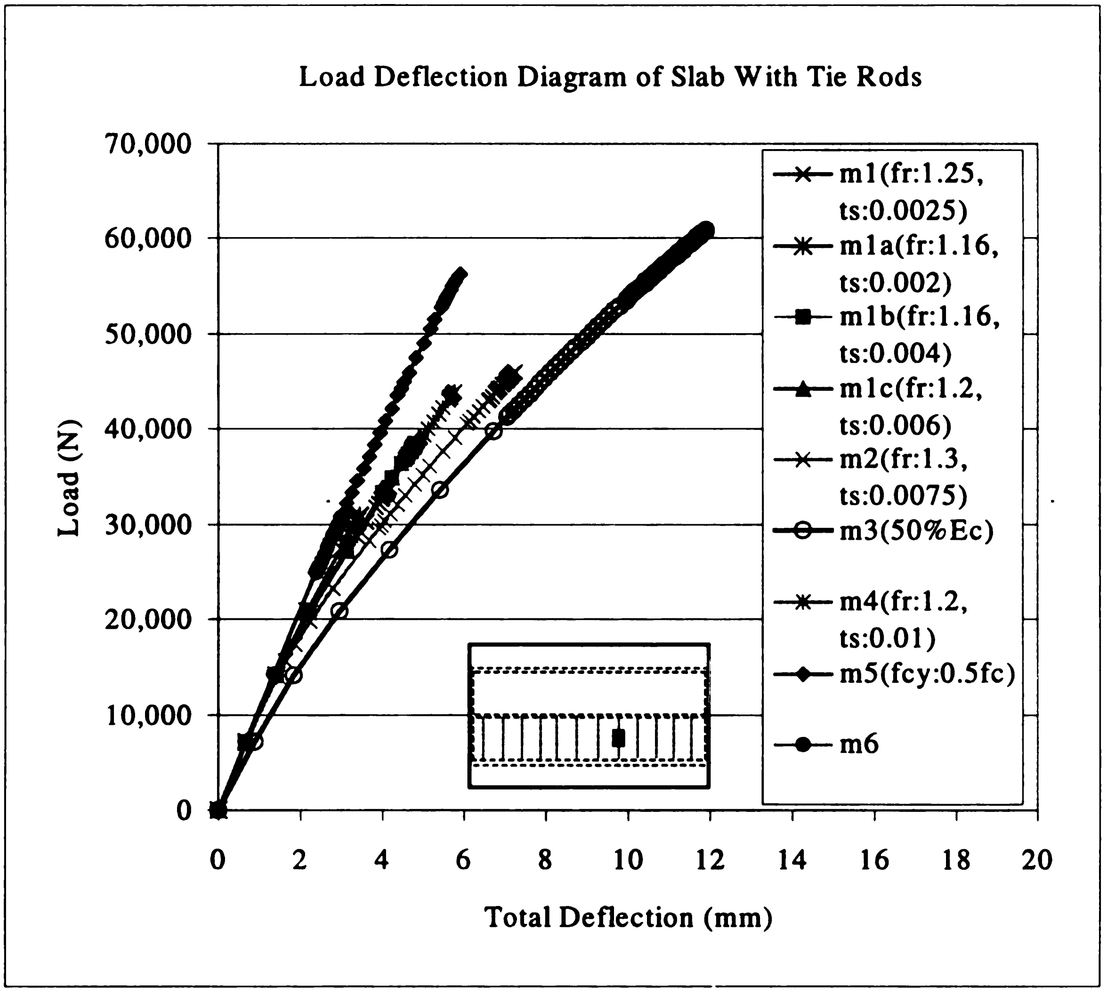

Figure 3.6 Predicted Load Deflection Diagram of Slab with Tie Rods

Models m5 and m6 show the stiffest response, in which the load deflection relation is nearly linear. Model m5 with a higher tension stiffening value provides a longer response than model m6. This shows that the tension stiffening value used in the ABAQUS example problem is not appropriate for the model in this study. Model m3 gives the longest response, which results in the highest failure load and the largest deflection of the slab. Some models are not included in the figures because they are on top of each other. The responses for these models can be seen in Table 3.4.

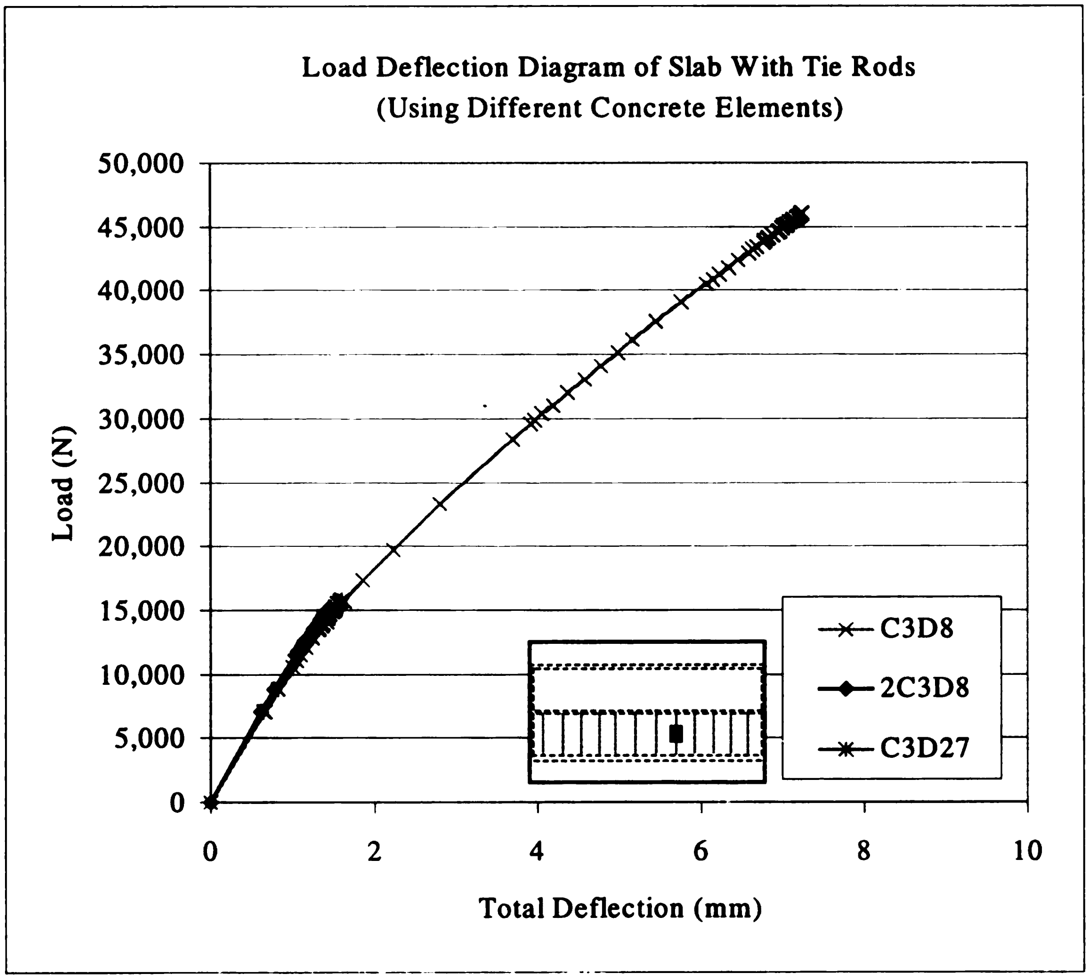

Figure 3.7 Load Deflection Diagram of Slab Using Different Elements

Figure 3.7 shows the effect of using different element types and configurations. The model using one 8-node element along the thickness of the slab provides the longest response. Using two 8-node elements and one 27-node element along the slab thickness, the models fail at a load much lower than those using one 8-node element. The load deflection curves however, are closely tied together.

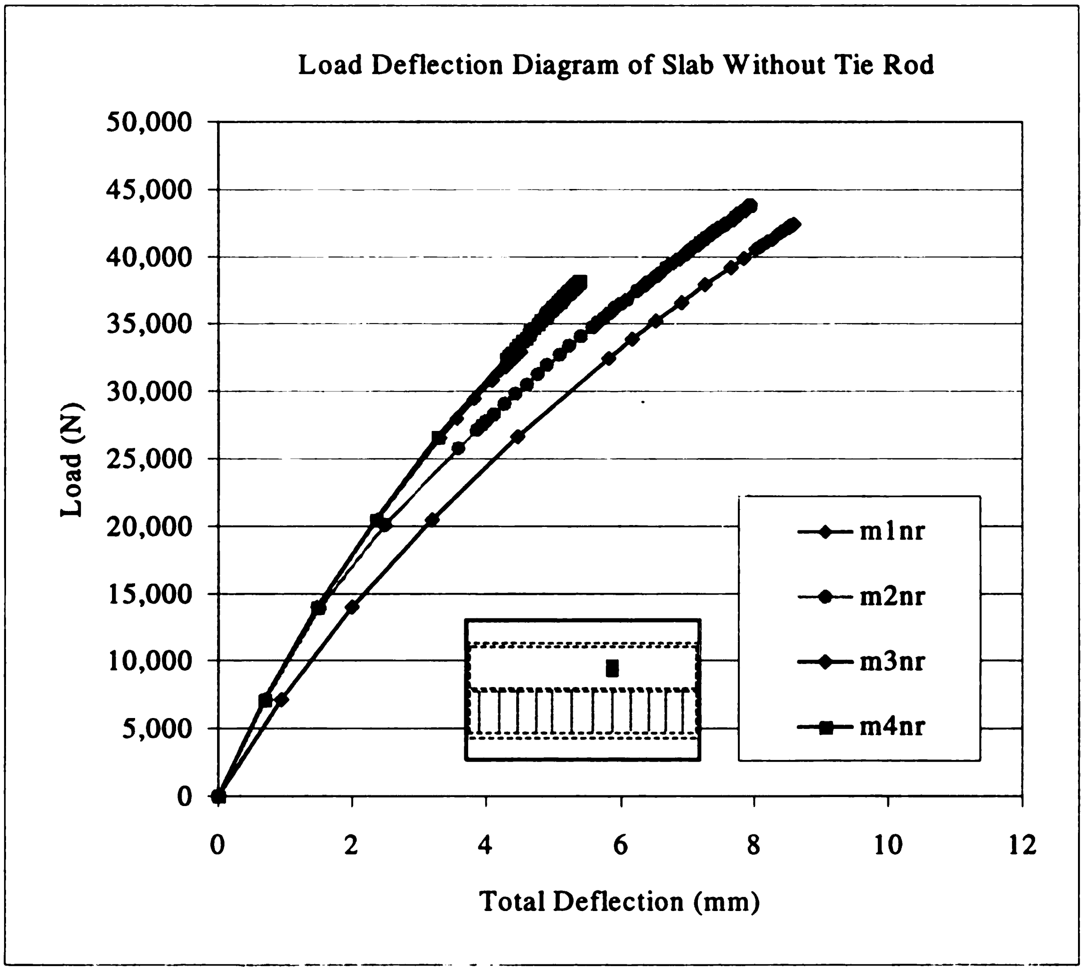

Figure 3.8 Predicted Load Deflection Diagram of Slab Without Tie Rods

The load deflection diagram for the FE models without tie rods is shown in Figure 3.8. Four FE models were developed to show the effect of material properties used for the models. Model m3nr, which uses a reduced value of Young's modulus, gives the largest deflection while models m1nr and m4nr give stiffer responses. The responses of model m2nr and m3nr are similar except that model m2nr is stiffer than model m3nr. These two responses show that the effect of modulus of elasticity is properly modeled in the FEA.

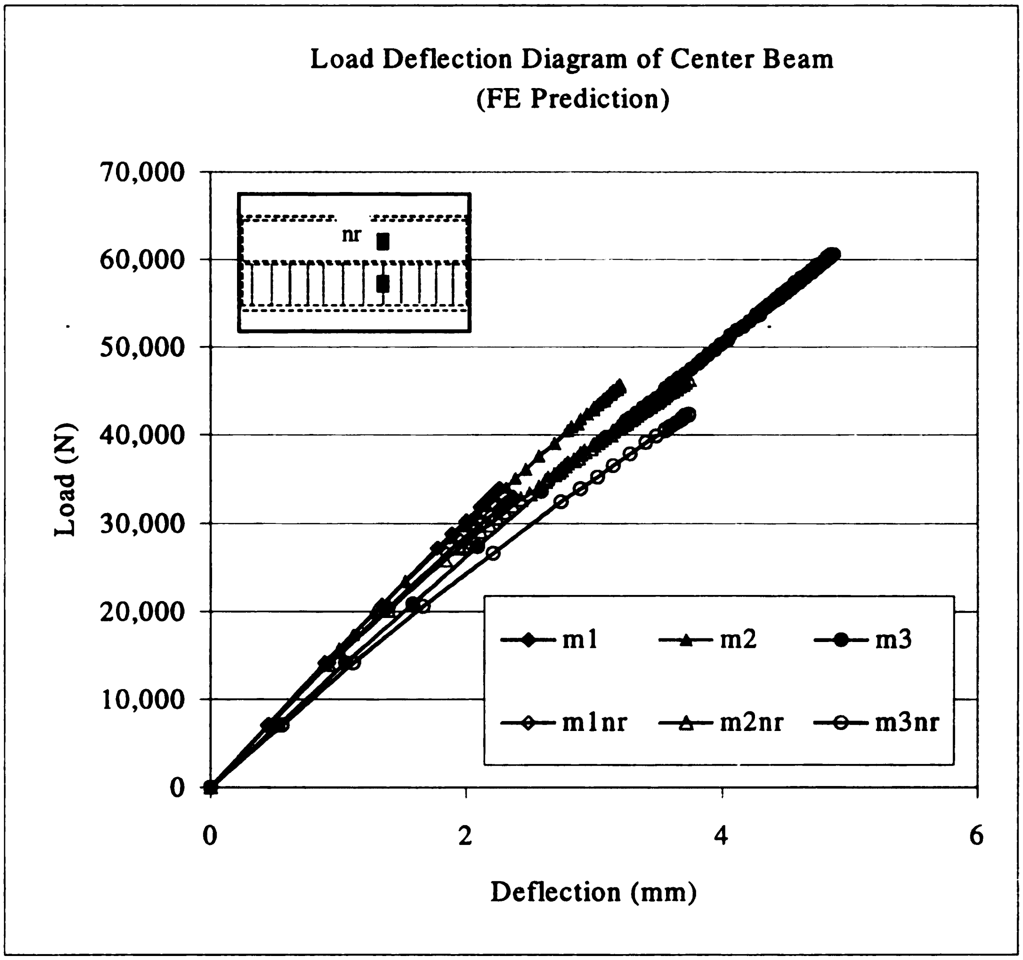

Figure 3.9 Predicted Load Deflection Diagram of Center Beam

Figure 3.9 shows the load-deflection curve for the center beam adjacent to the loaded slab. Similar to the result of slab deflection, the deflection of the center beam is significantly affected by the presence of tie rods. It can be seen from the response of model m1 and model m1nr that with tie rods, model m1 gives stiffer response than model m1nr without tie rods. Similar responses can be observed from the other models. It is also interesting to note that the load deflection relation in the center beam is obviously linear.

In addition to deflection of the center beam and the slab, the strain developed in the tie rods at a distance nearest to the load point is also recorded from the FEA. This strain is an important evidence of the presence of arching action in the slab that causes the supporting steel girders to move laterally. During the development of the FE models, shell elements were used to model the deck slab. However, no strain was developed in the tie rods, which meant that shell elements could not model the arching action developed in the deck slab.

The load strain relation in the tie rods underneath (S5) and immediately adjacent to the applied load (S4) are given in Figure 3.10. It is apparent from the figure that the higher the load the higher the strain in the tie rods, with strain rate higher than the rate of the load. It is also interesting to note that the development of strain in the tie rods started at a very low load level, under which bridge structures operate.

In general, the FEA results show that the effect of tie rods in the deck slab is properly modeled. The response of the FE models with and without tie rods show that the addition of tie rods improves the behavior of the slab through deflection reduction and strength enhancement in the slab. These results however, remain to be verified through the experimental test.

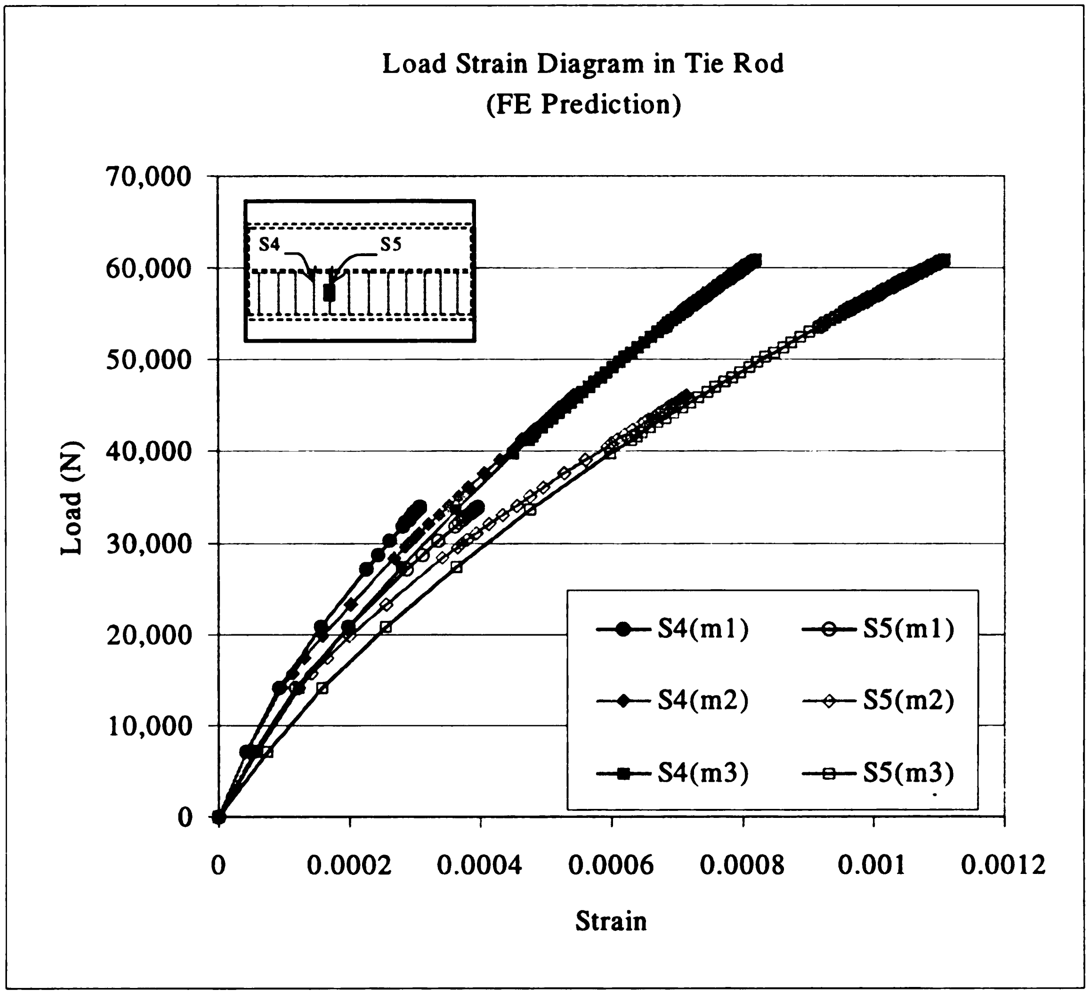

Figure 3.10 Predicted Load Strain Diagram of Tie Rods

CHAPTER 4

DESIGN AND CONSTRUCTION OF MODEL BRIDGE

4.1 Introduction

To study the effect of adding lateral restraint (i.e. tie rods) to an RC deck slab on its behavior under static concentrated load, laboratory load testing up to failure was decided upon. For that purpose, two different types of slab panels were planned: one panel without tie rods was used as a control panel, and the other panel with added tie rods served as a treated panel. In this study, both types of slab were incorporated into the construction of one bridge in order to obtain two slab panels with comparable properties. A bridge with three steel girders was adopted to obtain two similar slab panels. Therefore, the effect of adding tie rods could be observed by testing two similar rows of slab panels in the same bridge, in which one of the panels was treated by connecting the underside of the top flanges of the girders with tie rods.

Testing a full-scale prototype structure is ideal for accuracy as well as easy to design the structure. However, to build a full scale bridge is not only expensive but also time-consuming, particularly since the bridge will be tested up to failure. Therefore, a reduced scale model is more appropriate for the purpose of destructive testing.

The ACI Manual (1998) defines a small scale model as "any structural element or assembly of structural elements built to a reduced scale (in comparison with full size structures) which is to be tested, and for which laws of similitude must be employed to interpret test results." There are two commonly used approaches in designing a reduced scale model structure. The first approach is using scaled loads to design a model structure of the form of the prototype. The second approach is to scale the dimensions and sectional properties of a prototype structure to obtain a model structure. Previous researchers have used both approaches and obtained results with comparable accuracy. In this study, the second approach was adopted. For this purpose, a hypothetical prototype bridge was designed according to the AASHTO Specification, and then, each component of the bridge was scaled to obtain the model bridge. This way, the size of the model bridge could be adjusted according to the experimental condition. Following the design was the construction of the model-bridge. More detail on the design and construction of the model bridge is given in the following sections.

4.2 Design of Prototype Bridge

The hypothetical prototype bridge was designed according to AASHTO LRFD Bridge Design Specification, SI Units (Appendix B – Basic Steps for Steel Bridge Superstructures of AASHTO 1994). Three steel I-beams of Grade 250 MPa (36 ksi) were used with beam spacing of 2,540 mm (8 ft. – 4 in.). The simple span bridge was designed with a span length of 12,190 mm (40 ft) and a total width of 7,112 mm (23 ft.- 4 in.), that represents a one lane bridge at an exit ramp. The steel beams and the RC deck slab were designed to act as a composite beam utilizing shear connectors. Figure 4.1 shows a plan view of the hypothetical prototype bridge showing deck panels with and without tie rods. The design is summarized and presented in this section, while the details of the design of the prototype-bridge are not included in this thesis.

4.2.1 Reinforced Concrete Deck Slab

The behavior of RC deck slabs with and without additional lateral restraint is the primary interest of this study. For that reason, the deck was carefully designed by considering the test results from previous studies in addition to the AASTHO Specification (AASHTO 1994). The thickness of the RC deck slab was designed to be 203 mm (8 in), using a concrete compressive strength of about 28 MPa (4,000 psi). For the purpose of rebar development, the deck overhang was designed to be about 1,016 mm (40 in.), which is about five times the deck thickness.

Those numbers are within the AASTHO requirements for empirical design of RC deck slabs. The minimum concrete strength required by AASHTO was used for this project so that the experimental results could be used to interpret the punching strength of deck slabs with a wider range of compressive strengths. The thickness of the slab, however, was made thicker than the minimum requirement of 175 mm (7 in.), to represent common bridge deck design practice. No sacrificial wearing surface was included in the deck thickness for this design purpose. Accordingly, the steel reinforcement was placed symmetrically along the depth of the slab (using the same top and bottom concrete covers).

For the reinforcing steel, a smaller amount than that required by the Code was used in order to amplify the effect of adding lateral restraint (tie rods), provided such an effect could be shown to exist. It was also intended to verify the results of previous tests reported in the literature. The AASHTO minimum requirements for steel reinforcement are 0.57 mm^2/mm for each bottom layer, and 0.38 mm^2/mm for each top layer. With the

slab thickness of 203 mm, the above numbers correspond to steel ratios of 0.28 % and 0.19 % for the top and bottom layers, respectively.

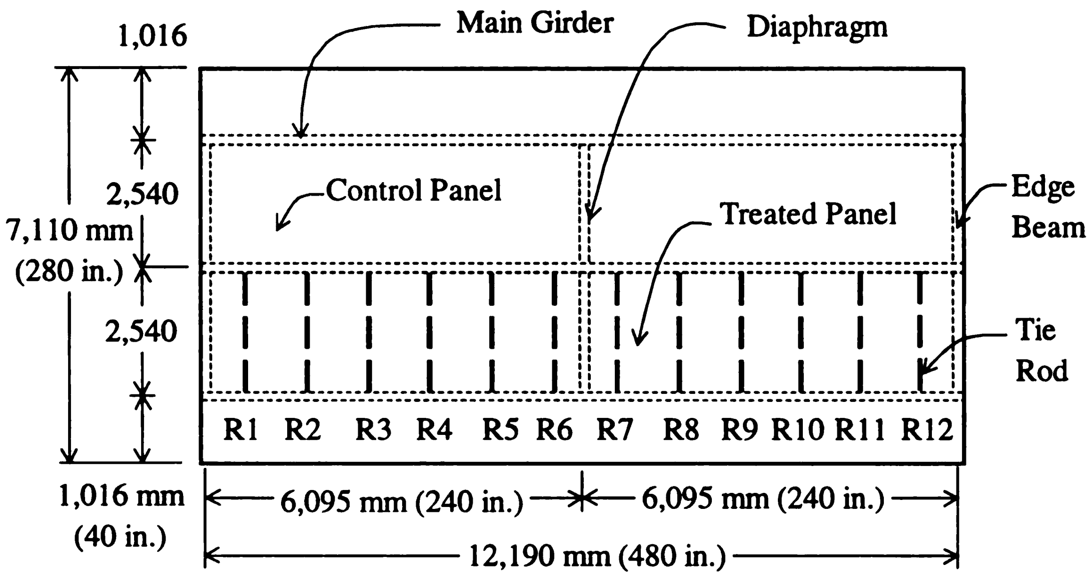
1,016
Main Girder
Diaphragm
2,540
7,110 mm
(280 in.)
Control Panel
Treated Panel
Edge
Beam
2,540
Tie
Rod
R1 R2 R3 R4 R5 R6 R7 R8 R9 R10 R11 R12
1,016 mm
(40 in.)
6,095 mm (240 in.)
6,095 mm (240 in.)
12,190 mm (480 in.)

Figure 4.1 Plan View of Prototype Bridge

In this study, a steel area of 0.40 mm^2/mm, which corresponds to a steel ratio of about 0.2 %, was used in all four layers with isotropic arrangement. Number 13 bars with 12.7 mm (0.5 in.) diameter and 305 mm (12 in.) spacing provides a steel area of 0.415 mm^2/mm. The minimum yield strength of steel reinforcement required by the code is 400 MPa (60 ksi). Steel with higher yield strengths could also be used as long as the minimum area is satisfied.

Using 0.2% isotropic steel results in lower steel ratio for the bottom layers but higher steel ratio for the top layers. The choice of isotropic steel arrangement was based on the possible benefit gained by using prefabricated steel such as welded wire fabric or wire mesh. Previous research also showed that an RC deck slab reinforced with 0.2 %

steel provides more than adequate strength to resist a concentrated load from a truck wheel (Hewitt 1972, Beal 1982). Therefore, the same steel ratio was adopted in this study, not only to amplify the effect of adding tie rods, but also to verify the adequacy of using minimum steel reinforcement in an RC bridge deck slab.

4.2.2 Design of Tie Rods

The design of steel tie rods was based upon previous research found in the literature (Newhook, 1997). The steel strap that is used in a fiber reinforced concrete deck slab, also known as a steel-free deck slab, is meant for a new construction where the strap was installed prior to the pouring of the concrete deck. In this study, the tie rods are intended to be installed after the concrete slab is constructed, because it is meant to improve the performance of an existing deck slab. Consequently, direct application of the strap design used for the steel-free deck slab is similar, but sufficiently different for the design of the tie rods. However, it was used as a nearest available guideline.

Considering their replaceability and ease of installation, the shape of the tie rods could be round or square with threaded ends to facilitate bolted connections. With bolted connections, the rods can be pre-tensioned by tightening the bolts prior to loading. The size of tie rods was determined following the Canadian Highway Bridge Design Code (CHBDC) requirements for fiber reinforced concrete deck slabs.

Another important issue in designing the tie rods was that their spacing should be small. Otherwise, they may not be effective if the slab is loaded at a distance away from the rods. The CHBDC requires that the maximum spacing of straps, S_l is 1.5 meter. For a slab thickness of 200 mm with a beam spacing of 2,500 mm, the minimum area of the strap required by CHBDC is about 938 mm^2 (Newhook, 1997). In this study tie rods with 40-mm (1.575 in.) diameter, spaced at 1 m (40 in) was adopted. The area of the rod was 1,257 mm^2, which is about 34% larger than the minimum area required by the CHBDC for a steel-free deck slab. A total of 12 rods were used and numbered R1 to R12 as shown in Figure 4.1.

4.2.3 Design of Steel Girders

The three main girders were designed using rolled steel wide flange sections. The section used for the prototype bridge was W760x160 (W30x108) of M270 Grade 250 MPa (36 ksi). The wide flange sections were designed as composite I-beams with a span length of 12,190 mm (40 ft. – 0 in.) and beam spacing of 2,540 mm (8 ft.-4 in.) from center to center. Shear studs of 3 x 19 mm (0.75 in.) diameter, spaced at 160 mm (6.3 in.) center to center were provided for that purpose. As required by the Code, the bridge was designed to have three diaphragms, one at mid-span and two at the ends of the bridge. Channel sections of MC450x86 (MC18x58), M270, Grade 250 MPa (36 ksi) were used for these diaphragms.

4.2.4 Design of Edge Beams

At the ends of the bridge, the top portions of the girders were connected together by means of steel channels termed the edge beams. These beams were also provided with shear connectors to obtain composite action between the beams and the deck slab. The strong axis of the channels was placed in the horizontal direction to provide greater lateral restraint to the slab near the longitudinal edges. The geometry of the edge beam is shown in Figure 4.2.

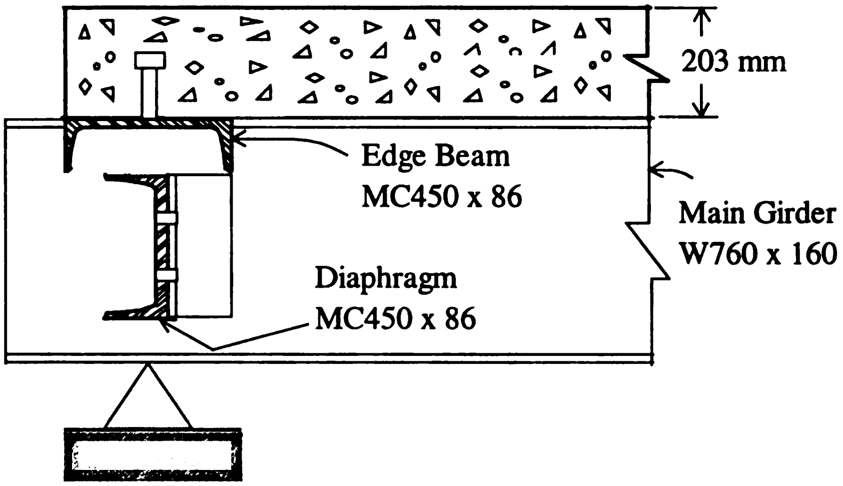

Figure 4.2 Longitudinal Section Showing Edge Beam and Diaphragm

The idea of using edge beams was based on previous research, in which it was shown that by adding lateral stiffeners at the ends of the slab, the strength of the slab become uniform along the slab (Bakht and Mufti, 1996). Without edge beams, the strength of the slabs near the edge were lower than that at a distance from the supports.

The CHBDC requirement for the flexural rigidity of an edge beam, EI is 3.5 L_u^4 in MN-m^2 unit, where L_u is the unsupported length of the edge beam which is equal to the span of the slab. For an L_u of 2.233 meter (beam spacing less the flange width), the required flexural rigidity EI was 87 MN-m^2. The channel section used for edge beam was the same as that used for diaphragms, which is MC450x86 (MC18x58) of M270 Grade 250 MPa (36 ksi). Considering composite action between the edge beam and the concrete deck slab, the moment of inertia of the edge beam was 4.837 x 10^{-4} m^4 (1,162 in^4). With

steel elastic modulus of 200,000 MPa (29,000 ksi), the flexural rigidity of the edge beam became 96.7 MN-m^2, that is about 11% higher than that required by CHBDC.

4.2.4 Design of Shear Connectors

The shear connectors for the steel girders were designed based on strength and fatigue requirements. The design was governed by fatigue requirement of the AASHTO Specification. Three studs of 19-mm (3/4 in.) diameter were used with spacing of 160-mm (6.3 in.) center to center. The properties of the shear studs and the other components of the prototype bridge are summarized in Table 4.1.

4.3 Design of Scaled Model Bridge

The two basic dimensions required in testing a model-structure for static loading are force and length, denoted F and L, respectively. For a practical true model, the scale factors of stress, strain, and the modulus of elasticity for both concrete and steel are all unity. Since the dimension of stress is $FL^{-2} = 1$, then the scale factor of force is the square of the scale factor of length.

Ideally, a length scale factor as close as possible to unity is preferable to avoid possible size effects and dimensional inaccuracy. In this study, however, to minimize the cost of construction, a length scale factor, s_L of 5 was adopted. A strength or realistic model, which is a direct model made of materials similar to that of the prototype materials, was used in order to predict the prototype behavior up to failure (Sabnis et al 1983, Aldridge and Breen 1970, and Harris et al. 1970).

Table 4.1 Properties of Prototype Bridge

No	Component	Properties
1	Deck Slab	203 mm (8 in.) thick of 28 MPa (4000 psi) concrete Isotropic steel ratio of 0.2 %.
2	Steel Girders	W760x160 (W30x108) of M270 Grade 250 MPa (36 ksi) Span length: 12,190 mm (40 ft.) Beam Spacing: 2,540 mm (8 ft. – 4 in.)
3	Diaphragm	MC450x86 (MC18x58) of M270 Grade 250 MPa (36 ksi).
4	Edge Beam	MC450x86 (MC18x58) of M270 Grade 250 MPa (36 ksi).
5	Shear Connectors	(3) 19-mm (3/4") diameter studs 160-mm (6.3") spacing.
6	Tie Rods	40 mm (1.575 in.) diameter 1015-mm (3' - 6") spacing.

For RC structures, the similitude requirements are expressed in term of the scale factor, s_i defined by

$$s_i = \frac{i_p}{i_m}$$

where i_p and i_m refer to prototype and model quantities, respectively. Using a length scale factor of 5 results in a scale factor of 25 for force. Therefore, a 1/5 scale deck slab that fails at an ultimate load of 1 kN, for example, will fail at a load of 25 kN in the full scale prototype structure. Accordingly, the scale factors for the other similitude requirements could be calculated as shown in Table 4.2.

Table 4.2. Scale Factor

Quantity	Dimension	Scale Factor
Stress	FL^{-2}	1
Strain	LL^{-1}	1
Modulus of elasticity	FL^{-2}	1
Length	L	5
Force	F	25
Deflection	L	5
Area	L^2	25
Section modulus	L^3	125
Moment of inertia	L^4	625
Density	FL^{-3}	1/5

The problem with a reduced scale model is related to the dead load induced stresses. The density or unit weight of a structural material is expressed in force per cubic length, FL^{-3}. By scaling the length, while keeping the stresses in prototype and model structures constant, it is required to scale the unit weight of the model structure by a factor of 1/5. However, in concrete structures the density of the material will affect their

properties. Accordingly, in this study, the density of the concrete was not scaled in order to get materials of comparable properties for both prototype and model structures.

It was assumed that the stress caused by the self-weight of the structure is relatively small compared to the live load induced stress, because punching shear capacity is related to a concentrated load instead of the distributed load due to self-weight. Therefore, the dead load induced stress was omitted in this study.

By not scaling the mass density of the model structure, the model becomes deficient as long as dead load stresses are of concern. If the dead load effects were to be properly scaled, a supplementary load equal to $(s_L - 1)$ times the actual model weight would have to be applied to the model structure. However, an earlier study showed that incorporating the effect of self weight by applying dead load compensation has little, if any, effect to the punching shear capacity of the deck slab (Hewitt, 1972). Accordingly, for practical purposes, it was recommended that any effect due to differential dead load stresses or deflection could be ignored.

Based on the above assumptions, the model structure was designed by dividing the properties of the prototype structure by an appropriate scale factor. The ratio between the scaled prototype and model structures should be as close as possible to unity. However, due to the availability of materials, some ratios could not be kept to unity.

Other difficulties were encountered in selecting the rolled steel sections that match the scaled properties of prototype structural component. Unless a built-up section was used, it was not possible to obtain rolled sections that matched all dimensions and sectional properties of the prototype section. Sections that match the cross sectional area may not match the moment of inertia and vise versa. However, the important or controlling factor was the moment of inertia, so that was used for the basis in the selection of the section. The same procedure has been used in bridge design practice, where the choice of a rolled section is dictated by the availability of the section in the market. In this study, however, special care was given to the modeling of the deck slab thickness, which proportionally affects the moment of inertia of the composite section. Figure 4.3 shows the cross section of the model bridge, while the complete dimensions of the prototype and model-bridges are given in Table 4.3.

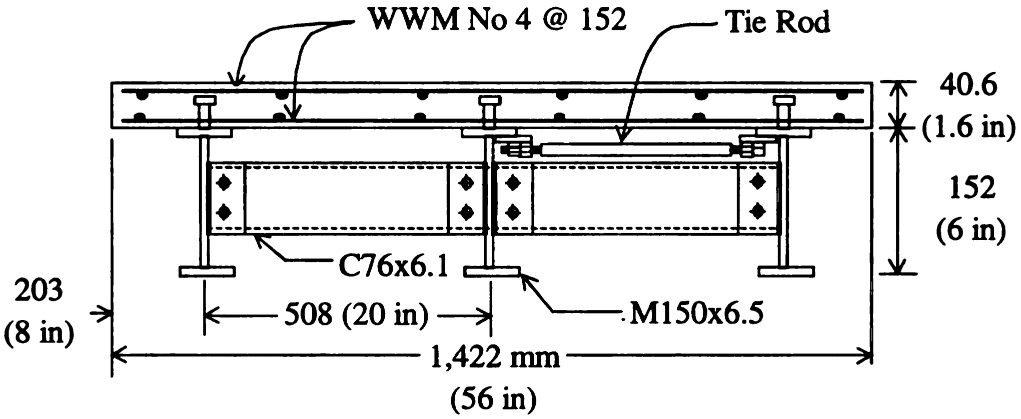

Figure 4.3 Cross Section of Model Bridge

For the model tie rods, a square bar was used to facilitate installation of strain gages in the rods. The ends of the bar were threaded with a net area equal to that required for the scaled rods. The threaded ends in the rods allowed the use of nuts to tighten the rod connection prior to load testing the slab. The detail of the tie rods is shown in Figure 4.4. Some difficulties related to the detail of the rod connection were anticipated mainly because of the limited space available. The flange width of the model girder was so small that an additional plate was required to facilitate the rod connection. This condition was not beneficial because the eccentricity caused by the additional plate would be the source of additional stress in the connection. In a full scale bridge, however, such problems would not exist because the flange width of the girder is usually large enough to accommodate the connection for the tie rods.

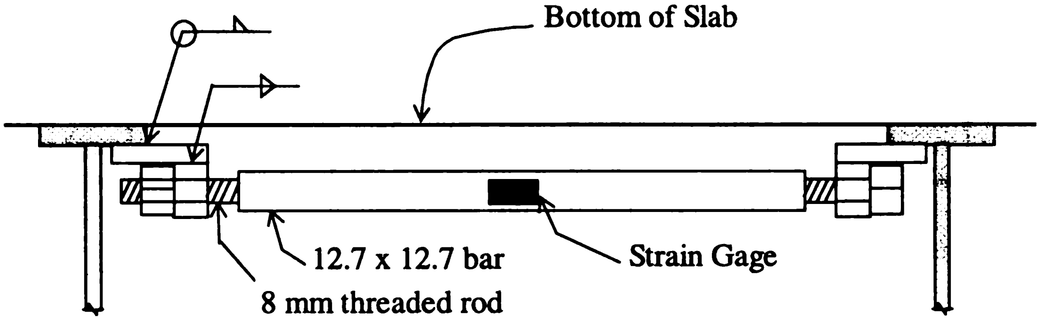

Figure 4.4 Detail of Tie Rods

4.4 Properties of Materials for Model Bridge

In order to obtain a true model, the properties of the materials in both prototype and model structures should be the same. In concrete structures, however, there are size effects that can not be avoided. It is generally believed that micro concrete exhibits higher strength but is more prone to shrinkage cracking than prototype concrete. In practice, modeling only the compressive strength of the concrete is considered acceptable for the purpose of experimental study. Special consideration for curing of micro concrete was recommended in order to prevent excessive cracking due to shrinkage. One way to control the shrinkage cracking problem is to cure the wet concrete under water as long as possible. The procedure of water curing is required by the AASHTO Specification for a prototype deck slab that is designed using the empirical method.

Table 4.3 Properties of Prototype and 1/5 Scale Model Bridge

Component	Prototype	Scaled	MODEL	Ratio
1. Deck Slab (fc' 28 MPa)				
Thickness (mm)	203	40.64	40.64	1.00
2. Steel Reinforcement	fy 400 MPa		fy 500 MPa	
	No 13 @ 317		No 4 @ 152	
Area (mm^2/mm)	0.400	0.080	0.083	1.04
3. Girders (fy 240)	W760 x 160		M150x6.5	
Area (mm^2)	20452	818	832	1.02
Ix (mm^4)	1.86 E9	2,976,000	2,996,866	1.01
Iy (mm^4)	60.77 E6	97,232	70,759	0.73
4. Diaphragms and Edge				
Beams (fy 240)	MC450x86		C75x6.1	
Area (mm^2)	11,032	441	781	1.77
Ix (mm^4)	2,813,724,444	450,196	690,944	1.53
Iy (mm^4)	7,408,919	11,854	83,246	7.02
5. Shear Stud (fy 240)	(3) ϕ 19 mm		(1) ϕ 8 mm	
Spacing (mm)	160		50.8	
Area (mm^2/mm)	5.316	1.06	0.99	0.93
6. Tie Rods (fy 240)	ϕ 40 mm		ϕ 8 mm	
Spacing (mm)	1000		203	
Area (mm^2/mm)	1.24	0.257	0.25	0.97

For a steel structure the mechanical properties of small and large size structures are considered the same. However, the availability of rolled sections in small sizes is limited. Consequently, slight distortions of a model structure can not be avoided. As long as the model does not significantly affect the behavior of the deck slab, the effect of adding tie rods could be measured properly. In this case, a slight distortion in the model for steel girders will not affect the test results as much as the distortion of the deck model. Accordingly, modeling the deck slab as accurately as possible is necessary.

As shown in Table 4.3, the ratio between the scaled prototype and model bridge components, are not equal to unity except that for the theoretical deck thickness. The exact thickness of the slab may vary due to imperfections during the construction. However, such variability is also found in the field, thus, with proper care in construction, it need not be considered in the design of the model. Since the effect of adding tie rods is of main concern, as long as the material properties are the same for both control and treated slab panels, the effect of the treatment could be measured properly. Further discussion of the material properties used for the model-bridge is given in the following sections.

4.4.1 Micro Concrete

The target value of compressive strength for the micro concrete was about 28 MPa (4000 psi), which is the minimum strength allowed by the AASHTO empirical design for deck slabs (AASHTO 1994). The compressive strength was the only concrete property to be modeled considering that the other properties such as tensile strength, the modulus of elasticity, and Poisson's ratio are related to the compressive strength. The mix design of regular (prototype) concrete recommended by ACI was used to design the mix proportion of the micro concrete, which in SI units proceeds as follows.

The maximum aggregate size for the prototype concrete was about 38 mm (1.5 in.). For the micro concrete, the maximum size of aggregate was scaled to about 7.6 mm (0.3 in.). In this study, a natural aggregate, so called "pea gravel", with maximum size of 9.5 mm (3/8 in.) was used. Only the maximum size of the aggregate was scaled in obtaining the mix design of micro concrete. Direct scaling of coarse and fine aggregate is not necessary because it may result in a large proportion of fines that require more absorption water. For this reason, regular sand with fineness modulus of 2.94 was utilized.

The micro concrete was intended to have a slump value of 100 – 125 mm (4 – 5 in.). Workability was another concern for the micro concrete because the slab was so thin that a special effort to compact the concrete to avoid segregation problem was required. Consequently, it was necessary to use highly workable, high slump micro concrete to assure good consolidation. With maximum aggregate size of 9.5 mm, the approximate mixing water required for the mix was about 230 kg/m^3 of concrete. To achieve a compressive strength of about 28 MPa (4000 psi), the maximum water cement ratio, w/c was about 0.54 as given by ACI 211, Table A1.5.3 (ACI 1994). Using fine aggregate with a fineness modulus of 2.94, the required volume of coarse aggregate per unit volume of concrete was 0.48 as shown in Table A1.5.3.6 of ACI 211.

The final weight of each ingredient for one cubic meter of concrete was; water: 230 kg, cement: 426 kg, fine aggregate: 986 kg, coarse aggregate: 768 kg. The final mix proportion by weight of water: cement: aggregate was 0.54: 1: 4.1. This mix proportion is very similar to that used by Hewitt (Hewitt, 1972), in which using this proportion a compressive strength of least 28 MPa (4,000 psi) was reported. Accordingly, in this

study, the mix proportion was directly used for the design of the micro concrete, no trial mix was conducted prior to using the mix design for the actual micro concrete.

4.4.2 Steel Reinforcement

Welded Wire Mesh (WWM) was used for the reinforcement of the model slab. The diameter of the wire was 4 mm (0.16 in.) with spacing of 152 mm (6 in.) in both directions. The wire that was readily available in the market had a minimum yield strength of 500 MPa (72.5 ksi). No attempt was made to anneal the wire as the process is complex and may introduce new variability in the properties of the wire. Bridge engineers have been reluctant to use welded wire mesh in highway structures. Their main concern is poor fatigue strength due to welded intersections. Nevertheless, there are many benefits to be gained from using WWM in bridge decks. Among the benefits are considerable savings of construction time, improved bonding and anchorage, small probability of error, and ease of placement.

A previous experimental testing program (Al-Mutairi 1989) showed that a deck slab reinforced with WWM performed well with the exception of a simply supported slab in the flexure test, where the slab had less ductility than an equivalent slab reinforced with conventional reinforcement. However, the welded wire mesh reinforced slab deformed sufficiently and showed clear signs of distress before failure, a behavior that can provide visual warning of imminent failure. In addition, knowing that a deck slab has a high reserve capacity compared to the maximum possible applied load, the ductility of the structure is not a concern. Csagoly et al. (1978) also recommended the use of welded wire mesh for the reinforcement of deck slabs. Finally, test results showed that the strain in a steel rebar induced by a truck load is so low that the steel is not required as far as strength is concerned (Beal 1982, Puckette et al. 1989). Thus, WWM can be used, with proper engineering judgment, as reinforcement of bridge decks.

4.4.3 Structural Steel

The structural steel for girders, diaphragms, edge beams, and tie rods, the properties of the material in both the model and prototype were the same. In this case, all of the steel used in the model bridge had a yield strength of 240 MPa (36 ksi). Therefore the material model for the structural steel was not distorted provided that the variability of the material properties are the same for large and small sections.

4.5 Construction of the Model Bridge

The model bridge was constructed in two phases, the steel framing phase and the concrete pouring phase. In the first phase, all steel framing for the girders, diaphragms, edge beams, and tie rods were prepared in the shop. The shear connectors were welded to the girders and edge beams prior to the frame assembly. The girders were cut longer than the designed span length and protruded beyond the bridge deck to facilitate supporting the bridge at the designed support points. Special structures for the supports were built high enough to provide clearance (working space) underneath the bridge. After all the dimensions were checked and verified, and formwork was prepared, the steel frame was transported in pieces to the Structural Lab of the Michigan Department of Transportation.

In the lab, the frame was re-assembled without the tie rods. The formwork and the reinforcing steel were put in place for pouring phase. The tie rods were not put in position prior to pouring of the concrete because it was meant to be added to an existing structure instead of being part of a new structure. During the pouring, two batches of concrete mix were required for the entire bridge and the associated preparation of concrete test cylinders. To avoid unwanted variability between the control slab panel and the treated one, pouring was started from the support end instead of from the side end of the bridge. One batch of concrete mix was enough for half the length of the bridge. In this way, similar concrete can be expected for both panels of the slab.

4.5.1 Concrete Cylinders

Scaled concrete cylinders are commonly used to determine the mechanical properties of the micro concrete. However, it is generally accepted that the strength of concrete cylinder in either compression or tension bears little relationship to the strength of the same concrete in a structure. The more accurate way to test the strength of concrete in a structure is by cutting cylinders out of the structure. In this study, however, since the thickness of the slab was only 40 mm (1.6 in.), it was not possible to cut a cylinder out of the slab. Accordingly, to determine the strength of the micro concrete, small concrete cylinders were cast from the same batch of concrete used for the deck slab. The suggested diameter of cylinder is about the least dimension of the structure, which in this case the thickness of the slab. However, a very small cylinder may not be effective for measuring the strength of the concrete (Aldridge and Breen 1970).

In this study, the size of the concrete cylinders used for compression and split-cylinder tests was 75 mm diameter by 150 mm (3 by 6 in.). The cylinders were cast using plastic molds, following the procedures suggested by the American Standard for Testing and Materials, ASTM C469 and ASTM C496 (ASTM 1996). The cylinders were cast at the time of pouring the concrete for the deck slab. Five cylinders were cast for each of the two batches. A total of ten cylinders were obtained, six for compression test and four for split-cylinder test.

The consistency of the mix was measured with a slump test according to the ASTM C143 (ASTM 1996). The value of the slump measured during the test was about 175 mm (7 in), which is higher than the expected value of about 100 to 125 mm (4 to 5 in). The higher slump value was partly attributed to the small maximum size of the coarse aggregate and the water content of the sand. For micro concrete, however, higher slump concrete is beneficial for workability, compaction, and finish without harmful segregation. It also indicates lower compressive strength.

4.5.2 Curing

Previous research on structural concrete modeling showed that curing is one of the most important factors affecting the properties of micro concrete. Extensive shrinkage cracking was reported for micro concrete cured under wet burlap or using a chemical compound (Hewitt, 1975). To avoid the same problem, it is necessary to cure the micro concrete well in the sense that the amount of lost water should be limited as far as possible. For the concrete cylinders, de-molding were done after 24 hours of casting. The cylinders were then cured in the curing room for 28 days. Curing of the model slab was done by ponding. For this purpose, the edges of the slab were made about 50 mm thicker to hold the ponding water. Ponding was continued for 28 days, until the removal of the formwork when the slab was ready for testing. In this way, the concrete cylinders and model slab were cured in a similar manner, and therefore, a better relationship can be expected between the concrete properties of the slab and the cylinders.

CHAPTER 5

EXPERIMENTAL PROGRAM

5.1 Introduction

The main purpose of the experimental program was to investigate the behavior and punching shear capacity of RC deck slabs with and without tie rods. For this purpose, a one-fifth-scale model bridge that incorporated two slab panels (with and without tie rods) was built and tested in the Structural Lab of the Michigan Department of Transportation. The behavior of deck slabs under varying magnitude of loads is of primary interest in this experiment. Moreover, the deflection of the beam and the strain developed in the tie rods were also investigated. The model bridge was instrumented accordingly.

A shored construction was adopted in this study to minimize the dead load induced stresses because neither density scaling, nor dead load compensation was planned for this experiment. The choice of shored construction was also intended to minimize dead load deflection, therefore, no cambering of the steel girder was necessary. Even though unshored construction was used, the dead load induced stress and deflection could still be disregarded for the purpose of testing a small-scale model structure (Hewitt 1972).

The instrumentation was designed to verify the focus of the experiment that was aimed at the effect of adding tie rods. Consequently, the instrumentation was directed toward measurements of the load deflection relationship in the slab and steel girder as well as the stress/strain developed in the tie rods. In this case, the quantities to be measured during the load test were the magnitude of applied loads, the deflection of the slab and the girder corresponding to the applied load, and the strain in the tie rods. More detail on the experimental program is explained in the following sections.

5.2 Instrumentation

Measurement of the load and the corresponding deflection of the slabs in the lab was done by applying a concentrated load generated incrementally by means of an instrumented ram (a hydraulic jack) reacting with a steel loading frame. The concentrated load was applied to the deck slab through a 50 by 100 mm (2 by 4 in.) neoprene pad of 13 mm (1/2 in.) thick, that corresponds to the nominal prototype wheel-print of a truck that is about 250 by 500 mm (10 by 20 in). The load was generated and recorded using a computer-based loading device that was capable of controlling the intended load magnitudes. A sketch of the experimental set up on the loading frame is shown in Figure 5.1.

The vertical deflection was measured using 0.025 mm. (0.001 in.) dial deflection gauges. The net deflection of the slab relative to the beam was measured by mounting the gage on the center beam adjacent to the load. When the beam and the slab deflect the same amount, then the gage reading will be zero. Likewise, if the beam and slab deflections are different then the gage reading will be the difference between the two deflections. A typical arrangement of the dial gauges to measure deflection, and the strain gage position in a tie rod are shown in Figure 5.2.

The measurement of strain in the tie rods was done using general-purpose strain gages, type CEA-06-250UW-120. The active length of the gage was 250 mils (0.25 in. or 6.35 mm) with a resistance of 120 Ohms and a gage factor of 2.065 at 24 °C. A total of 15 strain gages were mounted to 12 tie rods. To simplify the reading of the strains manually, each wire from the strain gage was connected to a low resistance switch box that can accommodate as many as 32 strain gages. The readings of the strain for each gage were obtained from a digital strain reader that was connected to the switch box by pressing the appropriate buttons that correspond to the strain gage.

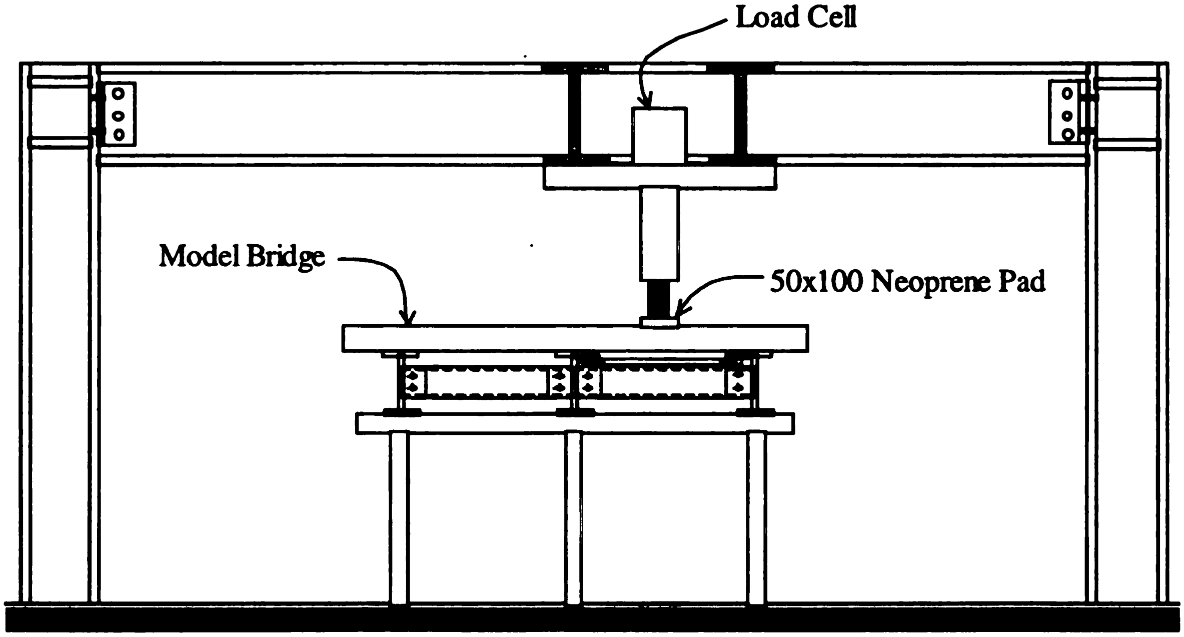

Figure 5.1 Experimental Set-Up on Loading Frame

5.3 Load Testing of the Model Bridge

Eight different load points, four for each slab panel, were planned for the loading test. The loading device could only be moved in one direction along the bridge. Therefore, to test the other panel of the slab, it was necessary to move the bridge. The diagram of the loading position showing tie rods and the strain gage positions on the tie rods are shown in Figure 5.3. A total of eight tests on eight loading positions, numbered LP1 to LP8, were conducted. The numbers that follow the two letters for the loading positions corresponded to the order of testing. The strain gages were also labeled S1 to S15 for identification purposes. As shown in Figure 5.3, two strain gages were mounted into each of the three tie rods located near the middle span of the bridge. The extra gages were stand by, meant to be used if some of the gages did not work properly.

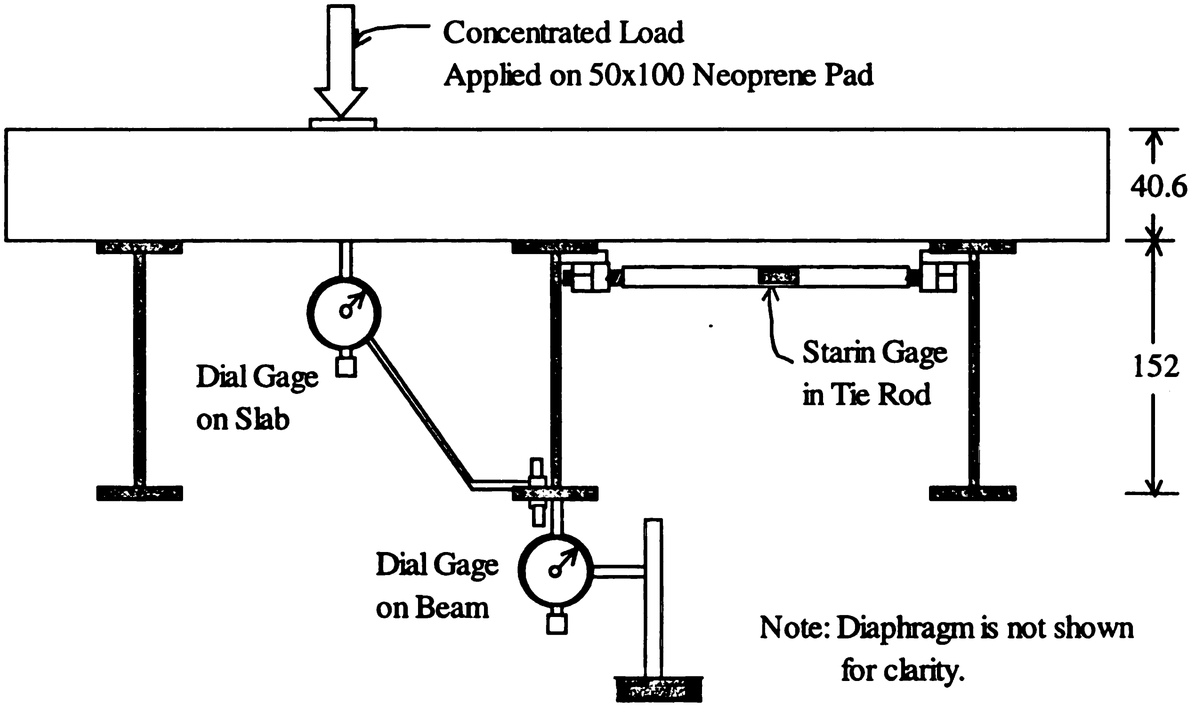
Concentrated Load
Applied on 50x100 Neoprene Pad
40.6
152
Dial Gage
on Slab
Starin Gage
in Tie Rod
Dial Gage
on Beam
Note: Diaphragm is not shown
for clarity.

Figure 5.2 Arrangement of Dial Gages and Strain Gage Position

The order of the testing at the various points of the slab was initially designed in order to minimize the influence of previous tests. The testing was started by applying the load near the end of the control slab panel (LP1) and continued on the other end of the strengthened slab panel (LP2). After three tests, however, it became apparent that such influence was so minimal that special precaution was unnecessary. Accordingly, the order of testing was rearranged to minimize the movement of the model bridge.

Using a load increment of 2.224 kN (500 lbs.), each test was continued until the slab failed. In each increment the load was applied for about two minutes to allow for the manual reading of deflections of the slab and the center beam, and strains in the tie rods (for the treated slab panel). Additional time was required for visual inspection of cracking in the slab as the load increased. The instance at which the first crack became visible was not easy to observe, however, with special precaution the load that caused the first visible crack could be approximately recognized.

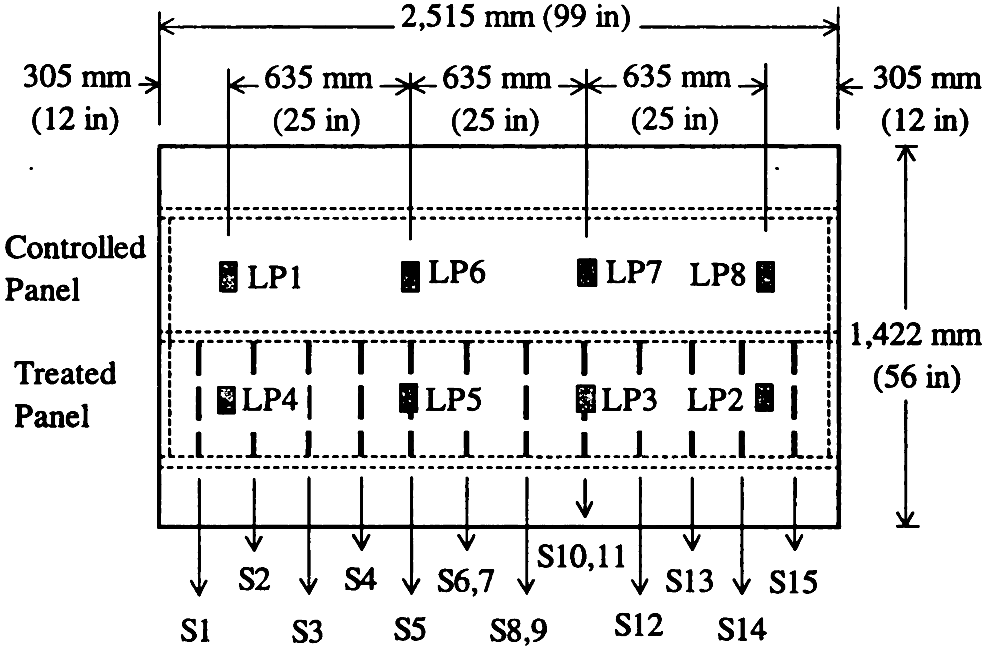
2,515 mm (99 in)
305 mm (12 in)
635 mm (25 in)
635 mm (25 in)
635 mm (25 in)
305 mm (12 in)
Controlled Panel
LP1
LP6
LP7
LP8
Treated Panel
LP4
LP5
LP3
LP2
1,422 mm (56 in)
S1
S2
S3
S4
S5
S6,7
S8,9
S10,11
S12
S13
S14
S15

Figure 5.3 Loading, Tie Rods, and Strain Gage Positions

For the eight tests conducted, each slab failed in punching shear and failures were marked by the formation of a punching cone with the top size slightly larger than the size

of the load pad. The bottom size of the cone, however, was significantly larger than the top size, which means the angle of the shear crack was greater than 45 degrees. Failure, in each case, was sudden with large slab deflection.

5.4 Recorded Data

Among the data recorded during the experiment were the load and the corresponding deflection of the slab and the center beam, and the strains in the tie rods. The data from the cylinder tests were also recorded to determine the strength of the micro concrete. The detail of the recorded data is summarized in the following sections.

5.4.1 Cylinder Test

The preparation of the test cylinders was discussed in chapter four where the cylinders were cast and cured following the ASTM procedures. Tests on the concrete cylinders were performed at the structural lab of Michigan State University prior to the load testing of the model slab. The original size of the cylinder was 76 m diameter by 152 mm (3 by 6 in). Prior to testing, the cylinders were cut to square their ends. Unfortunately, the surfaces of the cylinder ends could not be made perfectly square (parallel). Capping both ends of the cylinder, using a sulphur capping compound, would have been better than cutting them. Six cylinders were used for compression tests (ASTM C469), and four cylinders were used for split-cylinder tests (ASTM C496). The results of the tests are given in Table 5.1.

The cross sectional area of the cylinder was 4,560 mm2 (7.069 in2). With an average failure load of 116.00 kN (25,882 lbs.), the average compressive strength of the cylinder became 25,249 kPa (3,662 psi). For the split cylinder test, the average failure load was 51.79 kN (11,555 lbs). The average length of the cylinders, after they were cut, was 150 mm (5.91 in.). The relation between the failure load and the split tensile strength, f_{sp} (in psi unit) is given by

$$f_{sp} = \frac{2P}{\pi L D}$$

Where P is the failure load in lbs, L and D are the length and the diameter of the cylinder in inches, respectively. The corresponding average split tensile stress of the cylinder was 2,861 kPa (415 psi).

Table 5.1 Results of Cylinder Tests

No.	Failure Load, kN (lbs)	
	Compression Test	Split-Cylinder Test
1	121.01 (27,000)	46.84 (10,450)
2	114.65 (25,580)	50.20 (11,200)
3	114.07 (25,450)	55.89 (12,470)
4	118.55 (26,450)	54.23 (12,100)
5	114.47 (25,540)	
6	113.26 (25,270)	
Average	116.00 (25,882)	51.79 (11,555)

In general, the lower the compressive strength of the concrete, the higher it's relative tensile strength. The value of the splitting strength, f_{sp} of a normal weight concrete can be related to its compressive strength using a formula proposed by Mirza et al (Mirza et al, 1979) as given, in psi units, by

$$f_{sp} = 6.4\sqrt{f_c'}$$

For a split tensile strength of 2,861 kPa (415 psi), the corresponding compressive strength of the concrete would be 28.993 MPa (4205 psi).

The concrete strength obtained from the cylinder tests was 25.249 MPa (3662 psi). The result from compression tests was about 14.8% lower than the value calculated from the split-cylinder test. The main cause of the difference was suspected to be the cylinder ends that were not perfectly square. In this case, the result from the splitting test was more reliable than that from the uniaxial compressive test because the splitting test is not affected by the end surface condition of the cylinder. Accordingly, the result from the splitting test was used to determine the compressive strength of the model concrete.

The low value of compressive strength was also attributed to the high water cement ratio, which was meant to increase the workability of the micro concrete. For the purpose of the analysis, however, a value of 27.58 MPa (4000 psi) was assumed for the compressive strength of the model concrete. The sensitivity of the value of the compressive strength to the punching shear capacity of the concrete slab is low because the shear strength is related to the square root of the compressive strength of the concrete.

5.4.2 Loading Test

The data recorded during the testing of the slab included the load, the net deflection of the slab underneath the load application, the deflection of the center beam adjacent to the load, and the strain in the tie rods for the treated slab panel. The crack pattern of the slab was also observed. The cracking load, however, was very difficult to be recognized through visual inspection of the crack. Therefore, the crack load could not be determined accurately.

The mode of failure, for both types of slab panels, was punching shear, in which the failure surface was localized under the load in a circular manner. Prior to failure, flexural cracks developed on both surfaces of the loaded slab. On the bottom surface, the cracks originated from the center of the load and formed radial cracks. On the top surface, the flexural cracks started at the beam lines adjacent to the applied load. At a load near the failure load, shear cracks developed, originating on the bottom surface of the slab at a distance away from the load. As the load increased, the shear cracks grew to the top surface of the slab and formed the upper surface of the punch cone. Figures 5.4 (a) and (b) show the typical crack pattern on both surfaces of the slab.

The failure of the slabs was so sudden that it was difficult to observe the growth of the shear crack. After failure, however, the crack pattern was still visible even though the cracks closed as the load was removed. The load at which the slab started to crack was difficult to determine accurately because the initial crack was not visible. However, with some approximation and reference to the load deflection relationship, the cracking load could be recognized and shown in Table 5.2. The table also includes the load and maximum deflection at failure of the control and treated slab panels.

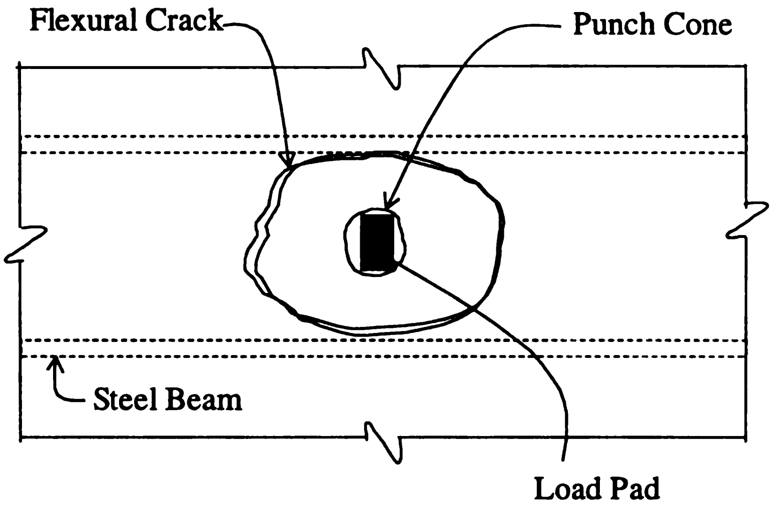
Flexural Crack
Punch Cone
Steel Beam
Load Pad

(a) Top Surface

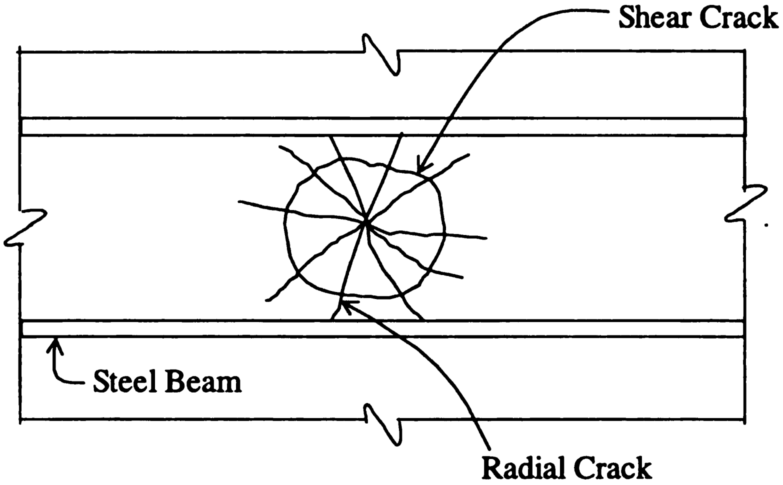
Shear Crack
Steel Beam
Radial Crack

(b) Bottom Surface

Figure 5.4 Typical Crack Pattern

Sample photographs of the top and bottom views of punched slab are shown in Figures 5.5 and 5.6. As can be seen from Figure 5.5, the top view of the failed slab loaded at LP3 shows the size of the upper cone (about the size of the load pad) that denotes a localized failure. Figure 5.6 shows the bottom part of the slab loaded at LP1, which shows a more extensive failure. In this case, however, the damage was caused by the penetration of the load pad into the slab due to delayed release of the hydraulic jack after failure. Nevertheless, the failure shows the radial and circular crack patterns similar to those reported in the literature.

Table 5.2 Crack Load, Failure Load, and Maximum Deflections of Test Slab

Load Position (Slab Type)	Crack Load kN (lbs)	Failure Load kN (lbs)	Max. Deflection, mm (in)	
			Beam	Slab
LP 1 (Control)	31.14 (7,000)	53.38 (12,000)	1.2 (0.049)	10.4 (0.409)
LP 6 (Control)	28.91 (6,500)	51.15 (11,500)	4.6 (0.182)	11.4 (0.450)
LP 7 (Control)	26.69 (6,000)	53.38 (12,000)	4.7 (0.186)	12.7 (0.500)
LP 8 (Control)	24.47 (5,500)	53.38 (12,000)	1.2 (0.046)	11.9 (0.468)
LP 2 (Treated)	40.03 (9,000)	60.05 (13,500)	1.4 (0.054)	5.7 (0.264)
LP 3 (Treated)	33.36 (7,500)	60.05 (13,500)	4.6 (0.180)	9.4 (0.370)
LP 4 (Treated)	31.14 (7,000)	60.05 (13,500)	0.9 (0.034)	9.2 (0.362)
LP 5 (Treated)	40.03 (9,000)	60.05 (13,500)	4.3 (0.170)	9.0 (0.356)

The load deflection relation of the slab and center beam, for each of the test point sets is given in Figures 5.7 and 5.8. It is apparent from Table 5.2 and Figure 5.7 that the slab with the additional tie rods cracked and failed at higher loads, and deflected less than the slab without tie rods. Comparing the load deflection curves of LP1 and LP2, and LP8 and LP4, it is apparent that the slab panel with added tie rods was significantly stronger and stiffer than that without tie rods. The same observation is obvious by comparing the curves for LP3, and LP5 and LP6, and LP7.

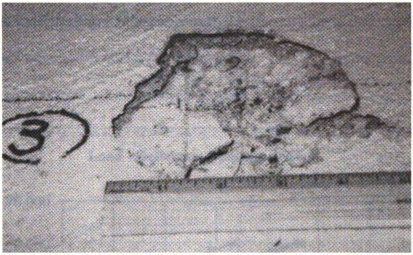

Figure 5.5 Top View of Punching Failure at LP3

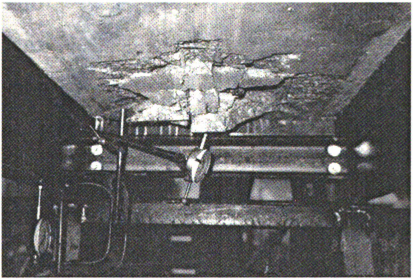

Figure 5.6 Bottom View of Punching Failure at LP1

The deflection of the center beam was also significantly affected by the addition of tie rods. From Figure 5.8, it is apparent that, when loaded near the supports, the deflection of the beam was less than that when loaded near the mid-span of the bridge. With added tie rods, the beam deflections were significantly lower than that without tie rods.

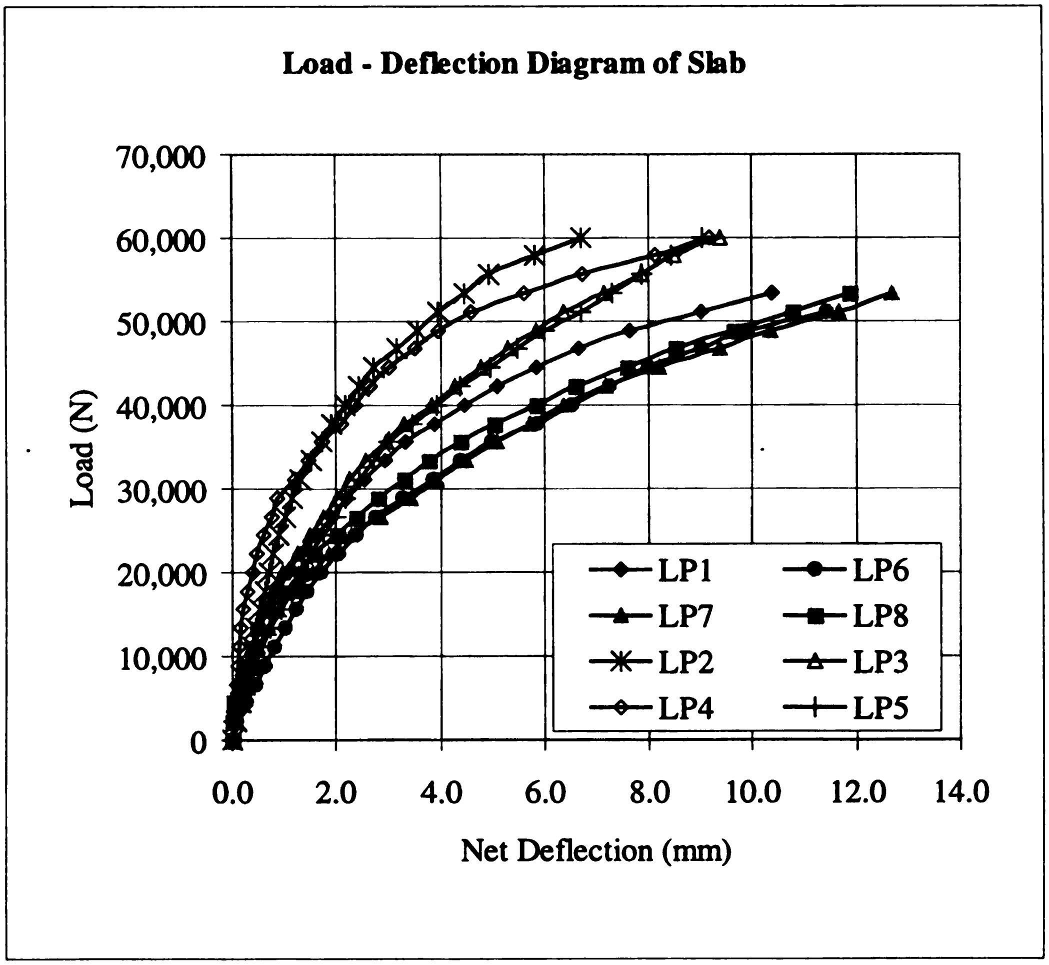

Figure 5.7 Load Deflection Diagram of Slab

Typical behavior of the rods is presented in the form of the load-strain curves given in Figure 5.9. When the load was applied at LP2 and LP3, most of the connection in the tie rods adjacent to the load failed (at a load of about 20 kN). This observation indicates that the welded connection was the weakest point in the structures. Therefore, prior to the next test, the welds were strengthened by adding another layer of weld. When loads were applied at LP4 and LP5, the strain developed in the tie rods was higher than that of the previous tests. Nevertheless, some of the welds also failed before the failure of

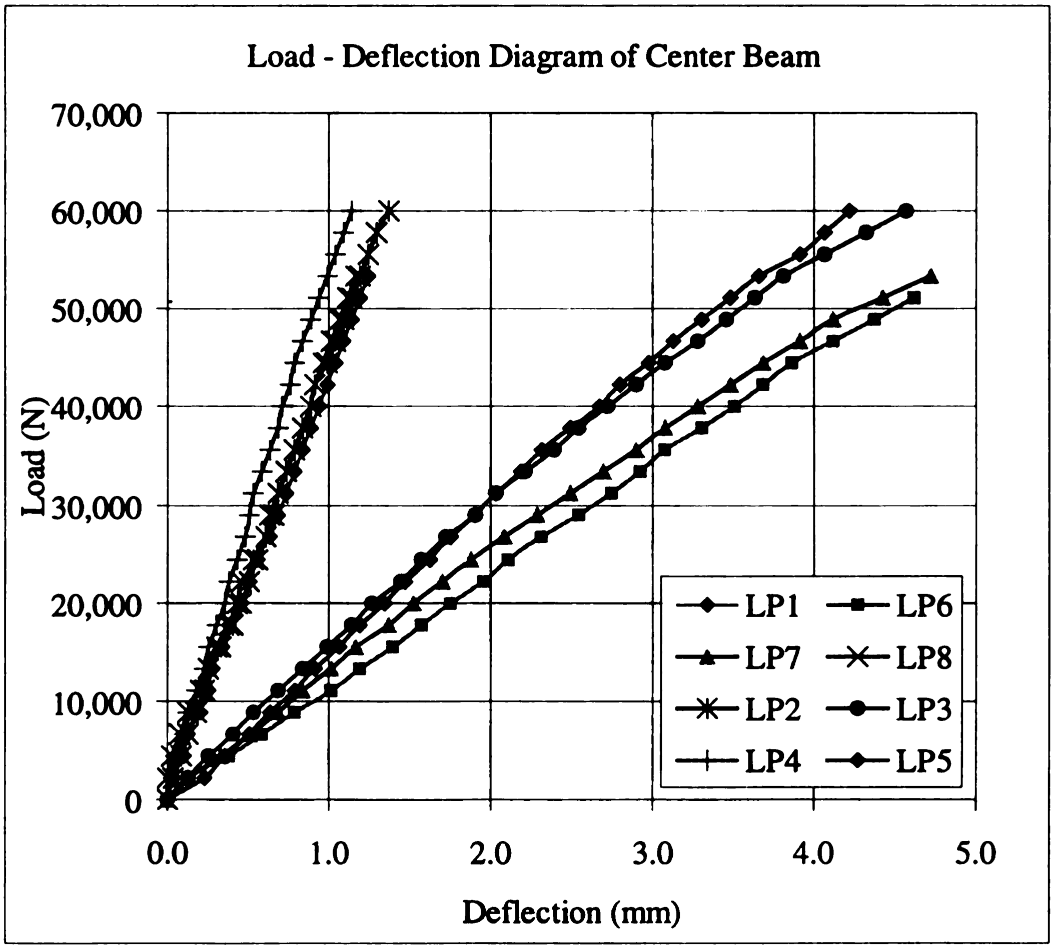

Figure 5.8 Load Deflection Diagram of Center Beam

the slab, but at a higher load level than those applied at LP2 and LP3. The failure of the weld, however, was a strong indication that the tie rods were under a high magnitude of stress due to the arching action developed in the slabs.

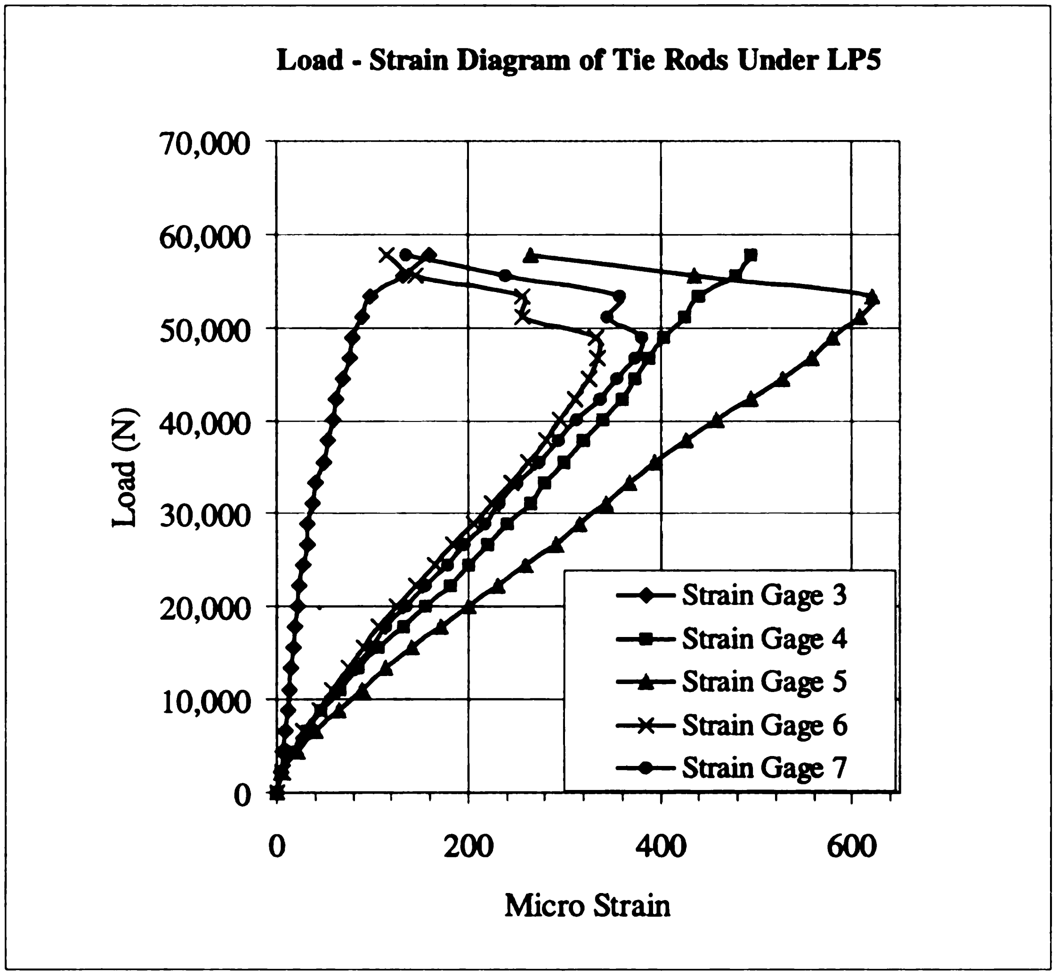

Figure 5.9 Load Strain Diagram of Tie Rods

As shown in Figure 5.9, the strain in tie rod 5 (S5 in Figure 5.3), and 6,7 (S6,7) dropped at a load about 50,000 N (11,240 lbs) because of the connection failure. Tie rods 3 and 4 (S3, S4) took over the tensile force until the slab failed. Strain developed in tie rod 3 (S3), which was two spaces away from the load, was so small compared to that of tie rod 5 (S5). The maximum strain in tie rod 5 (S5) was about 620 micro strain, which corresponds to about 50% of the yield strain of a 250 MPa (36 ksi) steel. At lower load levels, the strain in the tie rods was significantly lower.

Additional observations were made after the tests to inspect the steel reinforcement, shear connectors, and steel beams for stress development. The steel reinforcement around the failed slab was visually observed and yielding in the steel was detected. During the demolition of the concrete slab, there was no sign of yielding of the steel bars out side the load sites in the slab.

The 8 mm shear connectors, attached to the main girders and edge beams, were also carefully examined during the demolition of the slab. It was found that the connectors were perfectly bonded in the concrete and there was no sign of overstress in the connector or in the concrete around it. The bottom flanges of the steel beams were also observed for signs of overstress. However, no such sign was found which means that during the load testing the steel beams were within their elastic limit. Further discussion on the experimental results is given in Chapter 6 along with the results from the analyses.

CHAPTER 6

PRESENTATION AND DISCUSSION OF RESULTS

6.1 Introduction

The purpose of this chapter is to present and discuss the results from the analysis and experimental program presented in Chapter Three and Chapter Five. Analyses of the punching shear strength of RC deck slabs were conducted using the mechanical punching model of restrained slabs and the ACI Code provisions on punching shear strength of RC slabs. In addition, FEA were conducted to obtain the response of the deck under a full range of loads, from zero up to failure. Expectedly, the FEA would simulate the slab response observed during the experiment in the laboratories, which includes: the ultimate load and deflection of slabs, the load deflection relationships for the slab and the center beam, and the load strain relationship for the tie rods.

The results from the analyses are discussed and compared to the experimental results observed during the test. Direct comparison of the analyses and test results was possible because the actual dimensions of the model bridge, obtained from the measurements during the experimental program, were used in the analyses. Results from the FEA however, were discussed in more detail since these analyses provided more comprehensive responses of the structure. For the purpose of comparison between the test and FEA results, only the slab panels loaded near the mid-span of the bridge were considered. More detail on the results of the experiment and the analyses are presented and discussed in the following sections.

6.2 Punching Strength of Slabs (Analyses and Test Results)

The punching shear strength of the model slab, according to the punching theory of a restrained slab, was graphed for various values of restraint factor as shown in Figure 6.1. Inserted in the graph are the average values from the experimental program for the control and treated slab panels, and the results from the ACI Code formulae. The average test results were 60,050 N (13,500 lbs) and 52,822 N (11,875 lbs) for slab with and without tie rods, respectively. The ACI Code formulae gave nominal shear strengths of 25,162 N (5,657 lbs) for the RC slab, and 36,936 N (8,304 lbs) for the prestressed concrete slab.

From the graphs, it is apparent that with restraint factor values of 0.50 to 0.90 the strength of the slabs linearly increases from about 42.863 kN (9.636 kip) to 66.499 kN (14.95 kips). The corresponding uncorrected deflections of the slab with restraint factors of 0.5 and 0.9 were 1.76 mm (0.0694 in) and 1.26 mm (0.0498 in), respectively. The observed values for the deflections were 13.65 mm (0.537 in.) and 16.7 mm (0.657 in.) for the slab with and without tie rods, respectively. Comparing the analysis results to the observed values, it is apparent that the punching theory of a restrained slab could predict the punching load, but could not predict the deflection of the slab.

The plotted lines (Figure 6.1) for the observed strength of the slabs with and without tie rods cross the theoretical line at two different points that correspond to two different values of the restraint factor. Using linear interpolation, the failure loads of the test slab panels corresponded to a restraint factor of about 0.663 for the control slab panel, and 0.786 for the slab panel with tie rods (dashed area in Figure 6.1). The restraint factor values of deck slabs tested by Hewitt and Batchelor were between 0.52 and 0.74

(1975). Apparently, the restraint factor value of 0.663 for the control slab panels is in agreement with those reported in the literature. The 0.786 value for the slab with tie rods also in agreement with the Hewitt and Batchelor report, in which, with additional tie rods, the restraint factor of the slab becomes higher.

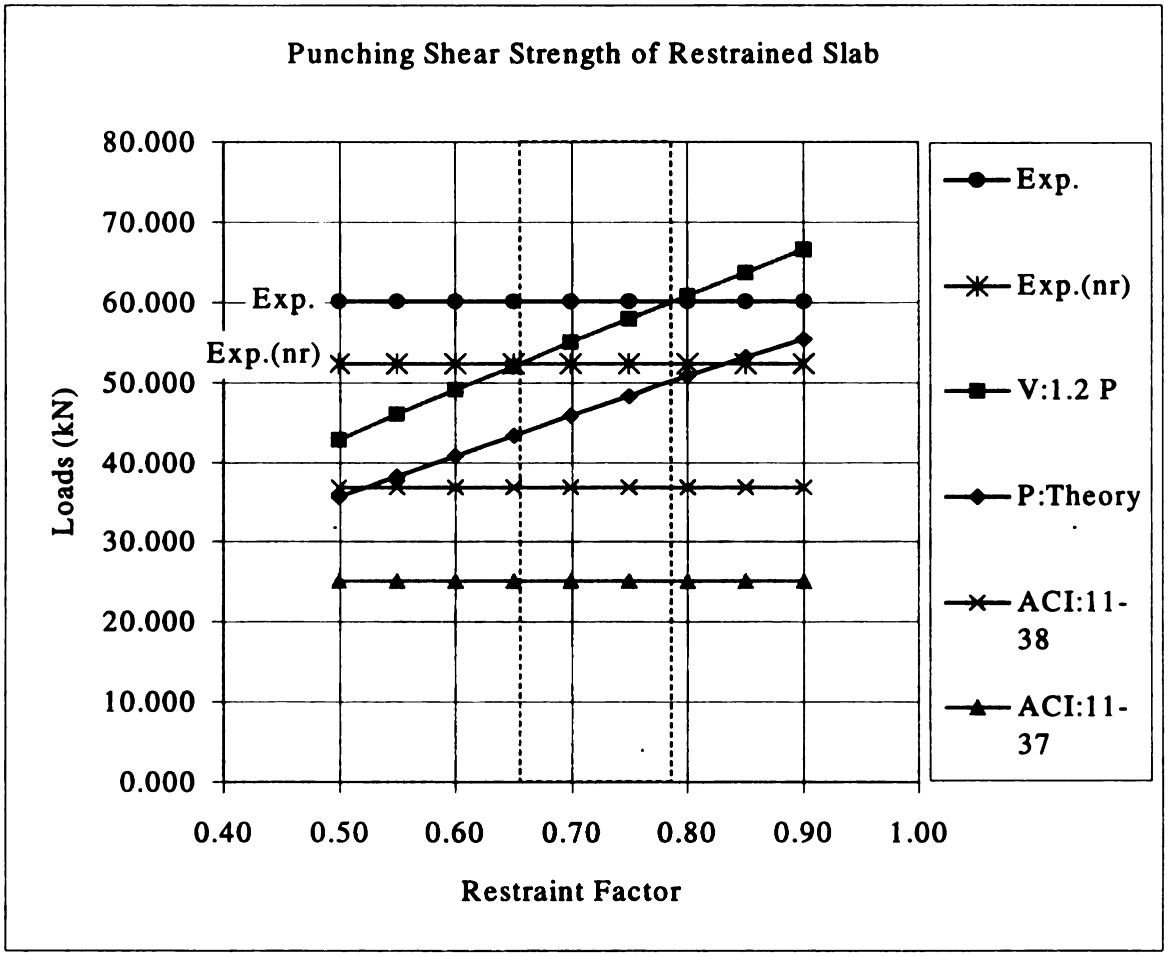

Figure 6.1 Analysis Results: Punching Strength of Slab

Referring to the test values, the addition of tie rods increased the lateral restraint of the slab by a factor of 18.2%. The corresponding increase in the strength of the slab was about 13.7%. The slight increase in restraint factor is attributed to the failure of the tie rod connections prior to failure of the slabs. Were the connections stronger, the slab with added tie rods would fail at a higher load, and therefore, the restraint factor of this slab will be higher.

The nominal punching shear strength of RC slabs, given by the ACI Code formula (ACI: 11-37), is substantially lower than that obtained from the punching shear theory of restrained slabs. Incorporating a compressive stress of 3.448 MPa (500 psi) into the ACI formula for prestressed concrete slabs (ACI: 11-38), however, increases the strength of the slab from 25.162 to 36.936 kN (from 5.657 to 8.304 kips), which is a 47% increase. ACI Equation 11-37 yields a strength value of about 48% of the measured strength of the control slab. ACI Equation 11-38 on the other hand, yields a value about 71% of the test value. This increase implies enhancement of shear strength due to the presence of compressive membrane stress.

The ACI formulae on punching shear strength of RC slabs are developed mainly for the purpose of designing the shear capacity of slabs loaded or supported by a column, such as in flat slab structures or in column footings. These formulae do not take into account any shear strength provided by the flexural reinforcement. They also neglect any conditions at the slab boundaries, so that is not appropriate for a restrained slab. Accordingly, the formulae give shear strength values lower than that obtained from the punching theory of a restrained slab.

FEA and Test Results

Data regarding the failure loads and deflections obtained from the FEA and test results are summarized in Table 6.1. It is apparent from the table that the FEA could not

Table 6.1 Data from FEA Compared to Test Results

FE Model					Slab With Tie Rods		Slab Without Tie Rods	
Name	f_{cy} / f_c	ε_{cy}	f. ratio	t. stiff.	P/ Pe.	Δ/Δe.	P/Penr	Δ/Δenr
M1	12.5%	0.0030	1.25	0.0025	57%	30%	63%	27%
m1a	10.0%	0.0015	1.16	0.0020	52%	25%		
m1b	12.5%	0.0030	1.16	0.0040	64%	35%		
m1c	12.5%	0.0030	1.16	0.0060	65%	36%		
m2	12.5%	0.0050	1.30	0.0075	77%	61%	84%	47%
m3*	12.5%	0.0050	1.30	0.0075	101%	87%	81%	51%
m4	12.5%	0.0030	1.20	0.0100	73%	42%	73%	32%
m5	50%	0.0030	1.20	0.0075	94%	43%		
m6	50%	0.0015	1.16	0.0020	51%	22%		
m82	12.5%	0.0050	1.30	0.0075	25%	11%		
m27	12.5%	0.0050	1.30	0.0075	26%	12%		

* This model uses reduced Young's modulus.
Pe is the average experimental load = 60,050 N (13,500 lbs),
Δe is the average experimental deflection = 13.65 mm (0.538 in.),
Penr is the average experimental load for control slab = 52,266 N (11,750 lbs),
Δenr is the average experimental deflection for control slab = 16.7 mm (0.659 in.).

predict the experimentally observed values at failure, in which the ratios between the analysis and the measured values are less than unity. Model m3 however, matched the measured load value well, but overestimated the slab stiffness at failure by 13%. However, in this model, the value for the concrete elastic modulus was arbitrarily

reduced to 50% of the commonly used value of 24,822 MPa (3.6E6 psi) for a 27.58 MPa (4,000 psi) concrete, in an attempt to study the effect of varying value of elastic modulus.

Models m1, m1a, m1b, and m1c show the effect of varying values of tension stiffening on the models' responses. In model m1, using a tension stiffening value of 0.0025 the analysis (therefore the solution) terminated at a load of 57% of the observed failure load. The strain at which the 500 MPa (72.5 ksi) steel reinforcement yields is about 0.0025. The value of 0.0025 also corresponds to a maximum tensile strain of 25 times the crack strain of plain concrete, which is about 0.0001. Therefore, model m1 was meant for the reference model to which the other models are compared.

Referring to the results of model m1, using tension stiffening of as much as the yield strain for the steel reinforcement does not seem to be appropriate for this problem. Accordingly, to study the effect of tension stiffening, values of 0.002, 0.004, and 0.006 were used for m1a, m1b, and m1c, respectively. The responses of these models were not distinguishable from each other in a load deflection diagram. The model with a higher tension stiffening value however, gave a longer (higher load and deflection magnitudes) response than the model with a lower value of tension stiffening.

In model m1c, using a tension stiffening value of 0.006, the ratios for the load and the deflection between the FEA and test results were only 65% and 36%. In model m4 using tension stiffening value of 0.01 results in load and deflection ratios of 73% and 42%, respectively. The tension stiffening value of 0.01 is the maximum value reported for heavily reinforced concrete (Schnobrich 1986). For the slab in the present study a lower value for tension stiffening is more appropriate. However, higher failure ratio is possible due to the confinement provided by the membrane action in the vicinity of the loaded slab area. Accordingly, a value as high as 1.3 was used for the failure ratio of concrete in compression.

In model m2, a tension stiffening value of 0.0075 was used with a failure ratio in compression of 1.3. The load and deflection ratios for this model were 77% and 53%, and 84% and 47% for the slab with and without tie rods, respectively. In models m5 and m6 the ratio of elastic stress limit and the ultimate compressive stress was set to 50%; means that the stress strain diagram of the concrete becomes nonlinear at a stress 50% of its compressive strength. Model m5, with tension stiffening value of 0.0075, gave a failure load ratio of 0.94, but a deflection ratio of 0.43. Model m6 on the other hand, gave ratios of 51% and 22% for the load and deflection, respectively. The material model used for model m6 is similar to that for model m1a, where the value for the tension stiffening was 0.002 with failure ratio of 1.16, and plastic strain ε_{pu} of 0.0015. With higher elastic stress limit, model m6 failed at a lower load and deflection than model m1a.

Models m82 and m27 gave very short responses compared to the observed response. The analysis for these models terminated at early stage of load increment because the system could not reach equilibrium conditions during the iteration process. The probable cause of this problem is the large size of the models that cause unstable analysis. The load deflection curves for these models however, fit the curve of model m2 very well, only they were shorter (see Figure 3.7 in chapter three).

6.3 Load Deflection Diagram of Slabs (FEM and Test Results)

The global behavior of the slab under varying load level could not be judged only from the failure load or deflection. The load deflection diagram of the slab would be a more appropriate measure of the effect of adding tie rods to the behavior of the deck slab. For this reason, the recorded data from the experimental program were analyzed and presented in Figures 6.2 and 6.3. In these diagrams, the total slab deflection was used instead of the net deflection to enable direct comparison to the diagram obtained from the FEA. During the experiment the net deflection of the slab (deflection of slab relative to the deflection of the center beam adjacent to the applied load) was measured. The total slab deflection was calculated as the sum of the net slab deflection and the center beam deflection. The consequence of this procedure is the introduction of a possible source of additional error in the test results.

In Figure 6.2, the observed load deflection diagrams of the slab loaded near the mid-span are presented. It is apparent that the slab panels with additional lateral restraint (tie rods), as shown by LP3 and LP5, are stronger and stiffer than the control slab without tie rods (LP6 and LP7). This statement also holds true for the slab panels loaded near the supports, as shown in Figure 6.3. Accordingly, from the experimental results, it is clear that the addition of tie rods increased the failure load, and at the same time, it significantly reduced the deflection of the slab. Therefore, additional tie rods improved the global behavior of the slab.

The diagrams for the slab panels near the mid-span of the bridge showed a good correlation where the two lines from two different tests were very close together. The test results for the slab panels near the support, however, were not as good as those near the middle span. For the slab panel loaded at LP1, the slab deflection is less than that when loaded at LP8. Theoretically, they should be the same since the slab panels are similar. One possible reason for the difference is the order of testing. The slab panel loaded at

LP1 was tested first while the later was tested last. When loaded at LP8, the slab panels adjacent to the tested slab panel were already tested and failed. Variability in the material properties may also contribute to this difference along with possible measurement error during the test. Despite the difference between the two, the lines for the slab panels with tie rods clearly deviated from those of slab panels without tie rods, which indicated an improvement in the slab behavior due to additional tie rods.

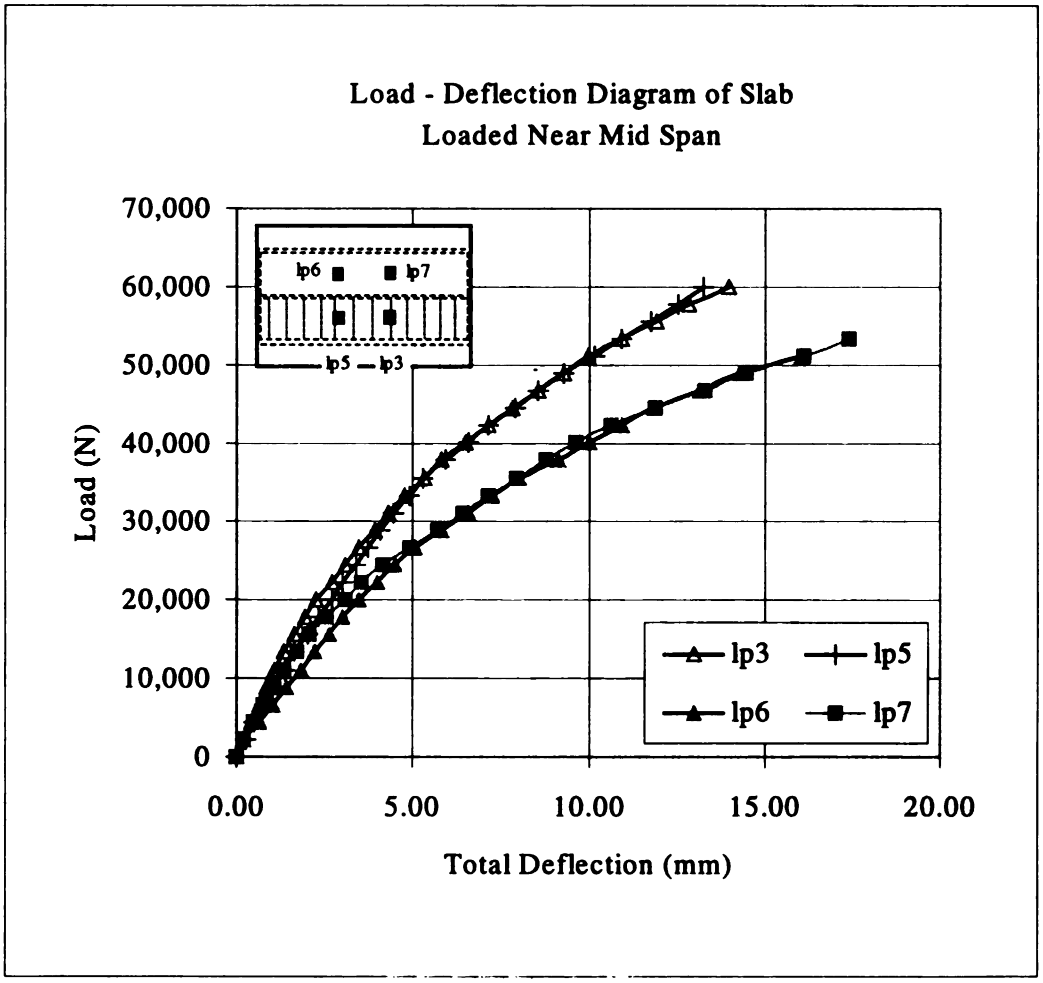

Figure 6.2 Observed Load Deflection Diagram of Slab Loaded near Mid-span

Figures 6.2 and 6.3 also showed that the slab panels with tie rods exhibited stiffer responses than those without tie rods. The deflections of the slab panels with tie rods were considerably lower than those of the control slab panels. These small deflections indicate smaller strains, and accordingly, lower stresses develop in the slab. From these figures, the effect of tie rods can be seen at a load less than 4,000 N (900 lbs), which in a prototype slab, the magnitude of the load would be less than 100,000 N (22,481lbs).

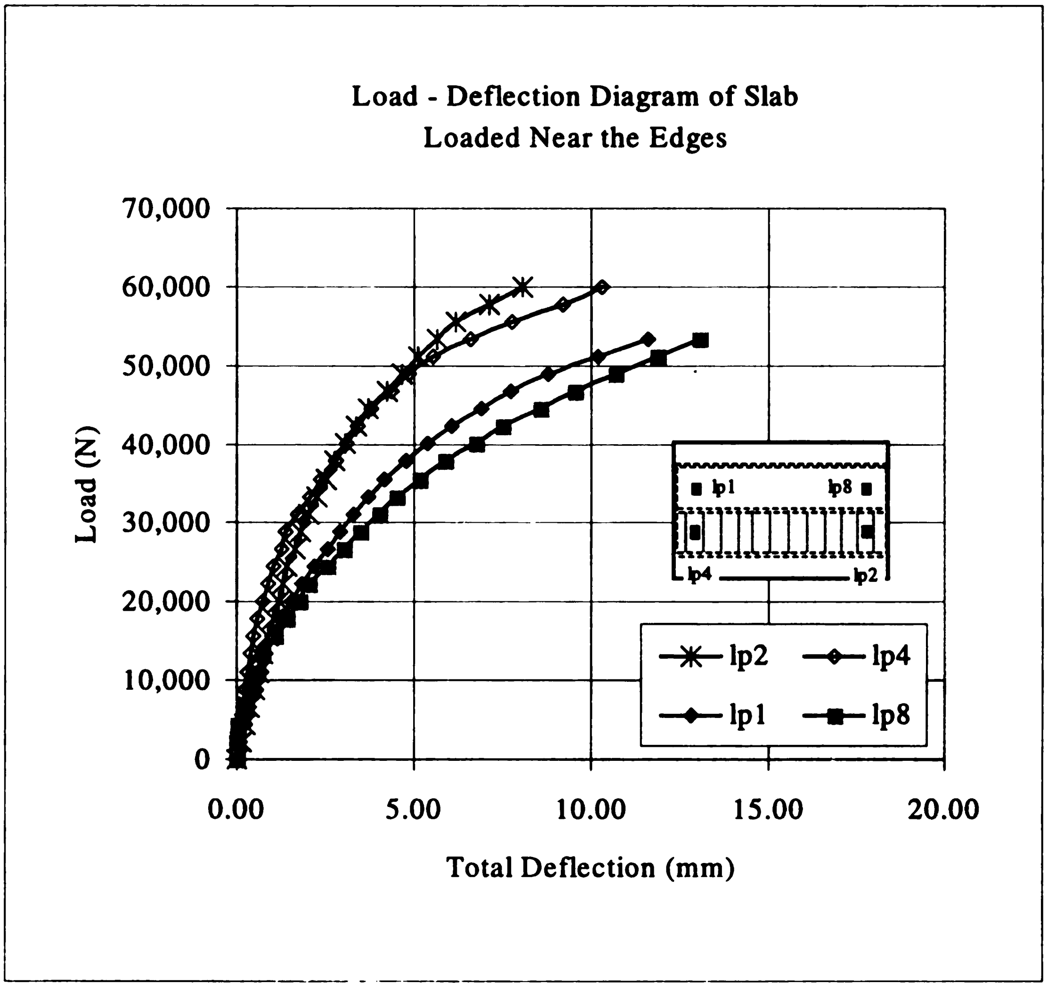

Figure 6.3 Observed Load Deflection Diagram of Slab Loaded Near the Edges

Knowing that the AASHTO wheel load (with 1.3 impact allowance) is about 95 kN (21 kip), then the tie rods would actually improve the behavior of the slab under service load. At higher load levels the improvement in the slab stiffness is more pronounced although such effect would be more desirable at a lower load level.

It is also apparent from Figures 6.2 and 6.3 that the load deflection relations of the tested slabs are highly nonlinear, starting at load levels below 10,000 N (2,248 lbs), which is about 10 to 15% of the failure loads. This is in agreement with the stress strain diagram of concrete material, where at lower stress levels the material behaves (nearly) linearly, and at higher stress levels the rate of strain becomes higher than the rate of stress.

In the FE models, the load was applied near the mid-span of the bridge for the following two reasons. Firstly, to avoid the effect of edge beams near the support. Secondly, to take advantage of the better test results near the mid-span in which the band of the data is narrower. The larger slab deflection near the mid-span of the bridge would also make comparison of he test and analysis results easier.

The FEA results are presented in Figure 6.4 for the slab with tie rods, and in Figure 6.5 for the slab without tie rods. Included in the figures are the test results of the slab panels loaded at LP3 and LP7 for the slab panels with and without tie rods, respectively. In Figure 6.4 only five models (out of eleven models listed in Table 6.1) were included. The rest of the models overly predicted the stiffness of the test slab, and are not included in the diagram.

From the five models, all but model m3 predicted the actual response of the slab at lower load levels very accurately. At higher load levels, however, the diagrams deviated from the observed response variously. From Figure 6.4 it is apparent that the model with higher failure ratio (m2) provided a response that best fits the observed response up to a load of about 35,000 N (7,868 lbs). Model m3, with failure ratio and tension stiffening values equal to those for m2, provided the best response at higher load levels.

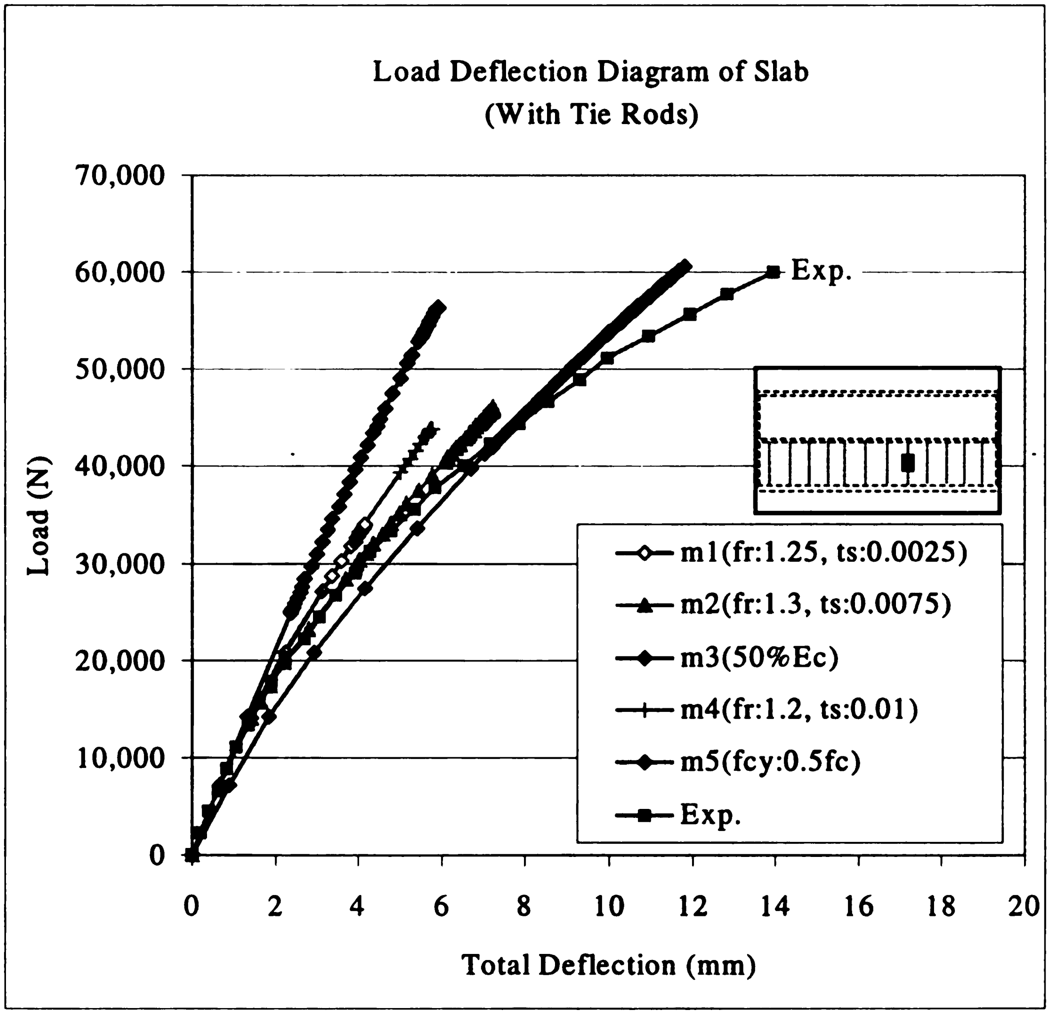

Figure 6.4 Measured and Predicted Load Deflection Diagram of Slab Loaded at LP3

The models with higher tension stiffening values gave solutions in which the models fail at higher load and deflection values. With a low value of tension stiffening, the analysis terminated at a lower load increment. The reason for this early termination of the analysis is due to a failure of convergence achieved during the iteration process.

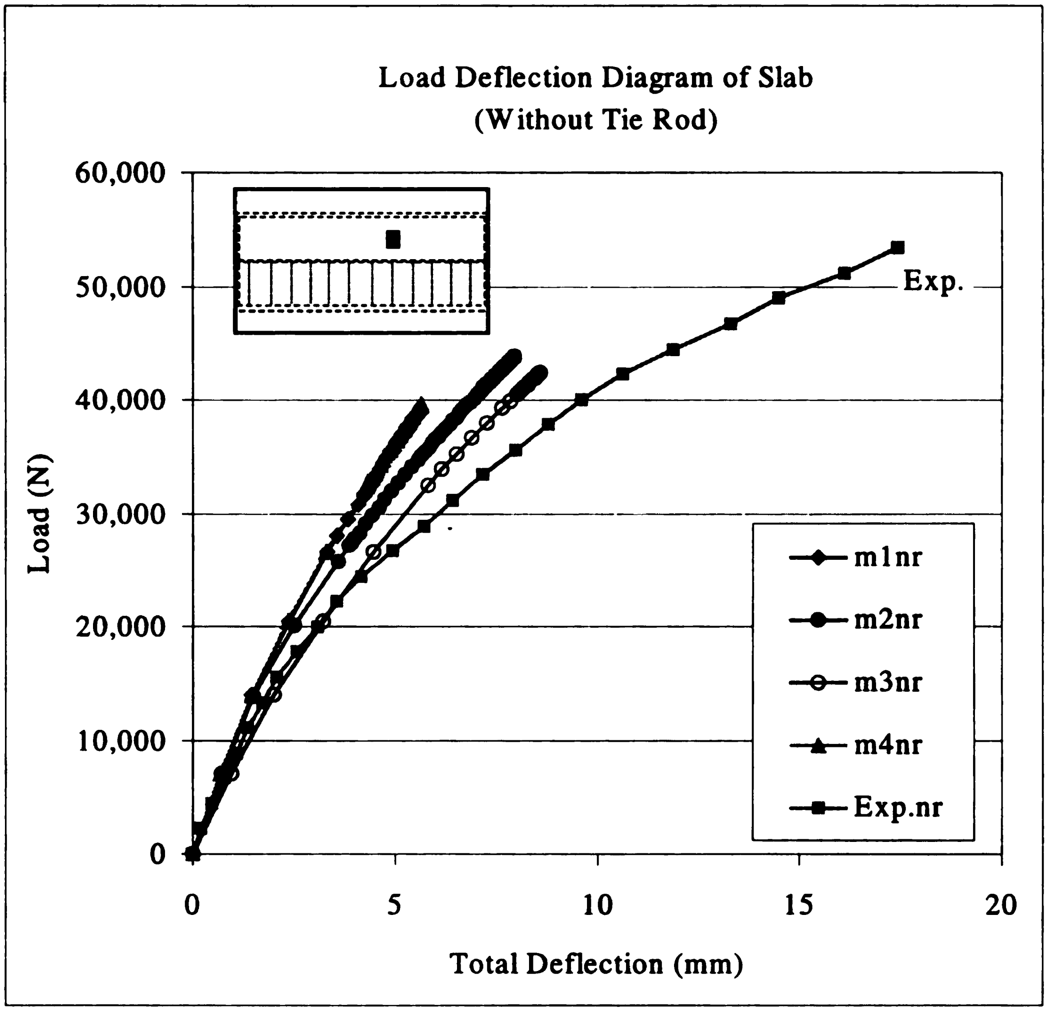

Figure 6.5 Measured and Predicted Load Deflection Diagram of Slab Loaded at LP7

The FEA results for the control slab panels shown in Figure 6.5 are not as satisfactory as those for the slab panels with tie rods. Among the four models, m3nr with a reduced modulus of elasticity fitted the experimental curve better than the other models. However, m2nr also yielded response reasonably close to the observed response. From the responses of models m2 and m2nr shown in Figure 6.4 and 6.5, it is apparent that the FE models appeared to fail at a load and deflection significantly lower than the observed values. Model m2 for the slab with tie rods ceased computing at a load of 77% of the observed failure load, and a maximum deflection of 52% of the observed value. In model m2nr, these ratios were 84% and 47% for the load and deflection, respectively. The models with a reduced Young's modulus gave better load and deflection ratios: 101% and 87% for m3, and 81% and 51% for m3nr. Despite the better load and deflection ratios, m3 underestimates the stiffness of the slab at lower load levels.

Judging from the response of m2 and m2nr, the FEA could not predict the load deflection diagram of the tested slab up to failure. The models failed at an average load about 20% below the observed failure load with a corresponding average deflection of 46% less than the observed value (see Table 6.1). During the tests however, the concrete slabs actually have failed at a load much lower than the ultimate load through the formation of shear cracks, which were not easy to observe. The dowel action between the steel reinforcement and the concrete made it possible for the slab to sustain a higher load after the cracks formed, as was marked by the excessive deformation in the slab prior to failure. In the FEA, failure was also determined by the failure of concrete. The dowel action was modeled in tension stiffening, and failure of concrete was modeled in failure ratios. As soon as the concrete stress reaches its limiting value the slab will not take additional load, and therefore the analysis terminates, which means that the slab has

failed. These arguments explain the reason the FE models fail at a significantly lower load than the observed value.

The model with a lower Young's modulus value gave a higher response because a smaller load increment is sufficient to cause additional deflection that helps the iteration process reaches convergence. Using higher values of the plastic strain and failure ratio also allows the analysis to continue to higher values.

During the test, the tie rod connections failed before the slab, which possibly caused larger deformation than if the tie rod connection were stronger. In the FEA the tie rods were not allowed to fail, so the model's response was stiffer than the observed response. This contributed to the difference between the FEA and measured responses at higher load levels (after the connections have failed).

Despite the differences between the observed and the FEA results, the FEA are more meaningful for studying the global behavior of the model slab up to relatively high load levels. Further discussion on the correlation between the observed and the FEA results on beam deflections and strains development in tie rods are continued in the next sections.

6.4 Deflection of Center Beam (FEA and Test Results)

The deflection of the center beam adjacent to the load was also recorded and its load deflection diagram was developed and is presented in Figures 6.6 and 6.7. Included in these diagrams are the results from the FEA. As expected, the deflection of the center beam was linearly proportional to the load up to failure. The reason for this linearity is that the beams were conservatively designed taking into consideration the failure load of the slab. Furthermore, the addition of tie rods significantly affected the deflection of the center beam. One possible reason for this effect is that with tie rods, the two beams share the applied better than without tie rods.

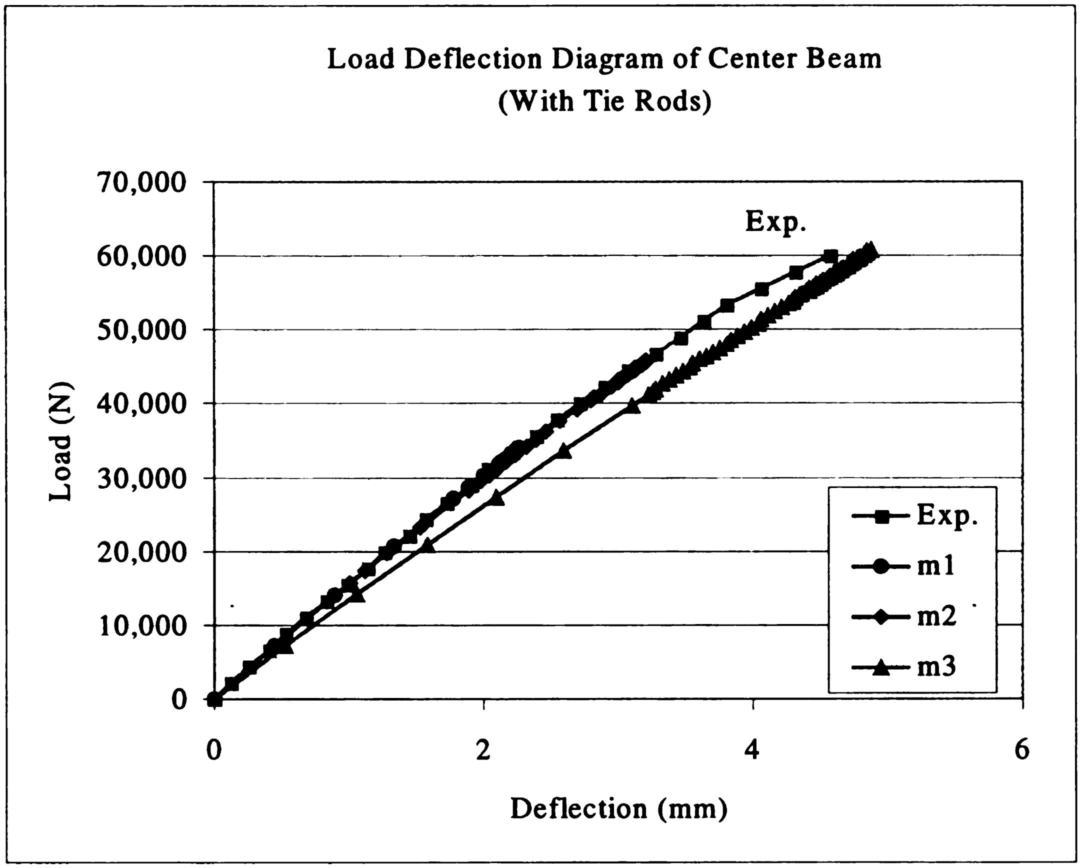

Figure 6.6 Measured and Predicted Load Deflection Diagram of Center Beam Loaded at LP3 (Slab with Tie Rods)

From Figure 6.6 it is apparent that FE models m1 and m2 mimic the load deflection diagram of the center beam very well. These models, however, failed at a load significantly lower than the actual failure load, in which failure was determined by the failure of the concrete slab. Model m3 matched the actual failure load, but slightly

underestimated the actual stiffness of the beam. From Figure 6.6 on the other hand, FE models m2nr, and m3nr predicted the load deflection curve of the center beam better than does m1nr. Model m2nr fitted the observed curve the best. These results agreed with the results for the slab deflection where model m2 gave responses better than the other models.

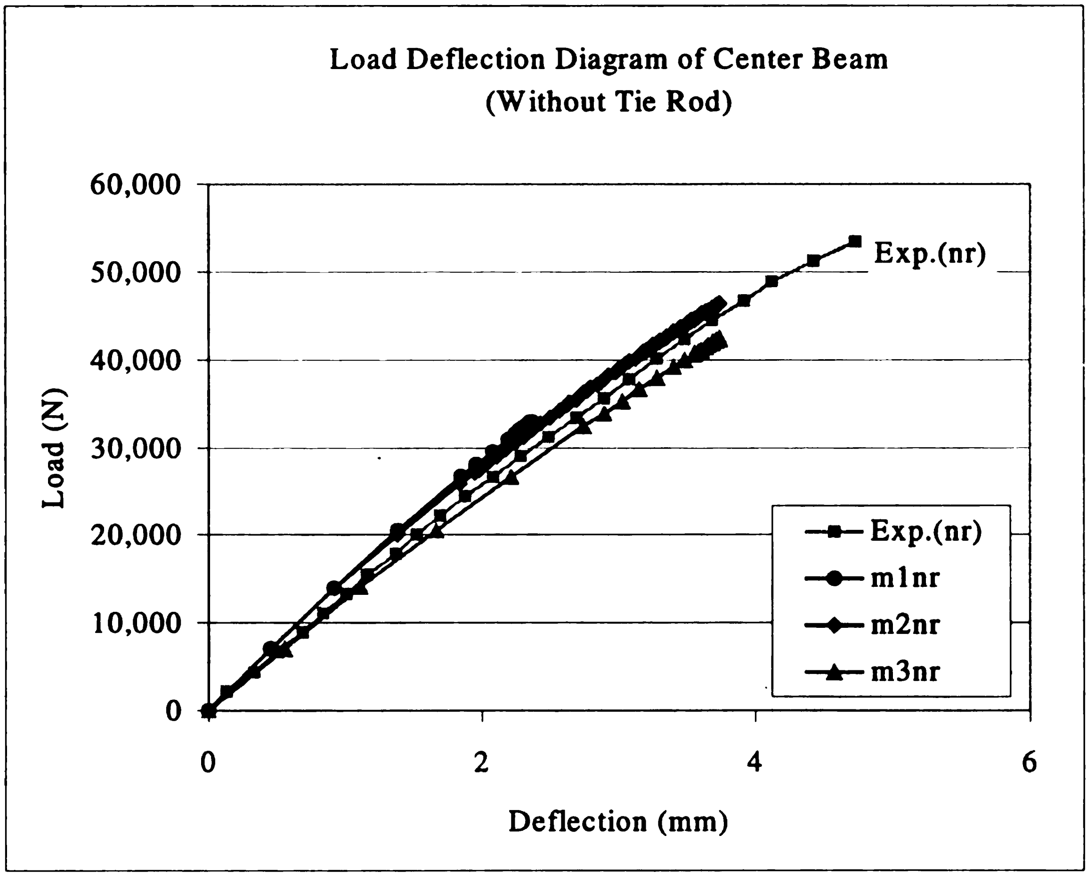

Figure 6.7 Measured and Predicted Load Deflection Diagram of Center Beam Loaded at LF7 (Slab without Tie Rods)

Comparing the curves for the slab and beam deflections, it is obvious that the FEA mimic the beam response much better than that of the slab. The explanation to this phenomenon lies on the variables associated with the modeling of the concrete material, which is not as simple as that for the steel material model. Steel on one hand is a relatively homogeneous material that behaves linearly up to a high stress level; in the present study the steel beams were within their elastic limit until failure of the slab. Concrete on the other hand, is a nonlinear material starting at a relatively low stress level. In addition, research on FEA of concrete structures is not yet as advanced as that of other structural materials because the application of concrete structures does not usually require analysis in great precision. In addition, FEA of RC structures involving true 3-D models are not yet as popular as applications that use shell or axisymmetric elements.

The observed behavior of the center beam loaded at LP3, LP5, LP6, and LP7 is presented in Figure 5.8 in chapter five. From this figure, the deflection of the beam when the load was applied to the slab with tie rods near the mid-span of the beam (at LP3 and LP5), was less than those when the load was applied at LP6 and LP7 of the control slab. The probable cause of the difference is the order of the testing; when the loads were applied at LP6 and LP7 the slab at LP3 and LP5 had already been tested and failed, that influenced the properties of the composite beam section, decreasing its stiffness. At load points near the support (LP1, LP2, LP4, and LP8), however, such effect was so small that it was not apparent.

In the FE models, the effect of testing order did not exist because the slab was loaded at one location at a time. Any differences between the observed and the FEA results could also be attributed to this factor. Nevertheless, the global behavior of the center beam was accurately modeled in the FEA. The model using a reduced Young's modulus (m3nr) produced larger beam deflection than did the other models, which means

that the FEA correctly modeled the composite action between the concrete deck and the steel beam.

6.5 Strain in Tie Rods (FEA and Test Results)

Another important parameter to study the effect of adding tie rods to a deck slab is the strain development in the tie rods. The effect is determined by the magnitude of strains at lower load levels under which the bridge slab operates. Figures 6.8 and 6.9 show a typical load strain diagram in the tie rods underneath and adjacent to the load when the load was applied at LP5.

The strains in the tie rods underneath the applied load started to develop at a very low load level, which means that the arching action in the slab is well developed under the service load. This verifies that the skepticism whether the arching action takes effect at low load levels is unjustified.

From the experimental program presented in chapter five, the average maximum strain in the tie rods in the vicinity of the load was about 0.00035. With steel Young's modulus of 200,000 MPa (29,000 ksi) the above strain corresponded to an average tensile force of 11.287 kN (2,538 lbs) in the 12.7 mm (0.5 in.) square bar. The corresponding stress in the 8 mm (0.315 in.) tie rods are about 224.6 MPa (32.6 ksi), which is within the elastic limit of the steel. Accordingly, the size of the tie rods used in the model-bridge is adequate even if the slab is overly loaded.

As shown in Figure 6.8, models m1, and m2 fitted the test curve better than model m3. It is also clear that at higher load levels the observed response was much stiffer than the model's curves, because the tie rod connection failed during the test. Were the connection stronger, the observed and FEA results would be better correlated up to a higher load level.

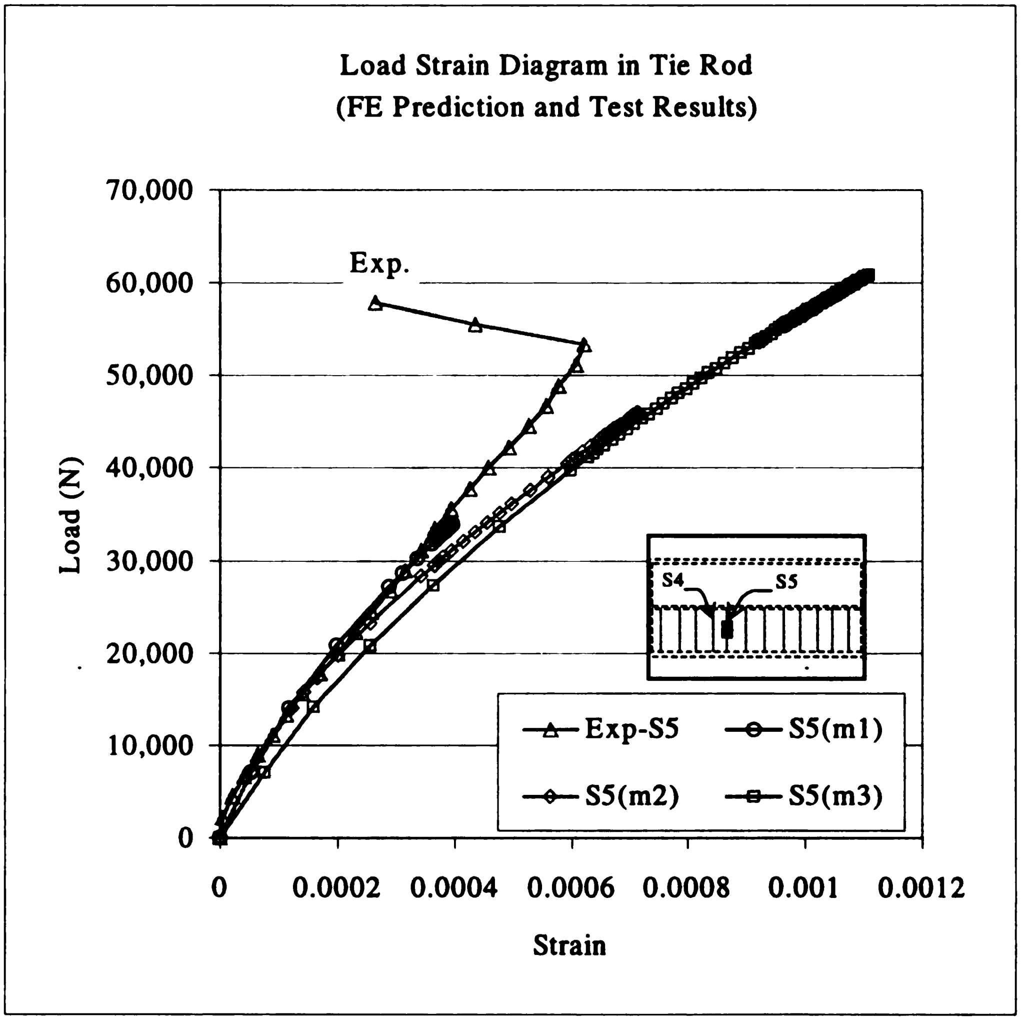

Figure 6.8 Measured and Predicted Load Strain Diagram of Tie Rods Directly Underneath the Applied Load

With 250 MPa (36 ksi) steel, the yield strain of the tie rods is about 0.0012. Figure 6.8 shows a nonlinear relation between the load and the strain in the tie rods, even at a very low strain value. The higher the load, the greater the strain rate in the tie rods.

This means that the magnitude of the arching action increases as the load increases as noted by the high strain rate developed in the tie rod.

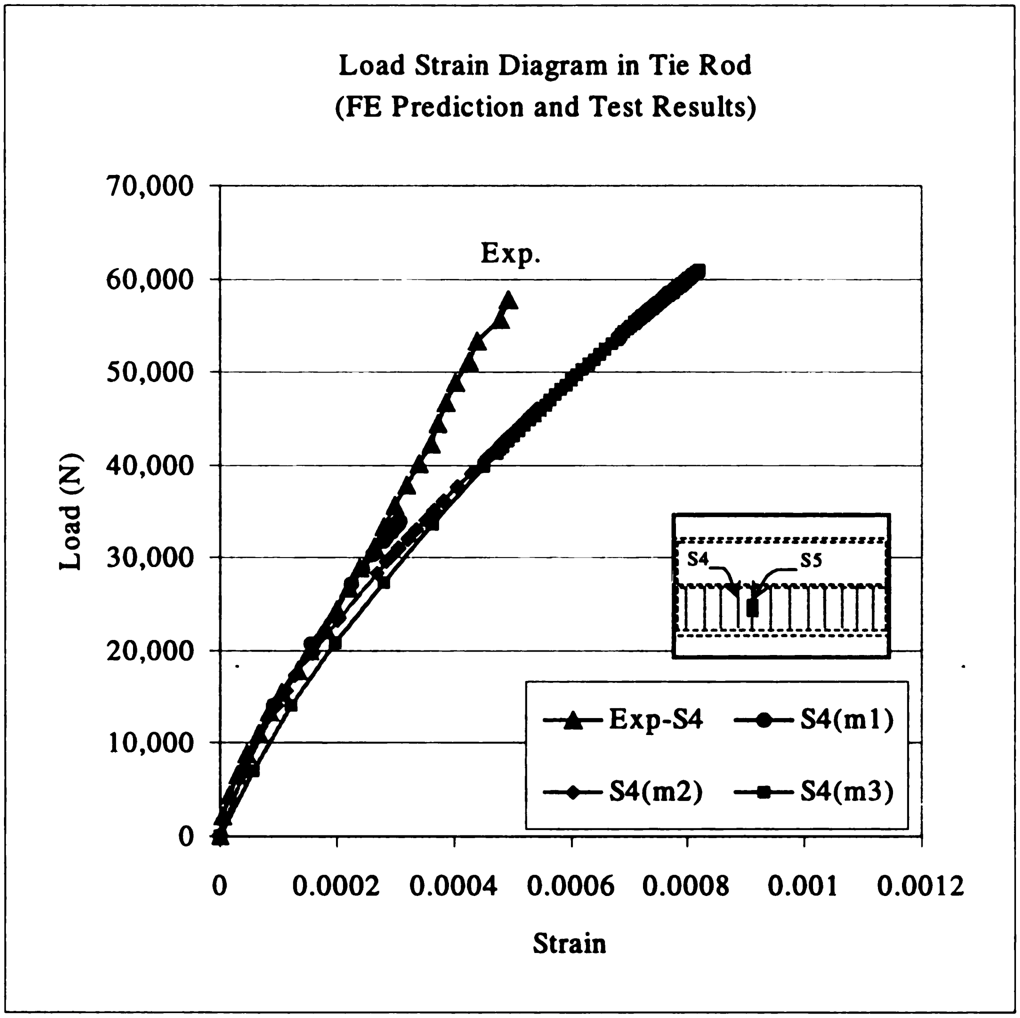

Figure 6.9 Measured and Predicted Load Strain Diagram of Tie Rods Adjacent to the Applied Load

The same argument holds true for the tie rods adjacent to the loaded area, as shown in Figure 6.9. At higher load levels, the test results showed less strain than did the FE models because during the test the tie rod connection failed before failure of the slab.

Model m3 gave a maximum strain value very close to the yield strain. However, under a load level of about 6 times the wheel load, the tie rods were still within its elastic limit.

The tie rods, at a distance from the loaded area, were not strained as much as that closer to the applied load. The strains diminished in tie rods at a distance two (tie rods) spaces away from the load (see Figure 5.9). This observation was also well modeled in the FEA. Therefore, the arching action is a highly localized phenomenon that causes enhancement of the concrete strength around the loaded area. This also suggests that the tie rods spacing should be small. A spacing of 1,000 mm in a prototype slab is sufficient, as shown in the test results.

6.6 Summary of Results

The behavior of deck slab panels with and without tie rods were experimentally observed and theoretically and numerically analyzed. The results were presented in the form of tables and diagrams and are summarized in the followings.

1. Experimental results showed that the slab panels with added tie rods were significantly stronger and stiffer than those without tie rods. A lower slab deformation means a lower stress magnitude, which accordingly, increases the fatigue resistance of the slab. As a result, addition of tie rods could improve the durability of the slab.
2. The effect of adding tie rods, observed through the development of strain in the tie rods, showed that the arching action developed in the slab starting at a load level lower than the service load. This means that it could improve the behavior of the slab under the service load, though the improvement is more pronounced at higher load levels.

3. Theoretical analysis using a punching shear model of a restrained slab predicted the punching load of the slabs with corresponding restraint factor values of 0.663 and 0.786 for the slab panels without and with tie rods, respectively. This theory however, could not predict the observed deflection of the slabs.
4. The ACI Code provision on punching shear strength of RC and prestressed concrete slabs gave significantly lower strengths (48% and 71%) than the observed values for the control slab. The formula for the prestressed concrete slab gave higher punching load than the formula for the RC slabs. This implies that the presence of compressive stress increase the punching shear capacity of the slab.
5. The finite element analyses of the model bridge showed that the response of the models were strongly dependent of the material model for the concrete. Among the variables affecting the FEA response were the tension stiffening, failure ratio, plastic strain, yield stress, and modulus of elasticity. The model with higher values for tension stiffening, failure ratio, and plastic strain gave a higher magnitude response than the model using the lower values. The model with higher value of yield stress gives a stiffer response. Using lower value of Young's modulus, the model provides higher response with less stiffness.
6. The FEA predicted the load deflection behavior of the slab well at the lower load levels (up to 60% of the observed failure load). At higher load levels however, the models showed stiffer response than the observed response. The model with tie rods was stronger and stiffer than the model without tie rods. This confirmed the experimental observation that the addition of tie rods improved the behavior of the slab.

7. The FEM mimic the observed load deflection diagram of the center beam very well until the model fails due to failure of the concrete slab. The model using a lower value of concrete elastic modulus gave a more flexible response, which means that the composite action between the concrete deck and the steel beam was properly modeled.
8. The strain developed in the tie rods was also properly modeled in the FEA. The observed response was stiffer than the model response at higher load levels, because during the test, the connection of the tie rods failed prior to the failure of the slab.
9. In general, the FEM could mimic very well the global behavior of the model bridge at lower load levels. Accordingly, the FEM is more appropriate for a non-destructive evaluation, in which the structure is not loaded up to failure. To predict the slab response up to failure, considerable efforts would be necessary to improve the material model as well as the mechanical constitutive models for concrete subjected to high magnitude three-dimensional stress states. Nevertheless, if properly understood, the FE method is one of the most powerful tools available for stress analyses.

CHAPTER 7

CONCLUSION AND RECOMMENDATION

7.1 Summary and Conclusion

Experimental investigation of the behavior of a reinforced concrete deck slab with additional lateral restraint (tie rods) was conducted by testing two different slab panels, which were incorporated into the construction of a 1/5 scale model bridge. The deck slab was reinforced with a 0.2% isotropic wire mesh arrangement that represented the minimum steel requirement for the empirical method of slab design in the AASTHO LRFD Bridge Design Specifications (1994). One slab panel was strengthened by connecting the top flanges of the steel girders with steel tie rods, immediately underneath the slab. The other slab panel served as a control slab without tie rods. Each slab panel was consecutively tested at four different load points with a full range static concentrated load. The load response history of the slab, the center beam, and the tie rods was observed under a load increment of 2,224 N (500 lbs). The effect of adding tie rods was measured from the stiffness and strength of each slab panel, as well as the strain developed in the tie rods.

To simulate the load response histories observed during the experiment, nonlinear three-dimensional finite element models were developed using a commercial finite element program, ABAQUS. The models incorporated each component of the bridge, including the deck, steel girders, edge beams, diaphragms, and the tie rods. The deck was modeled using 3-D solid elements where the steel reinforcement was modeled as layers of rebar embedded in the concrete elements. The finite element analyses involved several models to study the sensitivity of the models to various modeling parameters for concrete material.

In addition to the FEA, a rational punching shear theory of restrained slabs and the ACI Code provisions on punching shear strength of concrete slabs were also utilized to analyze the ultimate shear capacity of the slab. In the punching shear theory, the deck slab was transformed into an equivalent circular slab with diameter equal to the center to center spacing of the steel girders. For the ACI Code provision, two equations were utilized, one equation for RC slabs and the other for prestressed concrete slabs. The results obtained from the experiment and the analyses were carefully discussed toward the effect of adding tie rods on the behavior of the deck slab and the verification of the analysis methods.

From the experimental results, the following conclusions can be drawn:

1. The slab panel with tie rods was significantly stronger and stiffer than the slab panel without tie rods. The significant reduction in the slab deflection indicates a lower tensile strain in the slab, which accordingly, improves the crack resistance of the deck. Therefore, additional tie rods could improve the durability of an existing deck slab.
2. The strain developed in the tie rods is a strong indication of increased lateral restraint, which enhances the arching action in the deck slab and consequently, increases the stiffness and the strength of the deck.

3. With the addition of tie rods, the net deflection of the slab was reduced by a factor of 34% at lower load levels and 50% at higher load levels. The cracked and failure loads of the slabs with tie rods increased by factors of 30% and 13.7%, respectively.
4. The strength and stiffness enhancement in the slab with tie rods was observed starting at a load magnitude lower than the standard truck wheel load, which means that tie rods can improve the performance of a slab under service load conditions.
5. The present study verified the earlier findings that under static concentrated load, a deck slab reinforced with 0.2% steel exhibited a punching shear strength much higher than that required to support a standard truck loading. In a prototype bridge, the failure load of the slab with and without tie rods would be 1,501.268 kN (337.5 kip) and 1,306.659 kN (293.75 kip), respectively. Compared to a standard wheel load of 72.5 kN (16.3 kip) with an impact factor of 1.3, the expected safety factors of the slabs with and without tie rods are 15.9 and 13.9, respectively.

From the finite element analyses the following conclusions are drawn:

1. The observed nonlinear load response history of the model bridge was well simulated in the finite element models up to about 60% of the failure load. At higher load levels however, the FE models showed stiffer responses than the observed ones.
2. Solid 3-D elements could properly model the arching action in the RC slab through the development of strain in the tie rods. The shell elements in ABAQUS, however, were confined to flexural strains only and so the strain in the tie rods did not develop.
3. The responses of the finite element models were strongly dependent on the material model for the concrete slab. Among the variables that affect the model's responses

are tension stiffening, failure ratio, plastic strain, yield stress, and elastic modulus of concrete.

4. At higher load levels, the finite element models mimic the observed load deflection diagram of the center beam better than that of the concrete slab. This result indicates the needs for the improvement in modeling the post-cracking behavior of the reinforced concrete element.
5. The model using a lower value of concrete elastic modulus allowed larger deflection in the center beam, which means that the composite action between the concrete deck and the steel beam was properly modeled by the FEA.
6. In general, the finite element models could mimic very well the global behavior of the slab at lower load levels. To predict the slab response at higher load levels, considerable efforts are necessary to improve the material model as well as the mechanical constitutive models for the concrete. Accordingly, the FEA of RC structures is more appropriate for a non-destructive evaluation, in which the structure is not loaded up to failure.

From the rational punching shear theory of restrained slabs and the ACI Codes provision on punching shear strength of concrete slabs, the following conclusions can be drawn:

1. Theoretical analysis using the punching shear model of restrained slabs predicted the punching strength of the slabs with restraint factor values of 0.663 and 0.786 for the slab panel without and with tie rods, respectively. This theory however, gave a slab deflection about 10% of the observed value. For the purpose of design, a restraint factor value of 0.6 could be assumed for a deck slab of comparable design conditions.

2. The ACI Code provisions on punching shear strength of RC and prestressed concrete slabs gave punching shear strength of 48% and 71% of the observed strength of the control slab. These formulae however, are readily available for the purpose of design, or to rapidly estimate the punching shear strength of concrete slabs. Higher punching load for the prestressed concrete slab implies that the presence of compressive stress increases the punching shear capacity of the slab.

7.2 Recommendation

The present study showed that the newly constructed deck slab with additional tie rods exhibited better behavior than that without tie rods. Considering the extraneous possible benefits gained from the concept of adding tie rods to an existing deck slab, further research to study the long-term performance of slabs with varying degrees of deterioration is recommended. In addition, further study on the cost effectiveness of the concept is necessary. The effect of applying varying magnitudes of tension forces in the tie rods, to prestress the slab, would also be worth studying. For a newly constructed bridge, the concept could be applied with much less effort by prefabricating the rod connections. In addition, minimum steel reinforcement should be used to minimize the risk of corrosion-induced deterioration of the deck slabs.

For the purpose of applying the concept of adding tie rods to deck slabs of an existing bridge, the following notes are worth considering:

- The spacing of the tie rods should be kept small because the distribution of the stress in the tie rods is localized in the vicinity of the load. A 40 mm diameter tie rods with a 1,000 mm spacing would be sufficient for a full scale bridge.

- The tie rod connection should be designed to accommodate possible replacement and applying tension force in the tie rods. Fatigue resistance of the connection should also be considered.
- In the negative moment region, where the top flanges of the girders are in tension, bolted connections could be used to avoid welded connections.

Related to the finite element analysis, the present study verified the earlier findings that a true 3-D finite element modeling of RC structures could not predict the response of the structure up to failure. Accordingly, interpretation of the model response should be limited to the lower load levels. In addition, the application of modeling parameters used in the present study should be limited to untested models of similar configuration. Finally, development of material and constitutive models for the reinforced concrete element still remains to be investigated, taking advantage of test results reported in the literature.

REFERENCES

AASHTO (1994). *LRFD Bridge Design Specifications, SI Units,* First edition, American Association of State Highway and Transportation Officials, Washington, DC.

Abbasi, M.S., Baluch, M.H., Azad, A.K., Abdel-Rahman, H.H. (1992). "Nonlinear Finite Element Modeling of Failure Modes in R/C Slabs," *Computer & Structures*, Vol. 42, No. 5, 1992, pp. 815-823.

ACI Committee 318 (1995). *Building Code Requirements for Structural Concrete (ACI 318-95) and Commentary (ACI 318R-95),* American Concrete Institute, P.O. Box 9094 Farmington Hills, MI 48333.

Agarwal, A.C. (1990). "Load Testing of New Concrete Bridge Deck Slabs," *Third Int. Conference on Short and Medium Span Bridges*, Toronto, Canada, pp. 277-289.

Aldridge, W.W. and Breen, J.E. (1970). "Useful Techniques in Direct Modeling of Reinforced Concrete Structures," *Models for Concrete Structures,* ACI, SP 24-5.

Al-Mutairi, N.M. (1989). "The Structural Feasibility of Using Welded Steel Mesh in Bridge Decks," *Ph.D. Thesis*, University of Maryland College Park, 1989.

Aoyama, H., and Noguchi, H. (1986). "Future Prospect for Finite Element Analysis of Reinforced Concrete Structures," *Finite Element Analysis of Reinforced Concrete Structures, Proceeding of the International Workshop,* ASCE 345 East 47th Street New York, New York 10017-2398.

ASCE-ACI Task Joint Committee 426 on Shear and Diagonal Tension of the Committee on Masonry and Reinforced Concrete of the Structural Division (1974). "The Shear Strength of Reinforced Concrete Members – Slabs," *ASCE Journal of the Structural Division*, Vol. 100, No. ST8, pp. 1543-1591.

ASTM (1996). *Annual Book of ASTM Standards*, Section 4 Construction, Volume 04.02 Concrete and Aggregates, American Society for Testing and Materials, 100 Barr Harbor Drive, West Conshohocken, PA 19428.

Azad, A.K., Baluch, M.H., Abbasi, M.S., Kareem, K., (1994). "Punching Capacity of Deck Slabs in Girder-Slab Bridges," *ACI Structural Journal*, Vol. 91, No. 6, November-December 1994, pp. 656-662.

Bakht, B., and Mufti, A.A. (1996). "FRC Deck Slabs Without Tensile Reinforcement," *Concrete International*, Vol. 18, No. 2, pp. 50-55.

Barker, R.M., and Puckett, J.A. (1997). *Design of Highway Bridges Based on AASHTO LRFD Bridge Design Specifications,* John Wiley & Sons, Inc.

Batchelor, B. deV., Hewitt, B.E., Csagoly, P., and Holowka, M. (1978). "Investigation of the Ultimate Strength of Deck Slabs of Composite Steel/Concrete Bridges," *TRR Record No. 664 Transportation Research Board*, pp. 162-170.

Bathe, K-J., Walczak, J., Welch, A., and Mistry, N. (1989). "Nonlinear Analysis of Concrete Structures," *Computers & Structures,* Vol. 32, No.3 / 4, pp. 563-590.

Beal, D.B. (1981). "Strength of Concrete Bridge Decks," *Research Report 89,* Engineering Research and Development Bureau, New York State Department of Transportation.

Beal, D.B. (1982). "Load Capacity of Concrete Bridge Decks," *ASCE Journal of the Structural Division*, Vol. 108, No. ST4, April 1982, pp. 814-832.

Cook, R.D., Malkus, D.S., and Plesha, M.E. (1989). *Concept and Applications of Finite Element Analysis*, Third Edition, Wiley, New York.

Csagoly, P. (1997). "Testing of a Composite Steel-Concrete Bridge Deck," *Concrete International*, February 1997.

Csagoly, P., Holowka, M., and Dorton, R. (1978). "The True Behavior of Thin Concrete Bridge Slabs," *TRR Record No. 664 Transportation Research Board*, pp. 171-179.

Dorton, R.A., Holowka, M., and King, J.P.C. (1977). "The Conestogo River Bridge – Design and Testing," *Canadian Journal of Civil Engineers,* Vol. 4 No. 18, 1977, pp. 18-39.

Fang, I.-K., Tsui, C.K.T., Burns, N.H., and Klingner, R.E. (1990). "Load Capacity of Isotropically Reinforced, Cast-in-Place and Precast Panel Bridge Decks," *PCI Journal*, July-August 1990.

Fang, I.-K., Worley, J.A., Burns, N.H., and Klingner, R.E. (1986). "Behavior of Ontario-Type Bridge Decks on Steel Girders," *Research Report 350-1*, Center for Transportation Research, University of Texas at Austin.

Gilbert, R.I., and Warner, R.F. (1978). "Tension Stiffening in Reinforced Concrete Slabs," *Journal of the Structural Division, Proceeding of the ASCE,* Vol. 104, No. ST12, December 1978.

Gonzales-Vidosa, F., Kotsovos, M.D., and Palvovic, M.N. (1988). "Symmetrical Punching of Reinforced Concrete Slabs: an Analytical Investigation Based on Nonlinear Finite Element Modeling," *ACI Structural Journal*, May-June 1988.

Hand, F.R., Pecknold, D.A., and Schnobrich, W.C. (1973). "Nonlinear Layered Analysis of RC Plates and Shells," *Journal of the Structural Division*, Proceeding of the ASCE, Vol. 99, No. ST7, July, 1973.

Harris, H.G., Sabnis, G.M., and White, R.N. (1970). "Reinforcement for Small Scale Direct Models of Concrete Structures," *Models for Concrete Structures,* ACI, SP 24-6.

Hassoun, M.N. (1998). *Structural Concrete, Theory and Design,* Addison-Wesley.

Hewitt, B.E. (1972). "An Investigation of the Punching Strength of Restrained Slabs with Particular Preference to the Deck Slabs of Composite I-Beam Bridges," *Ph.D. Thesis,* Department of Civil Engineering, Queen's University at Kingston, Canada.

Hewitt, B.E., and Batchelor, B. deV. (1975). "Punching Shear Strength of Restrained Slabs," *ASCE Journal of Structural Division*, Vol. 101, No. ST9, pp. 1837-1853.

H, K & S, Inc. a (1998). *Abaqus Theory Manual,* Version 5.8, Hibbit, Karlsson & Sorensen, Inc. 1080 Main Street Pawtucket, RI. 02860-4847.

H, K & S, Inc., b (1998). *Abaqus/Standard User's Manual,* Version 5.8, Hibbit, Karlsson & Sorensen, Inc. 1080 Main Street Pawtucket, RI. 02860-4847.

H, K & S, Inc., c (1998). *Abaqus/Standard Example Manual,* Version 5.8, Hibbit, Karlsson & Sorensen, Inc. 1080 Main Street Pawtucket, RI. 02860-4847.

H, K & S, Inc., d (1998). *Abaqus/Post Manual,* Version 5.8, Hibbit, Karlsson & Sorensen, Inc. 1080 Main Street Pawtucket, RI. 02860-4847.

H, K & S, Inc. (1996). *Analysis of Concrete Structures with Abaqus,* Karlsson & Sorensen, Inc. 1080 Main Street Pawtucket, RI. 02860-4847.

Hsu, T.T.C. and Zhang, L. (1996). "Tension Stiffening in Reinforced Concrete Membrane Elements," *ACI Structural Journal,* Vol. 93, No. 1 January-February 1996.

Huria, V., Lee, K., and Aktan, A.E. (1993). "Nonlinear Finite Element Analysis of RC Slab Bridge," *Journal of Structural Engineering,* ASCE Vol. 119, No. 1, January 1993.

Jain, S.C., and Kennedy, J.B. (1974). "Yield Criterion for Reinforced Concrete Slabs," *Journal of the Structural Division,* Proceeding of the ASCE, Vol. 100, No. ST3, March, 1974.

Jiang Da-Hua and Shen Jing-Hua (1986). "Strength of Concrete Slabs in Punching Shear," *Journal of Structural Engineering,* ASCE, Vol. 112, No. 12, December 1986, pp. 2578-2591.

Jofriet, J.C, and McNeice, G.M. (1971). "Finite Element Analysis of Reinforced Concrete Slabs," *Journal of the Structural Division,* Proceeding of the ASCE, Vol. 97, No. ST3, March 1071.

Kinnunen, S. (1963). "Punching of Concrete Slabs with Two-way Reinforcement," *Transaction of the Royal Institute of Technology,* Stockholm, Sweden, No. 198.

Kinnunen, S., and Nylander, H. (1960). "Punching of Concrete Slabs without Shear Reinforcement," *Transaction of the Royal Institute of Technology,* Stockholm, Sweden, No. 158.

Kotsovos, M.D., and Pavlovic, M.N. (1995). *Structural Concrete Finite-Element Analysis for Limit-State Design,* Thomas Telford Services Ltd., Thomas Telford House, 1 Heron Quay, London E14 4JD.

Kuang, J.S., and Morley, C.T. (1992). "Punching Shear Behavior of Restrained Reinforced Concrete Slabs," *ACI Structural Journal,* Vol. 89, No. 1, January-February 1992, pp. 13-19.

Kupfer, H.B., and Gerstle, K.H. (1973). "Behavior of Concrete under Biaxial Stresses," *ASCE Journal of the Engineering Mechanics Division, Proceedings of the American Society of Civil Engineers,* Vol. 99, NO. EM4, August 1973, pp. 853-866.

Lin, C-S., and Scordelis, A.C. (1975). "Nonlinear Analysis of RC Shells of General Form," *Journal of the Structural Division,* Proceeding of the ASCE, Vol. 101, No. ST3, March, 1975.

Masajiro, K., Hiroshi, U., Masahito, U., and Takitaro, H. (1994). "Rehabilitation and Strengthening of Concrete Structures with Carbon Fiber," *Proceeding of 10th US-Japan Bridge Engineering Workshop,* Lake Tahoe - Nevada, pp. 304-319.

Mehta, P.K. and Monteiro, P.J.M. (1996) *Concrete Structure, Properties, And Materials,* Second Ed., Prentice Hall Inc., Englewood Cliffs, New Jersey 07632.

Mufti, A.A., and Bakht, B. (1996). "Design Provisions for Steel-free Deck Slabs on Beams," *Proceedings of the Sixth International Colloquium on Concrete in Developing Countries,* pp. 35-44.

Mufti, A.A., Jaeger, L.G., Bakht, B., and Wegner, L.D. (1993). "Experimental Investigation of Fiber-reinforced Concrete Deck Slabs without Internal Steel Reinforcement," *Canadian Journal of Civil Engineer,* Vol. 20, pp. 398-406.

Mufti, A.A., and Newhook, J.P. (1998). "Punching Shear Strength of Restrained Concrete Bridge Deck Slabs," *ACI Structural Journal,* Vol. 95, No. 4, July-August 1998, pp. 375-381.

Newhook, J.P. (1997). "The Behavior of Steel-Free Concrete Bridge Deck Slabs under Static Loading Condition," *Ph.D. Thesis,* Faculty of Engineering, Technical University of Nova Scotia, Halifax, Canada.

Ngo, D., and Scordelis, A.C. (1967). "Finite Element Analysis of Reinforced Concrete Beams," *ACI Journal* / March 1967.

Noguchi, H., and Schnobrich, W.C. (1991). "Finite Element Analysis of Reinforced Concrete in Japan and US," *Finite Element Analysis of Reinforced Concrete Structures II, Proceeding of the International Workshop,* ASCE, 345 East 47th Street New York, NY 10017-2398.

Perdikaris, P.C., and Beim, S. (1988). "RC Bridge Decks Under Pulsating and Moving Load," *ASCE Journal of Structural Engineering*, Vol. 114, No. 3, pp. 591-607.

Petrou, M.F. (1991). "A Model Study on Highway Concrete Bridge Decks Subjected to Concentrated Load (Ontario VS. AASHTO Design)," *MS Thesis,* Department of Civil Engineering, Case Western University May 1991.

Petrou, M.F. and Perdikaris, P.C. (1990). "Small Scale Model Tests: Arching Action in Reinforced Concrete Bridge Decks," *Third Int. Conference on Short and Medium Span Bridges*, Toronto, Canada, pp. 317-326.

Petrou, M.F. and Perdikaris, P.C. (1996). "Punching Shear Failure in Concrete Decks as Snap-Through Instability," *ASCE Journal of Structural Engineering*, Vol. 122, No. 9, September 1996, pp. 998-1005.

Polak, M.A. (1998). "Modeling Punching Shear of Reinforced Concrete Slabs Using Layered Finite Element," *ACI Structural Journal*, Vol. 95, No. 1, January-February 1998.

Puckett, J.A., Naiknavare, R.D., and Lohrer, J.D. (1988). "Evaluation of Bridge Deck Utilizing Ontario Bridge Deck Design Method," *Final Report, Project No. 38717*, Department of Civil Engineering, University of Wyoming, Laramie, WY, January 1988.

Sabnis, G.M., Harris, H.G., White, R.N., and Mirza, M.S. (1983). *Structural Modeling and Experimental Techniques*. Prentice-Hall, Inc., Eanglewood Cliffs, NJ. 07632.

Schnobrich, W.C. (1986). "The Role of Finite Element Analysis of Reinforced Concrete Structures," *Finite Element Analysis of Reinforced Concrete Structures, Proceeding of the International Workshop.* ASCE 345 East 47th Street New York, New York 10017-2398.

Wegner, L.D., Mufti, A.A. (1994). "Finite Element Investigation of Fiber Reinforced Concrete Deck Slabs without Internal Steel Reinforcement," *Canadian Journal of Civil Engineer*, Vol. 21, pp. 231-136.

Youn, S-G., and Chang, S-P. (1998). "Behavior of Composite Bridge Decks Subjected to Static and Fatigue Loading," *ACI Structural Journal*, Vol. 95, No. 3, May-June 1998.

Xanthakos, P.P. (1996). *Bridge Strengthening and Rehabilitation,* Prentice-Hall, Inc., Upper Saddle River, NJ. 07458.

APPENDIX A

PUNCHING SHEAR MODEL OF RESTRAINED SLAB

DERIVATION OF EQUATIONS

I. Mechanical Model for Simply Supported Slabs

Kinnunen and Nylander, based on observation made in their tests, argued that the outer portion of the slab, which is bounded by the shear crack and by radial cracks, is loaded through a compressed conical shell that develops from the column (load) to the end of the shear crack. The element shown in Figure A.1 is acted upon by reactions $P\beta/(2\pi)$ and by the following forces which are caused by rotation:

- The oblique compression force $T\beta/(2\pi)$ in the compressed conical shell.
- Tangential forces in the reinforcement at right angles to the radial cracks, with resultant R_1.
- Radial forces in the reinforcement cutting across to the radial cracks, with resultant R_2.
- Tangential compressive forces in the concrete under the center of rotation, with resultant R_3.

The conical shell was assumed to have the shape of Figure A.2, and its thickness varies in such a manner that the compressive stress at the intersection with the column and the root of the shear crack are approximately equal, as given by:

$$2\pi\frac{B}{2}(2c_2)f_t \cong 2\pi(\frac{B}{2}+y)(2c_1)f_t$$

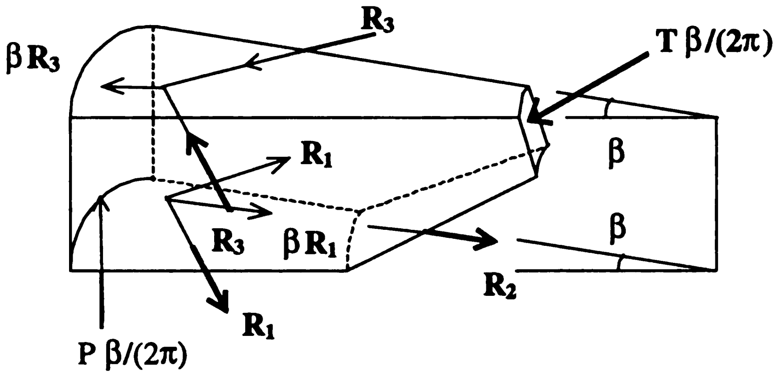
R₃
βR₃
T β/(2π)
R₁
β
R₃
βR₁
β
R₂
R₁
P β/(2π)

Figure A.1 Isometric View of Conical Shell Element for Simply Supported Slab

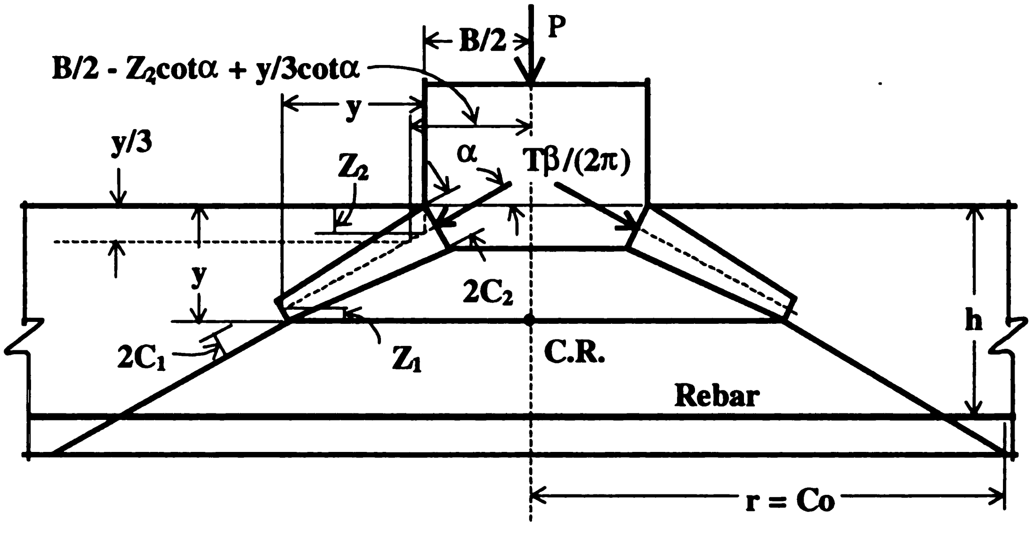
B/2
P
B/2 - Z₂cotα + y/3cotα
y
y/3
Z₂
α
Tβ/(2π)
y
2C₂
h
2C₁
Z₁
C.R.
Rebar
r = Co

Figure A.2 Cross Section of Mechanical Model Showing Notations

In this equation, f_t is the concrete compressive stress in the imaginary conical shell, $2c_2$ and $2c_1$ are the thickness of the conical shell as given by:

$$\frac{c_2}{c_1}=\frac{B/2+y}{B/2}=1+\frac{2y}{B}$$

Similarly, the following relation holds:

$$\frac{z_2}{z_1} = 1 + \frac{2y}{B}$$

From the geometry in Figure A.2 it can be seen that:

$$z_1 + z_2 + y\tan\alpha - y = 0$$

Therefore,

$$z_1 = y(1-\tan\alpha) - z_2 = y(1-\tan\alpha) - (1+\frac{2y}{B})z_1 = \frac{y(1-\tan\alpha)}{2(1+y/B)}$$

Over the cross section 2c$_1$ we have:

$$2c_1 = 2z_1\cos\alpha$$

The assumed compressive force, T, along the lower bounding surface of the cone can be approximated by:

$$T = 2\pi(B/2+y)2c_1 f_t$$

The force, P, which is transmitted through the conical shell is given by:

$$P = T\sin\alpha = 2\pi f_t(B/2+y)\frac{y(1-\tan\alpha)}{(1+y/B)}\sin\alpha\cos\alpha$$

Define:

$$f_{(\alpha)} = \sin\alpha\cos\alpha(1-\tan\alpha) = \frac{\tan\alpha(1-\tan\alpha)}{1+\tan^2\alpha} \qquad \text{Equation (1)}$$

Then P can be rewritten as

$$P = \pi\frac{B}{h}\frac{y}{h}\frac{(B+2y)}{(B+y)}f_t f_{(\alpha)}h^2 \qquad \text{Equation (2)}$$

If ψ is the angle of the rotation around the C.R., then the strain ε_s of reinforcing steel at a distance, r from the center of the slab is given by:

$$\varepsilon_s = \psi\frac{(h-y)}{r} = \frac{h}{r}\psi(1-\frac{y}{h})$$

The corresponding steel stress is given by:

$$f_s = k_1\varepsilon_s E_s = E_s\frac{h}{r}\psi(1-\frac{y}{h})$$

In this case k_1 is a coefficient greater than one (1), expresses the fact that the stress of steel varies between the radial cracks, and reaches a maximum value at the crack. Here k_1 is assumed as unity. At the boundary between the yield and elastic stress ranges, $r = r_s$, this expression holds:

$$\frac{r_s}{h} = \frac{\psi}{\varepsilon_s}(1-\frac{y}{h}) = \frac{E_s}{f_s}\psi(1-\frac{y}{h}) \qquad \text{Equation (3)}$$

In general, the resultant force in steel ring is given by:

$$R_1 = f_{sy}\left[\sum_{r=C_0}^{r=r_s} A_s + r_s\sum_{r=r_s}^{r=C/2}\frac{A_s}{r\cdot}\right]$$

Using $dA_s = \rho\ h\ dr$, then

For $r_s \geq C_0$: $R_1 = \rho f_{sy}h\left[\int_{C_0}^{r_s} dr + r_s\int_{r_s}^{C/2}\frac{dr}{r}\right] = \rho f_{sy}h\left[(r_s - C_0) + r_s\ln\frac{C/2}{r_s}\right]$

$$R_1 = \rho f_{sy}h^2\left[(\frac{r_s}{h}-\frac{C_0}{h}) + \frac{r_s}{h}\ln\frac{C/2}{r_s}\right] \qquad \text{Equation (4.a)}$$

For $r_s < C_0$: $R_1 = \rho f_{sy}h^2\left[\frac{r_s}{h}\ln\frac{C/2}{r_s}\right]$ Equation (4.b)

The stress in steel inside the shear crack is f_{sy} and correspondingly

For $r_s \geq C_0$: $R_2 = \varepsilon_s E_s\rho h\beta C_0 = f_{sy}h\rho C_0\beta = \rho f_{sy}h^2\frac{C_0}{h}\beta$ Equation (5.a)

For $r_s < C_0$: $R_2 = \rho f_{sy} h^2 \frac{r_s}{h} \beta$ Equation (5.b)

The Compressive Stress in Concrete

When the sector element outside the shear crack undergoes angular rotation around the C.R., compressive stress occurs in a tangential direction under a horizontal plane passing through the C.R. These stresses increase linearly as the distance from the above mentioned plane becomes greater. The strain is given by:

$$\varepsilon_{ct} = \psi \frac{y}{r}$$

The corresponding concrete stress in the tangential direction on the top surface of the slab, f_{ct} is

$$f_{ct} = k_2 \psi \frac{y}{r} E_c$$

where k_2 is a coefficient to reflect the stress variation which is again assumed as unity. The total compressive force acting on a radial crack is

$$R_3 = E_c \psi \int_{B/2+y}^{C/2} \left(\int_0^y y dy\right) \frac{dr}{r} = E_c \psi \int_{B/2+y}^{C/2} \frac{1}{2} y^2 \frac{dr}{r} = E_c \psi \frac{y^2}{2} \ln \frac{C/2}{B/2+y}$$

$$R_3 = E_c \psi \frac{h^2}{2} \left(\frac{y}{h}\right)^2 \ln \frac{C/2}{B/2+y}$$

Substituting the expression of:

$\psi E_c = f_{ct}\frac{r}{y} = f_{ct}\frac{B/2+y}{y}$ into the above equations, R_3 can then be written as:

$$R_3 = \frac{h^2}{2}(\frac{y}{h})^2 f_{ct}(\frac{B}{2y}+1)\ln\frac{C/2}{B/2+y}$$

The radial component of R_3 is $R_3\beta$.

Criteria of Failure

Failure occurs when ε_{ct} at the top of the slab (under the load) reaches a limiting value. The following expressions give an essential agreement with the test results reported by K and N:

For $0 < \frac{B}{h} \leq 2; \varepsilon_{ct} = \psi\frac{y}{r} = \frac{\psi}{1+B/2y} = 0.0035(1-0.22\frac{B}{h})$

For $\frac{B}{h} > 2; \varepsilon_{ct} = \frac{\psi}{1+B/2y} = 0.00195$

The following empirical expressions were also reported by K and N:

$$E_c = 10^5(0.35+0.3\frac{f_{cube}}{150}) \qquad \text{Equation (6)}$$

$$\frac{f_t}{f_{ct_{r=(B/2+y)}}} = 2.35 \qquad \text{Equation (7)}$$

Here f_{cube} is the 150 mm cube strength of concrete with unit of kilogram force per square centimeters.

The following expression was used by Hewitt and Batchelor to convert the compressive strength of a 6 in. diameter by 12 in. cylinder (f_{cyl}) in units of pounds per square inch into f_{cube}.

$$f_{cube} = \frac{f_{cyl}}{0.75 + 0.000025 f_{cyl}}$$ Equation (8)

Accordingly, the expression for ψ becomes:

For $\frac{B}{h} \le 2; \psi = 0.0035(1 - 0.22\frac{B}{h})(1 + \frac{B}{2y})$ Equation (9.a)

For $\frac{B}{h} > 2; \psi = 0.00195(1 + \frac{B}{2y})$ Equation (9.b)

The last two equations were derived on the basis of measurements of the concrete strain in a radial direction on the top surfaces of a slab with ring reinforcement. Kinnunen later proposed the following equation for slabs with two-way reinforcement.

And $\frac{C_o}{h} = \frac{B}{2h} + 1.8$ Equation (10)

The expression for the stress in the conical shell, f_t become as follows:

For $0 < \frac{B}{h} \le 2$: $f_t = 0.0035(1 - 0.22\frac{B}{h})E_c$

$f_t = 825(0.35 + 0.3\frac{f_{cube}}{150})(1 - 0.22\frac{B}{h})$ Equation (11.a)

For $\frac{B}{h} > 2$: $f_t = 0.00195 E_c = 460(0.35 + 0.3\frac{f_{cube}}{150})$ Equation (11.b)

Condition of Equilibrium

Taking moments with respect to the point of intersection of R_1 and $P\beta/(2\pi)$ gives:

$$2\pi R_3(h - y/3) + \frac{P}{\tan\alpha}(h - y/3) - P(C/2 - B/2) = 0$$

$$\frac{2\pi R_3}{P} = -\cot\alpha + \frac{C/2 - B/2}{(h - y/3)} = K_y - \cot\alpha$$

Here $K_y = \dfrac{C/2 - B/2}{(h - y/3)}$

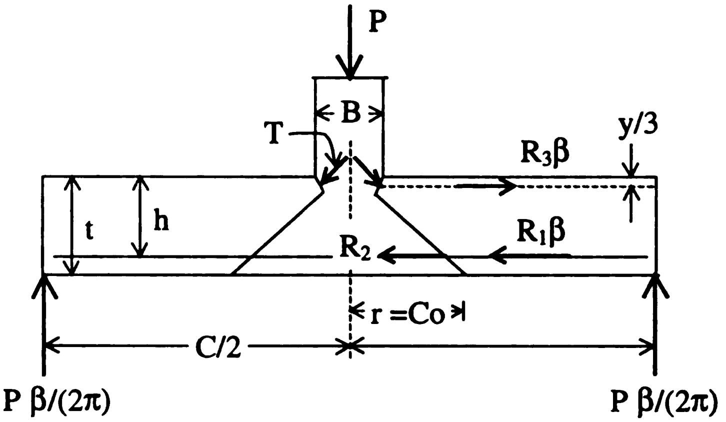

Figure A.3 Mechanical Model of Simply Supported Slab

Substituting the expression for P, R$_3$, and $f_t/f_{ct} = 2.35$ yields:

$$2\pi \frac{\frac{y^2}{2h} f_\alpha \left(\frac{B}{2y}+1\right)\ln\left[\frac{C/2}{B/2+y}\right]}{2\pi f_t f_\alpha B y \frac{B+2y}{B+y}} = \frac{y\left(\frac{B}{2y}+1\right)\ln\left[\frac{C/2}{B/2+y}\right]}{2.35B(B+2y)\frac{f_\alpha}{B+y}} = K_y - \cot\alpha$$

Rearrangement of terms yields

$$\frac{1}{4.7}\frac{(B+2y)(B+y)}{B(B+2y)}\ln\left[\frac{C/2}{B/2+y}\right] = (K_y - \cot\alpha) f_\alpha = (K_y - \cot\alpha)\frac{\tan\alpha(1-\tan\alpha)}{1+\tan^2\alpha}$$

Therefore,

$$(K_y \tan\alpha - 1)\left(\frac{1-\tan\alpha}{1+\tan^2\alpha}\right) = \frac{1}{4.7}\left(1+\frac{y}{B}\right)\ln\left[\frac{C/2}{B/2+y}\right]$$

The second equation of equilibrium for the sector element was obtained by taking moments about the point of intersection of Tβ/(2π) in the conical shell and the resultant of the forces R_3 (see Figure A.3).

$$\frac{P\beta}{2\pi}(C/2 - B/2) - (R_1\beta + R_2)(h - y/3) = 0$$

$$(R_1\beta + R_2) = \frac{P\beta}{2\pi}\frac{(C/2 - B/2)}{(h - y/3)} = P\frac{\beta}{2\pi}K_y$$

Therefore the second expression for P is given by:

$$P = \frac{2\pi}{K_y}(R_1 + \frac{R_2}{\beta}) \qquad \text{Equation (12)}$$

II Mechanical Model for Restrained Slabs

Hewitt and Batchelor, as shown in Figure A.4 proposed an idealized mechanical model of a restrained slab at punching failure. The model is basically that proposed by Kinnunen and Nylander, except a moment and force at the bottom compression reinforcement at the boundary have been included. M_b and F_b are respectively moment and force per unit length of slab acting in the plane of the slab.

Taking moments with respect to the point of intersection of the resultant of the forces R_1 and Pβ/(2π) gives:

$$2\pi R_3(h - y/3) + \frac{P}{\tan\alpha}(h - y/3) - P(C/2 - B/2) + M_b\pi C = 0$$

$$\frac{2\pi R_3}{P} = K_y - \cot\alpha - \frac{M_b}{P}\frac{\pi C}{(h - y/3)}$$

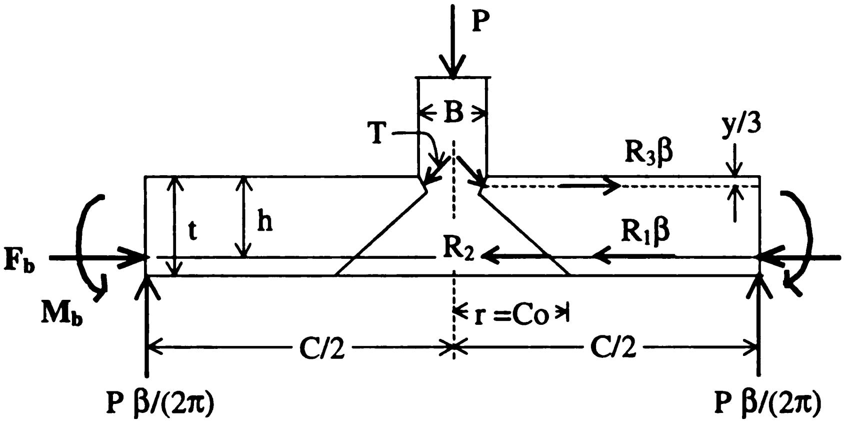

Figure A.4 Mechanical Model of Restrained Slab

For convenience, M_b/P is replaced by $X/(4\pi)$, in which X is a factor of the order unity (assuming a circular fan failure mode the resisting moments M_b, is given by $4\pi M_b$).

Thus $$X = 4\pi\frac{M_b}{P} \qquad \text{Equation (13)}$$

Then again assuming $f_t/f_{ct} = 2.35$ and substituting equations for P and for R_3, the following equations are obtained:

$$2\pi\frac{\frac{y^2}{2h}f_{ct}(\frac{B}{2y}+1)\ln\left[\frac{C/2}{B/2+y}\right]}{2\pi f_t f_\alpha By\frac{B+2y}{B+y}} = K_y - \cot\alpha - X\frac{C}{4(h-y/3)}$$

$$\frac{1+y/B}{4.7}\ln\left[\frac{C/2}{B/2+y}\right] = (K_y - \cot\alpha - \frac{XC}{4(h-y/3)})f_\alpha =$$

$$[(K_y - \frac{XC}{4(h-y/3)})\tan\alpha - 1]\frac{(1-\tan\alpha)}{(1+\tan^2\alpha)}$$

Define:

$$K_z = K_y - \frac{XC}{4(h-y/3)} \qquad \text{Equation (14)}$$

Then,

$$\frac{(1+y/B)}{4.7}\ln\left[\frac{C/2}{B/2+y}\right]=(K_z\tan\alpha-1)\frac{(1-\tan\alpha)}{(1+\tan^2\alpha)}\qquad\text{Equation (15)}$$

When $M_b = 0$, $X = 0$, and $K_z = K_y$, then Equation (15) is identical to that for a simply supported slab.

Taking moments about the point of intersection of $T\beta/(2\pi)$ in the conical shell and the resultant of the forces R_3, gives

$$\frac{P\beta}{2\pi}(C/2-B/2)-(R_1\beta+R_2+F_b\beta\frac{C}{2})(h-\frac{y}{3})-M_b\beta\frac{C}{2}=0$$

$$\frac{P\beta}{2\pi}(C/2-B/2)-XP\beta\frac{C}{8\pi}=(R_1\beta+R_2+F_b\beta\frac{C}{2})(h-\frac{y}{3})$$

$$\frac{P\beta}{2\pi}(\frac{C/2-B/2}{h-y/3}-\frac{XC}{4(h-y/3)})=(R_1\beta+R_2+F_b\beta\frac{C}{2})=\frac{P\beta}{2\pi}K_z$$

$$P=\frac{2\pi}{K_z}(R_1+\frac{R_2}{\beta}+F_b\frac{C}{2})\qquad\text{Equation (16)}$$

If $F_b = 0$ and $M_b = 0$, $X = 0$ and $K_z = K_y$, then Equation (16) is identical to Equation (12) for a simply supported slab.

Restraint Factor

In a practical situation, the boundary restraining forces on a slab loaded to punching failure are usually not known and would be difficult to either calculate or measure accurately, even under laboratory conditions. For these reasons a single factor, to be termed the 'restraint factor', was proposed by Batchelor and Hewitt. The factor ranges from zero for a simply supported slab to 1 (one) for a fully restrained slab.

The resultant maximum boundary stresses and forces are given in Figure A.5. The maximum tensile force, F_t, per unit length of the boundary, at the level of tensile reinforcement is given by:

$$F_t = h\rho f_{sy} \qquad \text{Equation (17)}$$

If the slab is not reinforced at the boundary, F_t is zero. The maximum compressive force per unit length of the boundary in the concrete is given by

$$F_c = kf_{\max}\left(\frac{t}{2} - \frac{\Delta}{4}\right) \qquad \text{Equation (18)}$$

where k is the ratio of the average stress to the maximum stress in the concrete, $f_{\max}$ and depends on the stress distribution, and Δ is the central deflection of the slab at failure. Assuming a parabolic distribution of stress, k = 2/3.

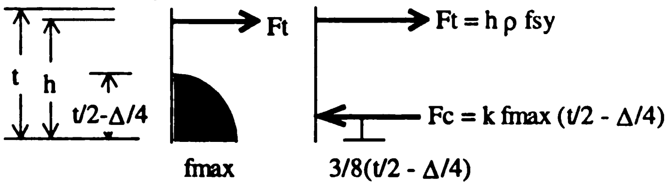

Figure A.5 Boundary Forces

Using a maximum concrete stress of 0.85 fc', the idealized maximum boundary restraints are then given by

$$Mb_{(\max)} = F_t(2h - t) - F_c\left(h - \frac{13}{16}t - \frac{3}{32}\Delta\right)$$

$$F_{b(\max)} = F_c - F_t$$

Realizing that the maximum boundary restraints would rarely occur at punching failure, the restraint factor, F_r was introduced. The actual boundary restraints at failure are then given by

$$M_b = F_r M_{b(\max)} = F_r\left[F_t(2h-t) - F_c(h - \frac{13}{16}t - \frac{3}{32}\Delta)\right] \qquad \text{Equation (19)}$$

$$F_b = F_r F_{b(\max)} = F_r\left[F_c - F_t\right] \qquad \text{Equation (20)}$$

The slab deflection, Δ, can be approximately expressed as

$$\Delta = \psi\frac{(C-B)}{2} \qquad \text{Equation (21)}$$

The uncorrected theoretical punching load, P, for a restrained slab is determined by iteration using Equations (1) through (21).

Using correction factor for dowel and membrane effects of 1.2, the following equation was adopted:

$$V = 1.2P$$

V is the corrected ultimate load of slab, and P is the load calculated without consideration of dowel or tensile membrane effects.

List of symbol and notations

- α - is the angel between the horizontal plane and $T\beta/(2\pi)$
- β - is the angel of sector element of the slab under the load.
- B - is the diameter of load (column).
- C - is the diameter of slab.
- $2c_1$ – is the thickness of conical shell at its lower boundary.

- $2c_2$ – is the thickness of conical shell at its upper boundary.
- C_o - is the distance from the center of slab to the shear crack.
- ε_{ct} - is the concrete strain at top of slab in tangential direction.
- ε_s - is the strain in reinforcing steel at a distance r from the center of the slab.
- f_{ct} - is the compressive stress at the top of slab in a tangential direction.
- f_{cube} - is the 150 mm cube strength of concrete with unit of kilogram force per square centimeters.
- f_t - is the compressive stress in the imaginary conical shell.
- F_b - is the boundary force at the boundary of restrained slab.
- F_c - is the concrete compressive force at the slab boundary.
- F_t - is the tensile force at the slab boundary.
- M_b - is the boundary moment at the boundary of a restrained slab.
- P - is the load (force) which is transmitted through the conical shell.
- R_1 - is resultant force in the ring reinforcement
- R_2 - is resultant force in the radial reinforcement acts at the section $r = Co$
- R_3 - is resultant force in the concrete acting in a radial crack
- r_s - is the radius of slab area in which the yield point stress is reached under the failure load.
- T - is oblique compressive force acting at the conical shell.
- y - is the distance from the top surface of the slab to the root of shear crack at failure.
- ψ - is the angle of rotation in a radial vertical plane of the slab portion adjacent to the load outside shear crack.

APPENDIX B

FLOW DIAGRAM AND CODE LISTING TO CALCULATE PUNCHING SHEAR STRENGTH OF RESTRAINED SLAB

I. Flow Diagram to Calculate Punching Strength of Restrained Slabs

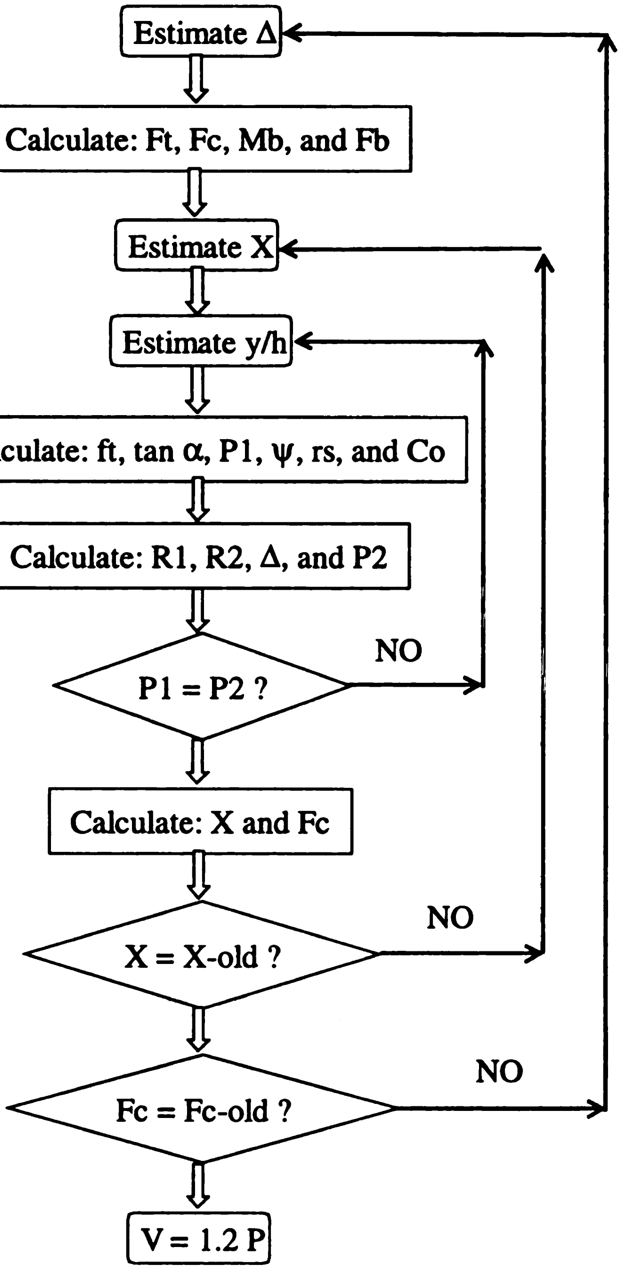
Estimate Δ
Calculate: Ft, Fc, Mb, and Fb
Estimate X
Estimate y/h
Calculate: ft, tan α, P1, ψ, rs, and Co
Calculate: R1, R2, Δ, and P2
P1 = P2 ?
NO
Calculate: X and Fc
X = X-old ?
NO
Fc = Fc-old ?
NO
V = 1.2 P

II. Code Listing to Calculate the Punching Strength of a Restrained Slab

```
{******* PROGRAM TO CALCULATE PUNCHING SHEAR STRENGTH *******}
{********* OF A RESTRAINED SLAB WITH KNOWN VALUE OF FR **********}
{***************** USING BORLAND DELPHI VERSION 3.0 ****************}

{***VARIABLES DECLARATION***}
VAR
 T, H, B, C, FCCYL, FCCUB, RHO, FSY, ES, RF, BF : double;
 X, PU, DEFL, PDIFF, XDIFF, FT, FC, V : double;
 BM, BMPF, YONH, HOLD1, HOLD2, HOLD3, HOLD4, HOLD5 : double;
 HOLD6, KY, KZ, TANA, FALFA, F, SIGT, P1, P2, PSI  : double;
 RS, CO, Y, PERR1, PERR2, PDHOLD, YHOLD, XCHECK, XDHOLD : double;
 CCHECK, R1, R2, BONH, CDIFF, PERR3 : double;
 cERR1,cERR2,cERR3: integer;

{*** PROCEDURE TO CALCULATE BOUNDARY RESTRAINING FORCES ***}
Procedure CalcBRes;
 begin
   FT:=RF*FSY*H*RHO;
   FC:=RF*((T/2)-(DEFL/4))*FCCYL*1.7/3;
   BF:=FC-FT;
   BM:=FT*(2*H-T)-FC*(H-T*13/16-DEFL*3/32);
   BMPF:=12.568*BM/1000;
 end;

{*PROCEDURE TO CALCULATE THE FIRST VALUE OF PUNCHING LOAD*}
Procedure CalcP1;
 begin
   Y:=YONH*H;
   HOLD1:=(1/4.7)*(1+Y/B)*Ln(C/(B+2*Y));
   KY:=(C-B)/(2*(H-Y/3));
   KZ:=KY-X*C/(4*(H-Y/3));
   HOLD2:=KZ+HOLD1;
   HOLD3:=-KZ-1;
   HOLD4:=HOLD1+1;
   HOLD5:=(HOLD3*HOLD3-4*HOLD2*HOLD4);
   IF HOLD5 < 0 THEN TANA:=-HOLD3/(2*HOLD2)
   ELSE
      TANA:=(-HOLD3-SQRT(HOLD5))/(2*HOLD2);
   FALFA:=TANA*(1-TANA)/(1+TANA*TANA);
   BONH:=B/H;
   F:=14.22;
   IF BONH < 2 THEN SIGT:=825*(0.35+FCCUB/(F*500))*(1-0.22*BONH)*F
   ELSE
      SIGT:=460*(0.35+FCCUB/(F*500))*F;
   P1:=3.142*BONH*YONH*(B+2*Y)*SIGT*FALFA*H*H/(B+Y);
 end;

{*PROCEDURE TO CALCULATE THE SECOND VALUE OF PUNCHING LOAD*}
Procedure CALCP2;
 begin
    IF BONH < 2 THEN PSI:=0.0035*(1-0.22*BONH)*(1+0.5*B/Y)
    ELSE
       PSI:=0.00195*(1+0.5*B/Y);
    RS:=H*ES*PSI*(1-YONH)/FSY;
    CO:=0.5*B+1.8*H;
    HOLD6:=RHO*FSY*H;
    IF RS <= CO THEN
       BEGIN
```

```
        R1:=HOLD6*RS*Ln(0.5*C/CO);
        R2:=HOLD6*RS;
        END
     ELSE
        IF RS > 0.5*C THEN RS:=0.5*C
        ELSE
              BEGIN
              R1:=HOLD6*((RS-CO)+RS*Ln(0.5*C/RS));
              R2:=HOLD6*CO;
              END;
    DEFL:=PSI*(C-B)/2;
    P2:=6.284*(R1+R2+BF*C*(H-Y/3-DEFL)/(2*(H-Y/3.0)))/KZ;
  END;

{***** THE MAIN PROGRAM *****}
Begin
T := StrToFloat(edT.Text);
H := StrToFloat(edH.Text);
B := StrToFloat(edB.Text);
C := StrToFloat(edC.Text);
FCCYL := StrToFloat(edFCCYL.Text);
RHO := StrToFloat(edRHO.Text);
FSY := StrToFloat(edFSY.Text);
ES := StrToFloat(edES.Text);
RF := StrToFloat(edRF.Text);
FCCUB:=FCCYL/(0.75+0.000025*FCCYL);
DEFL:=T/4;
PU:=0;
V:=0;
X:=1.0;
```

```
YONH:=0.5;
cERR1 := 0;
cERR2 := 0;
cERR3 := 0;
PERR3 := 1.1;
WHILE PERR3 > 0.1 DO
BEGIN
        Inc(cERR3);
        CalcBRes;
        PERR2 := 1.1;
        WHILE PERR2 > 0.1 DO
        BEGIN
   Inc(cERR2);
                PERR1 := 1.1;
                WHILE PERR1 > 0.1 DO
                    BEGIN
                            Inc(cERR1);
                        CALCP1; {*CALCULATE P1*}
                        CALCP2; {*CALCULATE P2*}
                        {**** COMPARE P1 & P2 ****}
                        PDIFF:=ABS(P1-P2);
                        PERR1:=100*PDIFF/P1;
                        {*** ITERATION WITH Y/H ***}
                        YONH:=YONH*0.5*(1+P2/P1);
                 END;
         PU:=(P1+P2)/2000;
         V:=1.2 * PU;
         XCHECK:=BMPF/PU;
         {*** COMPARE X & XCHECK ***}
         XDIFF:=ABS(X-XCHECK);
```

```
    PERR2:=ABS(100*XDIFF/X);
    X:=(X+XCHECK)/2;
    END;
{*** CHECK COMPRESSIVE BOUNDARY FORCE ***}
CCHECK:=RF*((T/2)-(DEFL/4))*FCCYL*1.7/3;
CDIFF:=ABS(FC-CCHECK);
PERR3:=100*CDIFF/FC;
END;

{*** PRINT OUTPUT ***}
lbP.Caption    := FloatToStr(PU);
lbV.Caption    := FloatToStr(V);
Label11.Caption := IntToStr(cERR1);
Label12.Caption := IntToStr(cERR2);
Label13.Caption := IntToStr(cERR3);
Label14.Caption := FloatToStr(YONH);
Label15.Caption := FloatToStr(X);
end;
end.
```

APPENDIX C

EXAMPLE OF FINITE ELEMENT INPUT AND OUTPUT FILES

I. Input File (ABAQUS/Standard Version 5.8)

```
*HEADING
 M1: Basic Model Using 8-node Elements (psi units).
**Node Definition
*NODE
 1,0.0,0.,0.
 19,36.,0.,0.
 23,40.,0.,0.
 51,96.,0.,0.
 201,0.0,7.,0.
 219,36.,7.,0.
 223,40.,7.,0.
 251,96.,7.,0.
 401,0.0,9.,0.
 419,36.,9.,0.
 423,40.,9.,0.
 451,96.,9.,0.
 801,0.0,16.,0.
 819,36.,16.,0.
 823,40.,16.,0.
 851,96.,16.,0.
 1001,0.0,20.,0.
 1019,36.,20.,0.
 1023,40.,20.,0.
 1051,96.,20.,0.
 1401,0.0,27.,0.
```

```
1419,36.,27.,0.
1423,40.,27.,0.
1451,96.,27.,0.
1601,0.0,29.,0.
1619,36.,29.,0.
1623,40.,29.,0.
1651,96.,29.,0.
2401,0.0,47.,0.
2419,36.,47.,0.
2423,40.,47.,0.
2451,96.,47.,0.
2601,0.0,49.,0.
2619,36.,49.,0.
2623,40.,49.,0.
2651,96.,49.,0.
2801,0.0,56.,0.
2819,36.,56.,0.
2823,40.,56.,0.
2851,96.,56.,0.
*NGEN, NSET=NL1
1,201,100
*NGEN, NSET=NL2
201,401,100
*NGEN, NSET=NL3
401,801,100
*NGEN, NSET=NL4
801,1001,100
*NGEN, NSET=NL5
1001,1401,100
*NGEN, NSET=NL6
1401,1601,100
```

```
*NGEN, NSET=NL7
 1601,2401,100
*NGEN, NSET=NL8
 2401,2601,100
*NGEN, NSET=NL9
 2601,2801,100
*NSET, NSET=NL
 NL1,NL2,NL3,NL4,NL5,NL6,NL7,NL8,NL9
*NGEN, NSET=NMID1
 19,219,100
*NGEN, NSET=NMID2
 219,419,100
*NGEN, NSET=NMID3
 419,819,100
*NGEN, NSET=NMID4
 819,1019,100
*NGEN, NSET=NMID5
 1019,1419,100
*NGEN, NSET=NMID6
 1419,1619,100
*NGEN, NSET=NMID7
 1619,2419,100
*NGEN, NSET=NMID8
 2419,2619,100
*NGEN, NSET=NMID9
 2619,2819,100
*NSET, NSET=NMIDL
NMID1, NMID2, NMID3, NMID4, NMID5, NMID6, NMID7, NMID8, NMI9
*NGEN, NSET=NMIR1
 23,223,100
*NGEN, NSET=NMIR2
```

```
223,423,100
*NGEN, NSET=NMIR3
423,823,100
*NGEN, NSET=NMIR4
823,1023,100
*NGEN, NSET=NMIR5
1023,1423,100
*NGEN, NSET=NMIR6
1423,1623,100
*NGEN, NSET=NMIR7
1623,2423,100
*NGEN, NSET=NMIR8
2423,2623,100
*NGEN, NSET=NMIR9
2623,2823,100
*NSET, NSET=NMIDR
NMIR1,NMIR2,NMIR3,NMIR4,NMIR5,NMIR6,NMIR7,NMIR8,NMI9
*NGEN, NSET=NR1
51,251,100
*NGEN, NSET=NR2
251,451,100
*NGEN, NSET=NR3
451,851,100
*NGEN, NSET=NR4
851,1051,100
*NGEN, NSET=NR5
1051,1451,100
*NGEN, NSET=NR6
1451,1651,100
*NGEN, NSET=NR7
1651,2451,100
```

```
*NGEN, NSET=NR8
 2451,2651,100
*NGEN, NSET=NR9
 2651,2851,100
*NSET, NSET=NR
 NR1,NR2,NR3,NR4,NR5,NR6,NR7,NR8,NR9
*NFILL, NSET=SLEFT
 NL,NMIDL,18,1
*NFILL, NSET=SMID
 NMIDL,NMIDR,4,1
*NFILL, NSET=SRIGHT
 NMIDR,NR,28,1
*NSET, NSET=STOP
 SLEFT,SMID,SRIGHT
*NODE
 50301,0.0,8.,-4.6
 50319,36.,8.,-4.6
 50323,40.,8.,-4.6
 50351,96.,8.,-4.6
 51501,0.0,28.,-4.6
 51519,36.,28.,-4.6
 51523,40.,28.,-4.6
 51551,96.,28.,-4.6
 52501,0.0,48.,-4.6
 52519,36.,48.,-4.6
 52523,40.,48.,-4.6
 52551,96.,48.,-4.6
*NGEN, NSET=WEBL1
 50301,50319,1
*NGEN, NSET=WMID1
 50319,50323,1
```

```
*NGEN, NSET=WEBR1
 50323,50351,1
*NGEN, NSET=WEBL2
 51501,51519,1
*NGEN, NSET=WMID2
 51519,51523,1
*NGEN, NSET=WEBR2
 51523,51551,1
*NGEN, NSET=WEBL3
 52501,52519,1
*NGEN, NSET=WMID3
 52519,52523,1
*NGEN, NSET=WEBR3
 52523,52551,1
*NCOPY, CHANGE NUMBER=40000, OLD SET=STOP, NEW SET=SBOT,
REFLECT=MIRROR
 0.,0.,-0.8,0.,1.,-0.8
 1.,0.,-0.8
*NSET, NSET=FTOPL
 40201,40301,40401,41401,41501,41601,42401,42501,42601
*NSET, NSET=FTOPR
 40251,40351,40451,41451,41551,41651,42451,42551,42651
*NCOPY, CHANGE NUMBER=20000, OLD SET=FTOPL, NEW SET=FBOTL,
REFLECT=MIRROR
 0.,0.,-4.6,0.,1.,-4.6
 1.,0.,-4.6
*NCOPY, CHANGE NUMBER=20000, OLD SET=FTOPR, NEW  SET=FBOTR,
REFLECT=MIRROR
 0.,0.,-4.6,0.,1.,-4.6
 1.,0.,-4.6
*NFILL,NSET=FBOT
```

```
 FBOTL,FBOTR,50,1
**End of Node Definition
**Start Element Definition

**Reinforced Concrete Element for Slab
*ELEMENT, TYPE=C3D8, ELSET=SLABTOP
 1,40001,40002,40102,40101,1,2,102,101
*ELGEN, ELSET=SLABTOP
 1,50,1,1,28,100,100
*SOLID SECTION, ELSET=SLABTOP, MATERIAL=RC
*MATERIAL, NAME=RC
*ELASTIC
 3.6E6,0.2
*CONCRETE
 500.,0.
 4000.,0.003
*FAILURE RATIOS
 1.25,0.1
*TENSION STIFFENING
 1.,0.
 0.,0.0025
*REBAR, ELEMENT=CONTINUUM, MATERIAL=WWM,
 GEOMETRY=ISOPARAMETRIC, NAME=YYBOT
 SLABTOP,.00333,1.,0.,0.1875,4,2
*REBAR, ELEMENT=CONTINUUM, MATERIAL=WWM,
 GEOMETRY=ISOPARAMETRIC, NAME=XXBOT
 SLABTOP,.00333,1.,0.,0.1875,1,1
*REBAR, ELEMENT=CONTINUUM, MATERIAL=WWM,
 GEOMETRY=ISOPARAMETRIC, NAME=YYTOP
 SLABTOP,.00333,1.,0.,0.8125,4,2
```

```
*REBAR, ELEMENT=CONTINUUM, MATERIAL=WWM,
GEOMETRY=ISOPARAMETRIC, NAME=XXTOP
 SLABTOP,.00333,1.,0.,0.8125,1,1
*MATERIAL, NAME=WWM
*ELASTIC
 29.E6
*PLASTIC
 72.5E3

**Shell Element for Steel Girders
*ELEMENT, TYPE=S9R5, ELSET=TOPFL1
 40001,40201,40203,40403,40401,40202,40303,40402,40301,40302
*ELGEN, ELSET=TOPFL1
 40001,25,2,1,
*SHELL SECTION, ELSET=TOPFL1, MATERIAL=A36ST1
 0.171,
*MATERIAL, NAME=A36ST1
*ELASTIC
 29.E6
*ELEMENT, TYPE=S9R5, ELSET=TOPFL2
 40101,41401,41403,41603,41601,41402,41503,41602,41501,41502
*ELGEN, ELSET=TOPFL2
 40101,25,2,1,2,1000,100
*SHELL SECTION, ELSET=TOPFL2, MATERIAL=A36ST2
 0.171,
*MATERIAL, NAME=A36ST2
*ELASTIC
 29.E6
*ELEMENT, TYPE=S9R5, ELSET=BOTFL1
 60001,60201,60203,60403,60401,60202,60303,60402,60301,60302
*ELGEN, ELSET=BOTFL1
```

```
60001,25,2,1,
*SHELL SECTION, ELSET=BOTFL1, MATERIAL=A36ST3
0.171,
*MATERIAL, NAME=A36ST3
*ELASTIC
29.E6
*ELEMENT, TYPE=S9R5, ELSET=BOTFL2
60101,61401,61403,61603,61601,61402,61503,61602,61501,61502
*ELGEN, ELSET=BOTFL2
60101,25,2,1,2,1000,100
*SHELL SECTION, ELSET=BOTFL2, MATERIAL=A36ST4
0.171,
*MATERIAL, NAME=A36ST4
*ELASTIC
29.E6
*ELEMENT, TYPE=S9R5, ELSET=WEB1
41001,60301,60303,40303,40301,60302,50303,40302,50301,50302
*ELGEN, ELSET=WEB1
41001,25,2,1,
*SHELL SECTION, ELSET=WEB1, MATERIAL=A36ST5
0.114,
*MATERIAL, NAME=A36ST5
*ELASTIC
29.E6
*ELEMENT, TYPE=S9R5, ELSET=WEB2
41101,61501,61503,41503,41501,61502,51503,41502,51501,51502
*ELGEN, ELSET=WEB2
41101,25,2,1,2,1000,100
*SHELL SECTION, ELSET=WEB2, MATERIAL=A36ST6
0.114,
*MATERIAL, NAME=A36ST6
```

```
*ELASTIC
 29.E6

**Beam Element for Edge Beams
*ELEMENT, TYPE=B31, ELSET=EDGEBM
 50001,40401,40501
*ELGEN, ELSET=EDGEBM
 50001,2,50,100,18,100,1
*BEAM SECTION, SECTION=RECTANGULAR, ELSET=EDGEBM,
MATERIAL=STEDGEBM
 2.758,0.95
*MATERIAL, NAME=STEDGEBM
*ELASTIC
 29.E6

**Truss Element for Tie Rods
*ELEMENT, TYPE=T3D2, ELSET=TIEROD1
 51001,40403,41403
*ELGEN, ELSET=TIEROD1
 51001,5,4,1
*SOLID SECTION, ELSET=TIEROD1, MATERIAL=STROD1
 0.25
*MATERIAL, NAME=STROD1
*ELASTIC
 29.E6
*ELEMENT, TYPE=T3D2, ELSET=TIEROD2
 51101,40425,41425
*ELGEN, ELSET=TIEROD2
 51101,7,4,1
*SOLID SECTION, ELSET=TIEROD2, MATERIAL=STROD2
 0.25
```

```
*MATERIAL, NAME=STROD2
*ELASTIC
 29.E6
*ELSET, ELSET=TIERODS
 TIEROD1, TIEROD2

**Beam Element for Diaphragms
*ELEMENT, TYPE=B31, ELSET=DIAPH1
 52001,50301,51501
*BEAM SECTION, SECTION=RECTANGULAR, ELSET=DIAPH1,
MATERIAL=STDIAP1
 0.95,2.758
*MATERIAL, NAME=STDIAP1
*ELASTIC
 29.E6
*ELEMENT, TYPE=B31, ELSET=DIAPH2
 52002,51501,52501
*BEAM SECTION, SECTION=RECTANGULAR, ELSET=DIAPH2,
MATERIAL=STDIAP2
 0.95,2.758
*MATERIAL, NAME=STDIAP2
*ELASTIC
 29.E6
*ELEMENT, TYPE=B31, ELSET=DIAPH3
 52003,50327,51527
*ELGEN, ELSET=DIAPH3
 52003,2,24,1,
*BEAM SECTION, SECTION=RECTANGULAR, ELSET=DIAPH3,
MATERIAL=STDIAP3
 0.95,2.758
*MATERIAL, NAME=STDIAP3
```

```
*ELASTIC
 29.E6
*ELEMENT, TYPE=B31, ELSET=DIAPH4
 52005,51527,52527
*ELGEN, ELSET=DIAPH4
 52005,2,24,1,
*BEAM SECTION, SECTION=RECTANGULAR, ELSET=DIAPH4,
MATERIAL=STDIAP4
 0.95,2.758
*MATERIAL, NAME=STDIAP4
*ELASTIC
 29.E6

**Boundary Conditions
*BOUNDARY
 60201,3
 60301,3
 60401,3
 61401,3
 61501,1,3
 61601,3
 62401,3
 62501,3
 62601,3
 60251,3
 60351,3
 60451,3
 61451,3
 61551,2,3
 61651,3
 62451,3
```

```
62551,3
62651,3

**Step Definition and Output Request
*RESTART, WRITE
*STEP, INC=100
*STATIC, RIKS
0.1,1.,,,,40921,3,-0.55
**Load Definition
*ELSET, ELSET=LOADEDEL
819,820,919,920
*DLOAD
LOADEDEL,P2,2000.
*EL PRINT, ELSET=TIERODS
E
*NSET, NSET=NODALDISP
40921,61521
*NODE PRINT, NSET=NODALDISP
U
*MONITOR, NODE=40921, DOF=3
*END STEP
```

II. ABAQUS/Standard Status File

```
SUMMARY OF JOB INFORMATION:
MONITOR NODE:  40921  DOF:  3
STEP  INC ATT SEVERE EQUIL  TOTAL  STEP      INC OF     DOF      IF
              DISCON ITERS  ITERS  TIME/LPF  TIME/LPF   MONITOR  RIKS
              ITERS
  1    1   1    0      3      3    0.0999    0.09995    -0.0264   R
  1    2   1    0      6      6    0.198     0.09815    -0.0553   R
  1    3   1    0      6      6    0.292     0.09364    -0.0883   R
  1    4   1    0      5      5    0.381     0.08966    -0.124    R
  1    5   2    0      5      5    0.403     0.02197    -0.133    R
  1    6   1    0      5      5    0.425     0.02177    -0.142    R
  1    7   1    0      5      5    0.447     0.02160    -0.151    R
  1    8   2    0      3      3    0.452     0.005430   -0.154    R
  1    9   1    0      4      4    0.458     0.005385   -0.156    R
  1   10   2    0      4      4    0.461     0.003041   -0.157    R
  1   11   1    0      5      5    0.465     0.004513   -0.159    R
  1   12   2    0      3      3    0.466     0.001149   -0.160    R
  1   13   1    0      3      3    0.467     0.001141   -0.160    R
  1   14   1    0      3      3    0.469     0.001694   -0.161    R
  1   15   2    0      3      3    0.470     0.0009607  -0.161    R
  1   16   1    0      4      4    0.471     0.001427   -0.162    R
  1   17   2    0      3      3    0.472     0.0008104  -0.162    R
  1   18   1    0      5      5    0.473     0.001204   -0.163    R
  1   19   2    0      3      3    0.474     0.0003035  -0.163    R
  1   20   1    0      3      3    0.474     0.0003035  -0.163    R
  1   21   1    0      3      3    0.475     0.0004545  -0.163    R
  1   22   1    0      4      4    0.475     0.0006827  -0.164    R
  1   23   2    0      3      3    0.476     0.0003859  -0.164    R
  1   24   2    0      3      3    0.476     0.0002182  -0.164    R
  1   25   1    0      3      3    0.476     0.0003228  -0.164    R
  1   26   2    0      3      3    0.476     0.0001816  -0.164    R
  1   27   1    0      4      4    0.477     0.0002716  -0.164    R
  1   28   2    0      3      3    0.477     0.0001533  -0.164    R
  1   29   1    0      4      4    0.477     0.0002311  -0.164    R
```

III. ABAQUS/Plot Output

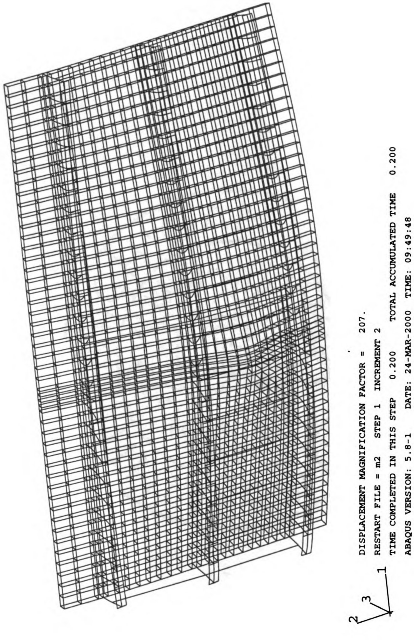
DISPLACEMENT MAGNIFICATION FACTOR = 207.
RESTART FILE = m2 STEP 1 INCREMENT 2
TIME COMPLETED IN THIS STEP 0.200 TOTAL ACCUMULATED TIME 0.200
ABAQUS VERSION: 5.8-1 DATE: 24-MAR-2000 TIME: 09:49:48
1
2
3

Figure C.1 Magnified Displaced Shape of FE Model of the Bridge

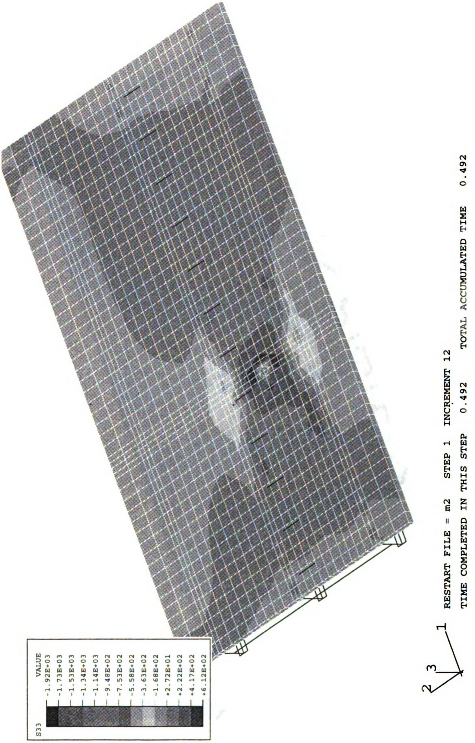

Figure C.2 Contour of S33, Stress in 3-direction

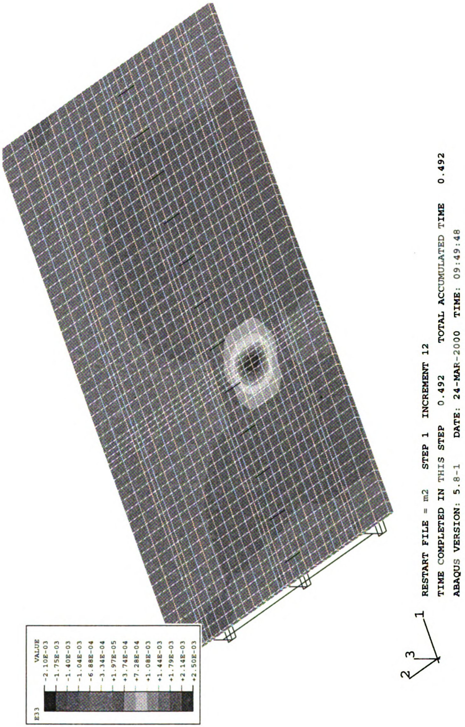

Figure C.3 Contour of E33, Strain in 3-direction

MICHIGAN STATE UNIVERSITY LIBRARIES
3 1293 02125 8938